

Proteomic Analysis of Benzo[a]pyrene-Mediated Bladder Toxicity

Inaugural Dissertation for the Degree of
Doctor of Natural Science
Dr. rer. nat.

A Thesis Presented to
The Faculty of Biology
University of Duisburg-Essen
Germany

Presented by
Nisha Verma
from Shimla, India
September, 2012

Die der folgenden Arbeit zugrunde liegenden Experimente wurden in der Arbeitsgruppe 'Toxicoproteomics' am Institut für Hygiene und Arbeitsmedizin der Universität Duisburg–Essen, durchgeführt.

1. Gutachter: Prof. Dr. Albert. W. Rettenmeier

2. Gutachter: Prof. Dr. Markus Kaiser

Vorsitzender des Prüfungsausschusses: Prof. Dr. Dr. H. de Groot

Tag der mündlichen Prüfung: 08.01.2013

Contents

1. Introduction.....	1
1.1 Benzo[a]pyrene (B[a]P)	1
1.2 Metabolism of B[a]P	3
1.3 Mechanisms of B[a]P-mediated toxicity.....	6
1.3.1 DNA and protein adducts	6
1.3.2 Oxidative stress	10
1.3.3 Disturbance of signal transduction pathways.....	12
1.4 Objective	12
2. Material and Methods	15
2.1 Cell Culture	15
2.1.1 Pig urinary bladder epithelial cells (PUBEC)	15
2.1.2 Evaluation of cell morphology and purity of PUBEC	16
2.1.3 RT4 cell line	16
2.2 Cell exposure.....	17
2.3 Uptake and metabolism.....	17
2.3.1 Determination of the time course of B[a]P uptake and subcellular distribution by confocal laser-scanning microscopy	17
2.3.2 Quantification of B[a]P uptake by spectrofluorometry	17
2.3.3 Quantification of B[a]P uptake by gas chromatography-mass spectrometry (GC-MS).....	19
2.3.4 Identification of 3-OH-B[a]P in PUBEC by GC-MS.....	20
2.4 Proteomic analysis	21
2.4.1 2D gel electrophoresis	21
2.4.2 Precipitation of phosphoproteins.....	21
2.4.3 Coomassie brilliant blue (CBB) staining of gels.....	22
2.4.4 Image acquisition and analysis.....	22
2.4.5 In-gel enzymatic digestion	22
2.4.6 MALDI-TOF-MS analysis and protein identification.....	23
2.4.7 TdT-mediated dUTP-X nick end labeling (TUNEL) assay	23
2.4.8 Western blot	24
2.4.9 Comet assay.....	25
2.4.10 Detection of the mitochondrial membrane potential (MMP).....	26
2.5 Two-dimensional Blue Native/SDS-PAGE (2D BN/SDS-PAGE).....	26
2.5.1 Sample preparation and subcellular fractionation of RT4 cells	26

2.5.2	2D BN/SDS-PAGE	28
2.5.3	Determination of intracellular chelatable iron by Phen Green TM SK.....	30
2.5.4	Determination of NO with the Griess test	32
2.5.5	Determination of intracellular calcium concentration.....	33
2.6	Bioinformatic analysis	35
3.	Exposure of PUBEC to B[a]P: <i>In vitro</i> uptake, intra-cellular concentration, and biological response	36
3.1	Objective	36
3.1.1	Morphologies and purity of PUBEC	36
3.1.2	Analysis of B[a]P uptake and its subcellular distribution	37
3.1.3	Quantification of intracellular B[a]P concentration by spectrofluoro-metry and GC-MS	39
3.1.4	Formation of 3-OH-B[a]P in PUBEC	42
4.	Proteome and phosphoproteome maps of PUBEC	43
4.1	Objective	43
4.2	2DE analysis and identity assignment	43
4.3	Physicochemical properties of identified proteins	49
4.4	Functional and subcellular annotation of proteins	50
4.5	Phosphoproteome profiling of PUBEC.....	53
5.	Toxicoproteomic analysis of apoptotic pathway in B[a]P- exposed PUBEC	55
5.1	Objective	55
5.2	2DE analyses of protein expression in control and B[a]P-exposed cells.....	55
5.3	Induction of DNA repair proteins and determination of DNA damage.....	56
5.4	Verification of DNA damage in PUBEC exposed to 0.5 μ M B[a]P	59
5.5	B[a]P induced changes expression of proteins involved in apoptosis	60
5.6	Analysis of mitochondrial alterations following B[a]P exposure	60
5.7	Application of western blot and TUNEL assay for analysis of apoptosis in PUBEC	61
6.	Blue Native PAGE analysis of B[a]P- and TCDD-exposed cells	63
6.1	Objective	63
6.2	Subcellular fractionation and 2D BN/SDS-PAGE analyses of fractionated samples for proteome map generation	64
6.2.1	Protein complexes of cytosolic fraction	64
6.2.2	Protein complexes of the membrane/organelle fraction.....	65
6.2.3	Protein complexes of the nuclear fraction	66
6.3	2D BN/SDS-PAGE analyses of fractionated samples of B[a]P-and TCDD-exposed cells	67

6.4	Alterations in calcium- and iron-containing proteins	67
6.5	Analysis of intracellular calcium changes after B[a]P and TCDD exposure.....	69
	Effects of B[a]P and TCDD on the labile iron pool (LIP) and the possible role of calcium	71
6.6	Possible involvement of nitric oxide (NO) in calmodulin-modulated iron content of cells	72
7.	Discussion	74
7.1	Uptake and subcellular distribution of B[a]P.....	74
7.2	Development of 2DE proteome map of PUBEC	76
7.3	Toxicoproteomic analysis of B[a]P-mediated toxicity in PUBEC	78
7.4	2D BN/SDS-PAGE analysis for the identification of protein complexes involved in B[a]P toxicity	80
8.	Summary.....	86
9.	References.....	89
10.	Annex	108
10.1	Annex I - Representative 2D-gel image after B[a]P exposure.....	108
10.2	Annex II – Protein complexes of subcellular fractions of RT4 cells identified by using MALDI-TOF-MS	109
10.3	Annex III – List of protein complexes of subcellular fraction identified after exposure to B[a]P and TCDD	117
10.4	Annex IV – Representative 2D BN/PAGE gel images after exposure to B[a]P and TCDD.....	123
10.5	Annex V - Cell culture media, reagents, and instrumentation	126
10.6	Annex VI - Curriculum Vitae	130
10.7	Annex VII - Acknowledgement.....	134
10.8	Annex VIII - Declaration	135

Figure Index

Figure 1:	Chemical structure of benzo[a]pyrene.	1
Figure 2:	Pictorial representation of the aryl hydrocarbon receptor (AhR)	2
Figure 3:	Representation of steps involved in the metabolism of B[a]P to reactive intermediates by the activity of phase I and phase II enzymes.....	5
Figure 4:	Metabolic pathways of B[a]P to different configurational isomers of B[a]P-7,8-diol-9,10-epoxide and formation of DNA adducts.	6
Figure 5:	Generation of reactive oxygen species by B[a]P <i>via o</i> -quinone.	10
Figure 6:	Generation of covalent and oxidative DNA adducts with <i>o</i> -quinones..	11
Figure 7:	Spectral characteristics of B[a]P in cytosolic medium	18
Figure 8:	Calibration curves for the determination of intracellular B[a]P concentrations by spectrofluometry.	19
Figure 9:	Calibration curve obtained from B[a]P standards.....	20
Figure 10:	Pictorial representation of subcellular extraction by using S-PEK.....	28
Figure 11:	Principle of 2D BN/SDS-PAGE.....	29
Figure 12:	Measurement of the labile iron pool by using the Phen Green TM SK.....	31
Figure 13:	Mechanism of nitrite detection by using the Griess reagent.....	32
Figure 14:	Chemical structures of intracellular calcium staining dye Fluo-4 and calcium store staining dye Rhod-2/AM.....	34
Figure 15:	Establishment and characterization of porcine bladder epithelial cell culture....	37
Figure 16:	Box plots representing the time-dependent increase in B[a]P fluorescence of different PUBEC pools exposed to 0.5 μ M B[a]P.....	38
Figure 17:	Subcellular distribution of B[a]P in PUBEC	39
Figure 18:	(A) A representative single ion chromatogram obtained from the supernatant of a PUBEC pool exposed to 0.5 μ M B[a]P for 24 h. (B) GC-MS separation of the B[a]P metabolite (3-OH-B[a]P) in unexposed samples and cells exposed to 0.5 μ M and 10 μ M B[a]P	41
Figure 19:	Representative 2DE gel image of PUBEC.....	44
Figure 20:	Theoretical isoelectric point (pI) (A) and molecular weight (MW) distribution (B) of proteins from pig bladder epithelial cells	49
Figure 21:	Ontological classification of the identified proteins according to the PANTHER prediction	51
Figure 22:	Subcellular location of the identified proteins according to DAVID prediction.	52
Figure 23:	Classification of the identified phosphoproteins from PUBEC based on their predicted biological function	53
Figure 24:	Potential protein-protein interactions of all differentially expressed protein species associated with B[a]P exposure as suggested by the STRING 9 database	58

Figure 25:	Concentration-dependent increase in B[a]P-induced DNA damage evaluated with the Comet assay..	59
Figure 26:	Determination of the MMP of PUBEC by using Rhodamine 123.....	60
Figure 27:	Analysis of pig urinary epithelial cell apoptosis by the TUNEL assay..	61
Figure 28:	Immunoblot analysis of differentially expressed proteins.	62
Figure 29:	Representative 2D BN/PAGE gel of the cytosolic fraction of RT4 cells.	65
Figure 30:	Representative 2D BN/PAGE gel of the membrane/organelle fraction of RT4 cells.	66
Figure 31:	Protein complexes differentially expressed in control and TCDD exposed RT4 cells	69
Figure 32:	Alterations of cellular calcium homeostasis after exposure to B[a]P or TCDD..	70
Figure 33:	Measurement of the chelatable iron pool by PG SK.....	72
Figure 34:	NO production after exposure to TCDD or B[a]P in normal and W-7 inhibited RT-4 cells.....	73
Figure 35:	Ontological classification of the proteins present in different subcellular fractions by using the PANTHER software.....	81
Figure 36:	Pictorial representation of the hypothesis proposed for the interactions between calcium and iron.....	83
Figure 37:	Representative 2D-gel image representing the differentially expressed proteins after B[a]P exposure.	108
Figure 38:	2D BN/PAGE gels representing proteins differentially expressed in the cytosolic fraction of RT4 cells after 24 h exposure to TCDD or B[a]P	123
Figure 39:	2D BN/PAGE gels representing proteins differentially expressed in the membrane/organelle fraction of RT4 cells after 24 h exposure to TCDD or B[a]P	124
Figure 40:	2D BN/PAGE gels representing proteins differentially expressed in the nuclear fraction of RT4 cells after 24 h exposure to TCDD or B[a]P	125

Table index

Table 1:	Primary and secondary metabolites of B[a]P.	3
Table 2:	Albumin and hemoglobin adducts of B[a]P.	7
Table 3:	An overview on similarities between pigs and humans.	13
Table 4:	Spectrofluorometric quantification of B[a]P concentrations in pig urinary bladder epithelial cells.	40
Table 5:	Summary of the proteins of primary cultured PUBEC identified by 2DE separation and peptide mass fingerprinting.	45
Table 6:	List of phosphoproteins identified in PUBEC after precipitation by La ³⁺ ions. ...	54
Table 7:	Proteins with altered expression (≥ 2) after B[a]P exposure compared to controls.	57
Table 8:	List of calcium- and iron-associated proteins with altered expression (≥ 2) after B[a]P or TCDD exposure compared to controls	68
Table 9:	Mass spectrometric data of proteins identified in the cytosolic fraction of RT4 cells, used for the generation of a proteome map.	109
Table 10:	Mass spectrometric data of proteins identified in the membrane/organelle fraction of RT4 cells, used for the generation of a proteome map	112
Table 11:	Mass spectrometric data of proteins identified in the nuclear fraction of RT4 cells, used for the generation of a proteome map	114

List of Abbreviations

1D	one-dimensional
2D	two-dimensional
2DE	two-dimensional electrophoresis
8-‘OH-dG	8-hydroxydeoxyguanosine
ACN	acetonitrile
AhR	aryl hydrocarbon receptor
AhRE	aryl hydrocarbon responsive element
AKR	aldo-keto reductase
ALDH	aldehyde dehydrogenase
amu	atomic mass unit
ANX	annexin
APS	ammoniumperoxodisulfate
ATP	adenosine triphosphate
AR	aldose reductase
ARNT	aryl hydrocarbon nuclear translocator
Asp	aspartic acid
B[a]P	benzo[a]pyrene
BPDE	benzo[a]pyrene-7,8-dihydrodiol-9,10-epoxide
BPM	beats per minute
BN	blue native
BSA	bovine serum albumin
BSTFA	<i>N,O</i> -bis(trimethylsilyl)trifluoroacetamide
CaM	calmodulin
CAPS	<i>N</i> -cyclohexyl-3-aminopropanesulfonic acid
CALR	calreticulin
CAPN	calpain
CBB	Coomassie brilliant blue
CDD	charged-coupled device
cDNA	complementary deoxyribonucleic acid

CHAPS	3-[(3-cholamidopropyl)dimethylammonio]-1-propanesulfonate
CHCA	α -cyano-4-hydroxycinnamic acid
CLIC	chloride intracellular channel protein
Cys	cysteine
CTSD	cathepsin D
CYP	cytochrome P450
DAPI	4',6-diamidino-2-phenylindole
DAVID	Database for the Annotation Visualization and Integrated Discovery
DMSO	dimethyl sulfoxide
DNA	deoxyribonucleic acid
dNTP	dexynucleotide triphosphate
dNu	deoxynucleotide
DTT	1,4-dithiothreitol
EDTA	ethylenediaminetetraacetic acid
EEF2	elongation factor 2
EGF	epidermal growth factor
EH	epoxide hydrolase
ENU	<i>N</i> -ethyl- <i>N</i> -nitrourea
ETF	electron transfer flavo protein
FAD	flavin adenine dinucleotide
FCS	fetal calf serum
GRAVY	grand average of hydropathy
G6PD	glucose-6-phosphate-1-dehydrogenase
GAPDH	glyceraldehyde-3-phosphate dehydrogenase
GC-MS	gas chromatography-mass spectrometry
Glu	glutamic acid
GSH	glutathione
HBSS	Hanks balanced salt solution
HEPES	4-(2-hydroxyethyl)-1-piperazineethanesulfonic acid
HNRNP	heterogeneous nuclear ribonucleoprotein
HSP	heat shock protein

IAA	iodoacetamide
IARC	International Agency for Research on Cancer
IEF	isoelectric focusing
IPG	immobilized pH gradient
kDa	kilodalton
KRT	keratin
LSM	laser scanning microscopy
LDH	lactate dehydrogenase
LMNB2	lamin B2
LIP	labile iron pool
MALDI	matrix-assisted laser desorption/ionization
MFO	mixed-functional oxidase
MEM	minimal essential medium
MSDB	Mass Spectrometry protein sequence DataBase
MHC	major histocompatibility complex
MS	mass spectrometry
MMP	mitochondrial membrane potential
MOWSE	molecular weight search
MW	molecular weight
n.a.	not applicable
NAD	nicotinamide adenine dinucleotide
NADP	nicotinamide adenine dinucleotide phosphate
NCBI	National Center for Biotechnology Information
NEDA	naphthylamine dihydrochloride
NO	nitric oxide
NOS	nitric oxide synthase
OTM	olive tail moment
PAGE	polyacrylamide gel electrophoresis
PANTHER	Protein Analysis Through Evolutionary Relationships database
PAH	polycyclic aromatic hydrocarbon
PBS	phosphate-buffered saline

PG	Phen Green [®]
PHE	phenanthroline
Pen/Strep	penicillin/streptomycin
<i>pI</i>	isoelectric point
PKC	protein kinase C
PMF	peptide mass fingerprinting
PRDX	peroxiredoxin
PTM	posttranslational modification
ppm	parts per million
PUBEC	pig urinary bladder epithelial cells
PVDF	polyvinylidene fluoride
ROI	region of interest
rcf	relative centrifugal force
ROS	reactive oxygen species
rpm	rounds per minute
RT	room temperature
SAA	sulfanilamide
SDS	sodium dodecyl sulfate
SEM	standard error of the mean
SQ	semiquinone anion radical
SOD	superoxide dismutase
SDS	sodium dodecyl sulfate
STRING	Search Tool for the Retrieval of Interacting Genes/Proteins
TFA	trifluoroacetic acid
TCA	trichloroacetic acid
TCDD	2,3,7,8-tetrachlorodibenzo- <i>p</i> -dioxin
TfR	transferrin
TdT	terminal deoxynucleotidyl transferase
TEMED	tetramethylethylenediamine
TMS	trimethylsilyl
TOF	time-of-flight

TPT	translationally-controlled tumor protein
TRIS	tris(hydroxymethyl)aminomethan
TUNEL	terminal deoxynucleotidyl transferase-mediated biotinylated UTP nick end labeling
2D-BN	two-dimensional blue native
UDP	uridine diphosphate
UTP	uridine triphosphate
UV	ultra violet
Uniprot	universal protein
VDAC2	voltage-dependent anion-selective channel protein 2
v/v	volume/volume
Vh	volt hours
w/v	weight/volume
XPC	Xeroderma pigmentosum, complementation group C

List of peer-reviewed publication list

The following articles have been produced on the course of this PhD thesis at the Institute of Hygiene and Occupational Medicine, University Hospital Essen, and are partially attached to this thesis:

Published papers

Verma N., Pink M., Petrat F., Rettenmeier A.W. & Schmitz-Spanke S. (2012) Exposure of primary porcine urothelial cells to benzo[a]pyrene: *In vitro* uptake, intracellular concentration and biological response. *Archives of Toxicology* 86(12): 1861-1871.

Verma N., Pink M., Rettenmeier A.W. & Schmitz-Spanke S. (2012) Review on proteomic analyses of benzo[a]pyrene toxicity. *Proteomics* 12(11): 1731-1755.

Verma N., Bäuerlein C., Pink M., Rettenmeier A.W. & Schmitz-Spanke S. (2011) Analysis of the proteome and phosphoproteome of primitively cultured pig urothelial cells. *Electrophoresis* 32(24): 3600-3611.

Verma N., Rettenmeier A.W. & Schmitz-Spanke S. (2011) Recent advances in the use of Sus scrofa (pig) as a model system for proteomic studies. *Proteomics* 11(4): 776-793.

Pink M., **Verma N.**, Polato F., Hideo B.A., Rettenmeier W.A., & Spanke-Schmitz S. (2011) Precipitation by lanthanum ions: an improved approach to isolate phosphoproteins. *Journal of Proteome Research* 10(2): 375-83.

Pink M., **Verma N.**, Rettenmeier A.W. & Schmitz-Spanke S. (2010) CBB staining protocol with higher sensitivity and mass spectrometric compatibility. *Electrophoresis* 31(4): 593-598.

Pink M, Stein C, **Verma N.**, Rettenmeier A.W. & Schmitz-Spanke S. (2012) Gel-based separation of phosphoproteins in samples stored in urea/thiourea after precipitation by lanthanum chloride. *Electrophoresis* (doi: 10.1002/elps.201200278).

Manuscripts submitted

Pink M., **Verma N.**, Rettenmeier A.W. & Schmitz-Spanke S. (2012) Integrated proteomic and metabolomic analysis to assess the effects of carbon black nanoparticles on energy metabolism in the human endothelial cell line EA.hy926 (submitted).

Published Abstracts

Verma N., Pink M., Rettenmeier A. W., Schmitz-Spanke S. (2012) Identification of protein complexes involved in calcium and iron homeostasis after TCDD exposure. *Naunyn-Schmiedeberg's Archives of Pharmacology* 385 (1), pp 99-99.

Verma N., Rettenmeier A.W. & Schmitz-Spanke S. (2010) Proteomic analysis of primary porcine bladder epithelial cells after B[a]P exposure. *Toxicology Letters* 196: S571-S571.

Verma N., Rettenmeier A.W. & Schmitz-Spanke S. (2009) Pig as a model organism for toxicoproteomic studies on bladder cancer. *Toxicology Letters* 189: S194-S194.

1. Introduction

1.1 Benzo[a]pyrene (B[a]P)

Benzo[a]pyrene (B[a]P) is a highly persistent environmental contaminant, known for its cytotoxic, mutagenic, and carcinogenic properties [1]. B[a]P first attracted wide attention in the 1933's when it was revealed as the compound responsible for the 19th century incidences of scrotal cancer among workers in the chimney sweep trade of London [2]. Since the discovery of its carcinogenic nature and because of its ability to accumulate in various organs it has become a model compound for many toxicological investigations.

Belonging to the large family of polycyclic aromatic hydrocarbons (PAHs) [3], B[a]P (**Figure 1**) is listed among the group of chemicals known as particulate polycyclic organic matter that are registered as federal hazardous air pollutants [4]. Based on epidemiological evidence, the International Agency for Research on Cancer (IARC) has classified B[a]P-containing mixtures such as soot, mineral oils, shale-oils, and coal tars as Group 1 carcinogens in humans [5].

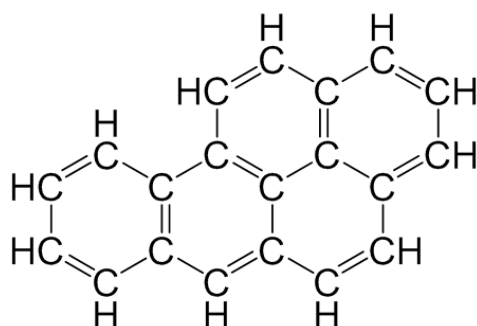


Figure 1: Chemical structure of benzo[a]pyrene.

B[a]P enters the environment from multiple sources including coal-processing waste products, petroleum sludge, asphalt, creosote, and tobacco smoke [6]. The long half-life of B[a]P in soil, water, air, and subsequently our food makes it a persistent contaminant that can be absorbed by the oral, inhalation and dermal routes of exposure [7-9]. Many studies have shown the accumulation of B[a]P in liver, lung, kidney, placenta, and bladder after its uptake from food or aerosols [10-18]. B[a]P that enters the bloodstream is believed to be transported by chylomicrons and lipoproteins [19].

Once inside the body, B[a]P requires activation to reactive primary and secondary metabolites both for mediating or protection against its toxic effects. In particular, its carcinogenic effect is induced by these metabolites that ultimately interact with critical cellular constituents such as DNA. These ultimate carcinogens are usually electrophilic intermediates that attack the nucleophilic sites of vital macromolecules in the cells, thus initiating the process of carcinogenesis. The metabolic activation of B[a]P to DNA-binding carcinogens is catalyzed by cytochrome P450 (CYP). Moreover, once inside the cytosol, B[a]P also initiates the induction of genes for CYP *via* a ligand-receptor mechanism [20]. The aryl hydrocarbon receptor (AhR) is a cytosolic receptor involved in the transcriptional regulation of drug metabolizing enzymes for which xenobiotics such as 2,3,7,8-tetrachlorodibenzo-*p*-dioxin (TCDD) and B[a]P act as ligands [21]. B[a]P binding to AhR induces the translocation of the AhR-B[a]P complex into the nucleus, where it interacts with the aryl hydrocarbon nuclear translocator (ARNT) forming the AhR-ARNT heterodimer. This heterodimer then binds with aryl hydrocarbon response elements (AhRE) in the regulatory regions of CYP and forms a positive feedback regulatory loop that sustains the metabolism of B[a]P [22-25] (**Figure 2**).

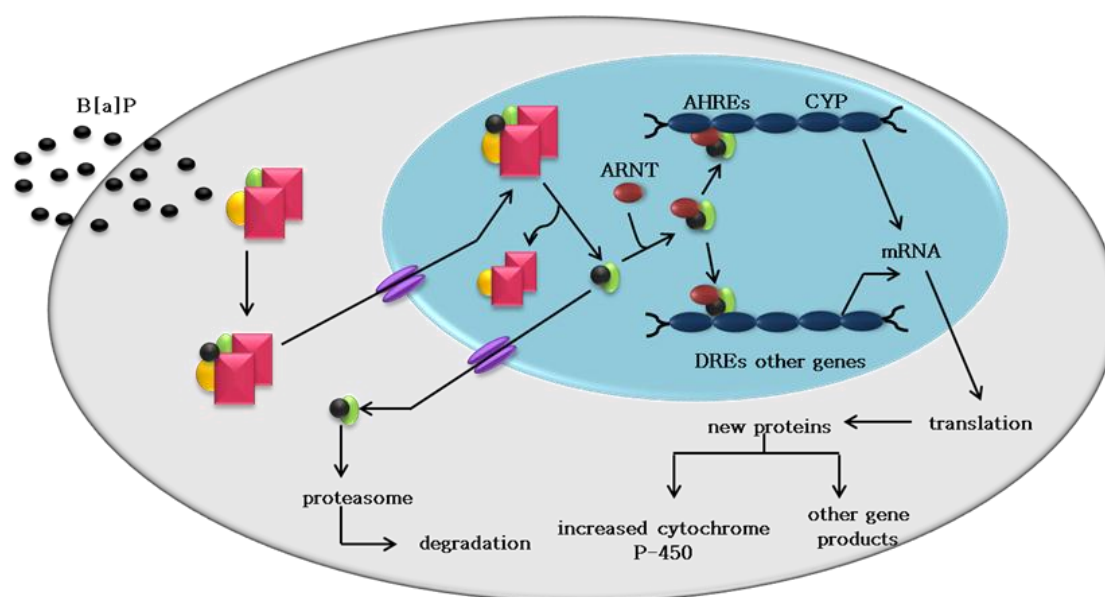


Figure 2: Pictorial representation of the aryl hydrocarbon receptor (AhR). AhR (●), a cytosolic receptor protein, is present in the cytoplasm as a heterodimer complex (■) in an inactive form. B[a]P a ligand to AhR, triggers the “transformation” of the receptor into a DNA-binding protein (■). The B[a]P-AhR complex translocates into the nucleus and dimerizes with its nuclear partner protein, ARNT (●). The ligand-AhR-ARNT complex binds specific DNA sequences known as aryl hydrocarbon responsive elements (AhREs) located in the 5’-flanking region of target genes. This provides a platform for recruiting multiple co-activator proteins that increase or decrease gene transcription. Figure adapted from **Denison et al.**, [26].

1.2 Metabolism of B[a]P

B[a]P is metabolized to approximately 20 primary and secondary oxidative metabolites and to a variety of conjugates by the activity of phase I and phase II enzymes (**Table 1**).

Table 1: Primary and secondary metabolites of B[a]P.

Metabolites	Types	Enzymes involved	References
Epoxides	1,2-epoxide 2,3-epoxide 4,5-epoxide 7,8-epoxide 9,10-epoxide	mixed-function oxidases	[27-29]
Phenols	1-OH 3-OH 6-OH 7-OH 9-OH	mixed-function oxidases / NIH shift	[30-34]
Quinones	1,6-quinone 3,6-quinone 6,12-quinone	mixed-function oxidases	[35, 36]
Dihydrodiols	(-)- <i>trans</i> -4,5-diol (-)- <i>trans</i> -7,8-diol (-)- <i>trans</i> -9,10-diol	epoxide hydratase	[37-41]
Glucuronides	1-O-glucuronides 3-O-glucuronides 6-O-glucuronides 7-O-glucuronides 9-O-glucuronides 4,5-diol-glucuronides 7,8-diol-glucuronides 9,10-diol-glucuronides	UDP-glucuronyl transferase	[42-44]
Sulfates	1-sulfate 3-sulfate 7-sulfate 9-sulfate 6-sulfate 4,5-sulfate 7,8-sulfate 9,10-sulfate	sulfotransferase	[45-48]
GSH conjugates	4,5-SG 7,8-SG 9,10-SG	glutathione-S-epoxide transferase	[48-50]
Diol epoxides	7,8-diol-9,10-epoxide I 7,8-diol-9,10-epoxide II	epoxide hydratase	[51-55]
Tetrols	tetrol 1 (7,10/8,9) tetrol 2 (7/8,9,10) tetrol 1 (7,9,10,8) tetrol 2 (7,9/8,10)	H ₂ O	[54, 56]
Triols	triol (7/8,9) triol (7,9,8)	non-enzymatic conversion + NADPH/NADH ⁺	[51, 54]

These enzymes are the initial biological receptors for B[a]P after its ingestion, absorption, and transport into the body [57] [58]. Among all organs, liver contains most enzymes required for the bioactivation of B[a]P [59, 60]. Phase I reactions involve enzymes such as cytochrome P450 mixed-function oxidases (MFOs), epoxide reductases, and epoxide hydrolases, while phase II enzymes include conjugating enzymes such as glutathione transferases, UDP-glucuronyl transferases, and sulfotransferases (Figure 3). The first step of metabolic activation to genotoxic metabolites is initiated by endoplasmic reticulum-based CYPs that introduce oxygen to the parent compound to form the most genotoxic metabolites, the 2,3-, 4,5-, 7,8-, and 9,10-epoxides [29]. These epoxides undergo hydration in the presence of epoxide hydrolase to the corresponding 4,5-, 7,8-, and 9,10-*trans*-dihydrodiols. B[a]P 7,8-*trans*-dihydrodiol that has been reported to be carcinogenic to animal cells [56, 61] can be converted by the activity of dihydrodiol dehydrogenase to a catechol that is subsequently autoxidized to B[a]P 7,8-quinone [62].

Other than dihydrodiols, epoxides undergo non-enzymatic rearrangement (NIH shift) to form phenolic intermediates such as 1-, 3-, 6-, 7-, and 9-OH-B[a]P [63, 64]. The 3- and 6-OH phenolic isomers can also be formed by direct hydroxylation [65] and are further involved in the formation of quinones. In the presence of peroxidases or CYP, 6-OH-B[a]P undergoes one-electron oxidation to the toxic radical cation 6-oxy-B[a]P that is further oxidized to 1,6-, 3,6-, or 6,12-quinones *via* hydroquinone and semiquinone radicals [66, 67]. On the other hand, 3-OH-B[a]P upon incubation with heat-inactivated microsomes can be metabolized to B[a]P 3,6-quinone [66-68]. Quinones are known to cause many cytotoxic effects through the generation of reactive oxygen species (ROS) [69, 70]. Furthermore, the phenols, quinones, and dihydrodiols form conjugates with glucuronic and sulfuric acid or are hydrolyzed to triols and tetrols [32, 65] to form water-soluble intermediates that can be excreted from the body as part of the detoxification process. On the other hand, B[a]P 7,8-dihydrodiol undergoes further oxidation to form 7,8-dihydrodiol-9,10-epoxide that is considered the most important carcinogenic metabolite of B[a]P due to its ability to form adducts with DNA [53, 71].

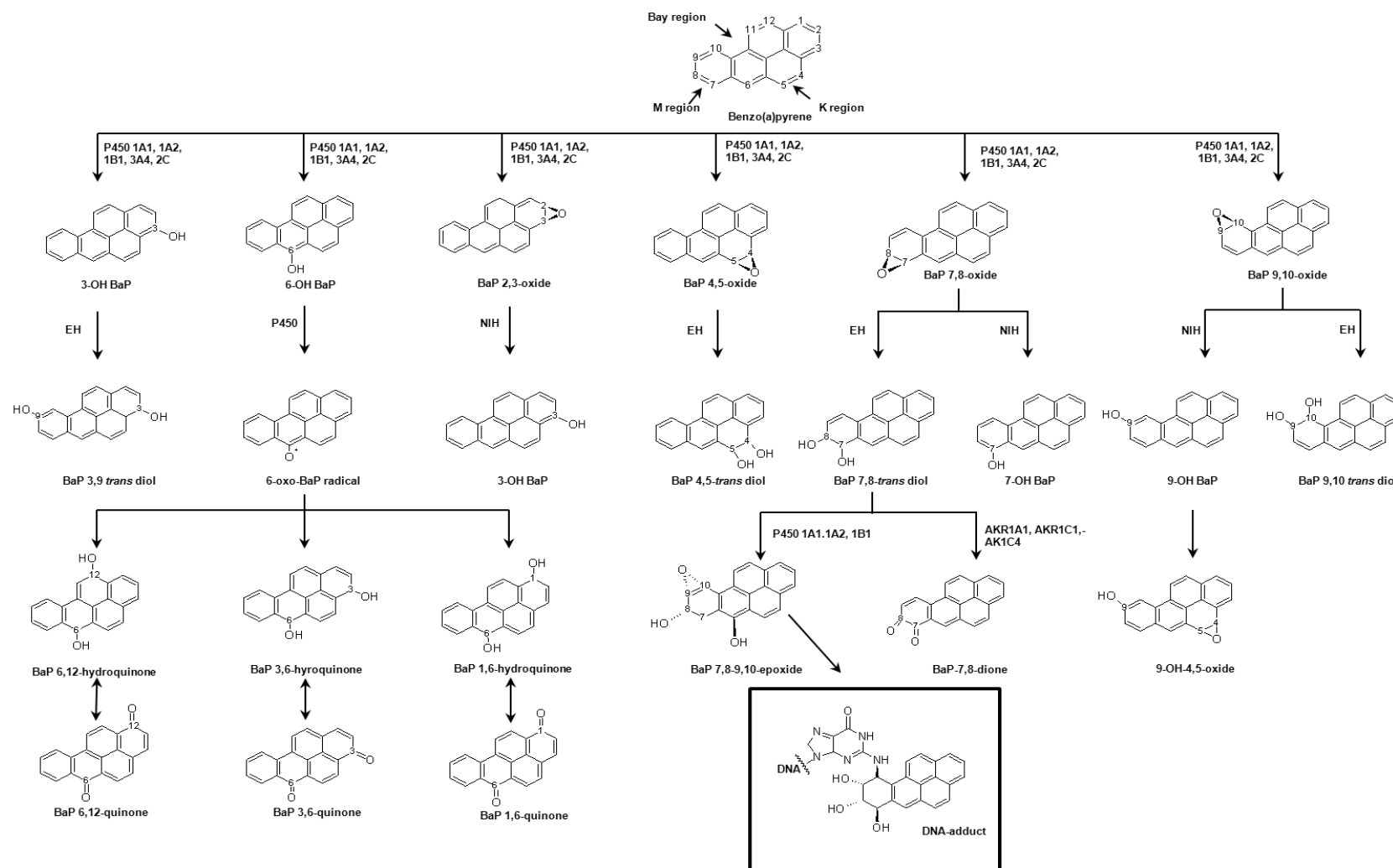


Figure 3: Representation of steps involved in the metabolism of B[a]P to reactive intermediates by the activity of phase I and phase II enzymes. P450: cytochrome P450; EH: epoxide hydrolase; AKR: aldo-keto reductases; NIH shift: hydroxylation-induced migration. Figure taken from *Verma et al., Proteomics 2012, 12, 1731–1755*.

1.3 Mechanisms of B[a]P-mediated toxicity

1.3.1 DNA and protein adducts

DNA damage is the important first step in the process of cancer development. B[a]P is a strong genotoxic compound, a property attributed to the ability of some of its metabolites to form DNA adducts. The formation of these adducts results from the presence of reactive sites known as bay region [72]. The bay region is an angular ring formed by fusion of a saturated benzene ring encompassing carbons 9-12 with the active center (α -carbon) at C-10 (**Figure 4**). These angular rings are prone to easy oxidation or radical ion formation but immune to conjugation and detoxification [73]. B[a]P 7,8-dihydrodiol-9,10-epoxide (BPDE), a compound arising from oxidation of B[a]P 7,8-dihydrodiol at the C-10 position, preferentially forms an adduct with DNA at the N2 position of guanine [53, 71]. These epoxides are capable of undergoing ring opening to form carbonium ions, electrophiles that are highly susceptible to nucleophilic attack by macromolecules such as DNA [63].

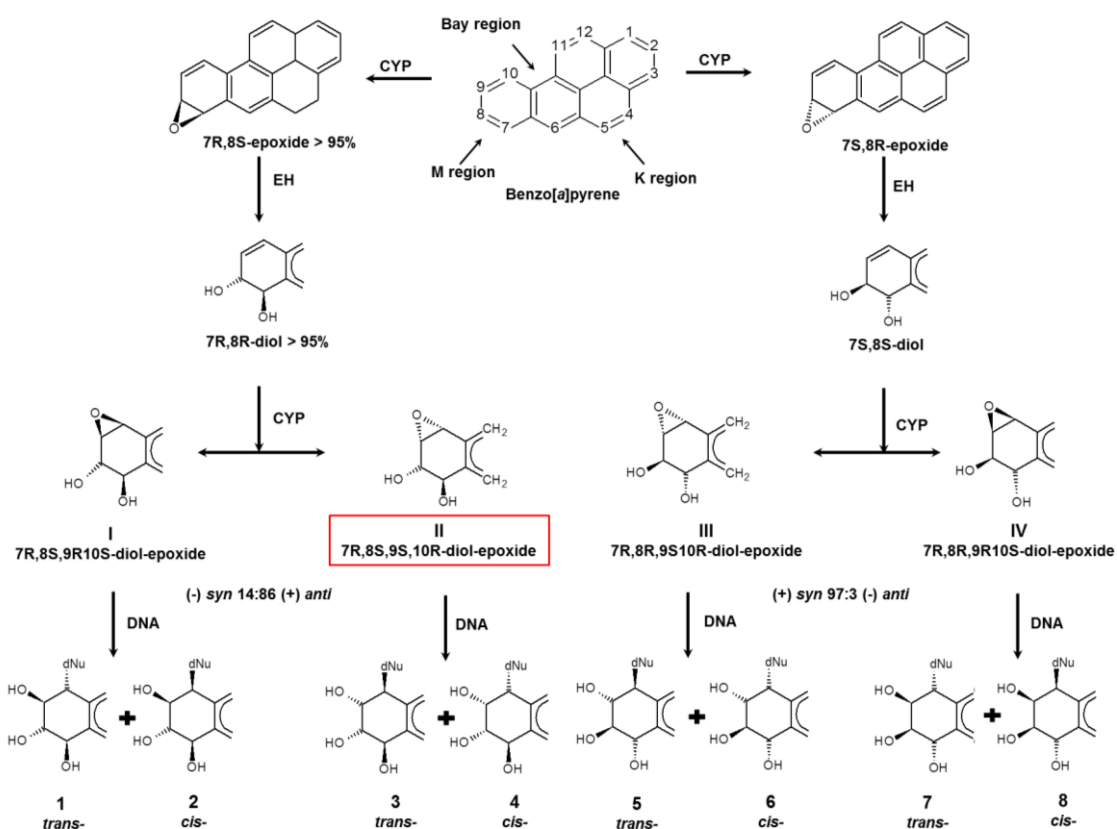


Figure 4: Metabolic pathways of B[a]P to different configurational isomers of B[a]P-7,8-diol-9,10-epoxide and formation of DNA adducts. dNu: deoxynucleotide, CYP: cytochrome P450; EH: epoxide hydrolase, DNA: deoxyribonucleic acid. Figure adapted from **Xue et al.**, [74].

The CYP enzymes and the microsomal epoxide hydrolase involved in B[a]P metabolism are highly stereoselective. BPDE itself is known to occur in four different isomers, however, (+)-*anti*-BPDE, derived from (-)-B[a]P 7,8-dihydrodiol has been found to possess greater biological activity than the other three isomers [75] (**Figure 4**). In addition, B[a]P metabolites are also nucleotide-specific. More than 90 % of racemic *anti*-BPDE target deoxyguanosine residues [76]. However, the K region (carbon 4-5 of B[a]P) metabolite B[a]P 4,5-oxide has also been reported to form adducts with DNA [63]. Other than the 7,8-dihydrodiol-9,10-epoxide and B[a]P 4,5-oxide, 9-OH-B[a]P-4,5-oxide, an intermediate of 9-OH-B[a]P, is also capable of binding to DNA [77].

These adducts when formed cause mutations by inducing changes in the nucleotide sequences due to misincorporation of a nucleotide opposite to the damaged base during DNA replication. The most common transversions associated with B[a]P exposure that cause cancer are G → T and C → A transversions [78, 79]. In fact, most of these transversions are responsible for mutations found in tumor suppressor genes in B[a]P-induced cancers [18]. A deficient repair of these adducts increases the rate of mutations and hence favors carcinogenesis. A number of different studies have revealed the formation of these adducts upon B[a]P exposure, but the effects are dose-, species-, tissue-, and strain-specific [80-82] [83]. Other than DNA adducts, hemoglobin and serum albumin are known to form stable adducts with *anti*-BPDE. These protein adducts have been suggested as biomarkers of cumulative human PAH exposure (**Table 2**) [84, 85] because of the long lifespan of these proteins (24 days for albumin and 120 days for hemoglobin).

Table 2: Albumin and hemoglobin adducts of B[a]P. Table taken from *Verma et al., Proteomics 2012, 12, 1731–1755*.

Adduct	Characteristics	Number of subjects	Technique used*	Protein adduct levels	References
Albumin-BPDE	non-smokers	74	ELISA	4.54 (2.12-7.12) fmol/μg	[86]
	non-smokers	29		3.54 (1.50-9.95) fmol/μg	
	non-smokers	17		n.a.	
Albumin-BPDE	at work	13	ELISA	5.22 ± 1.49 fmol/μg	[87]
	after one month vacation	12		4.18 ± 1.43 fmol/μg	
	control	10		4.07 ± 2.14 fmol/μg	
	at work	12		5.19 ± 4.02 fmol/μg	
	control	12		3.28 ± 2.07 fmol/μg	

Adduct	Characteristics	Number of subjects	Technique used*	Protein adduct levels	References
Albumin-BPDE	sample assessment in summers	36	ELISA	4.34 ± 0.335 fmol/μg	[88]
	sample assessment in winters	59		3.06 ± 0.187 fmol/μg	
	sample assessment in summers	45		4.55 ± 0.296 fmol/μg	
	sample assessment in winters	48		3.04 ± 0.184 fmol/μg	
		45		232 (108) fmol/mg	
Albumin-BPDE	non-smokers	26	ELISA	102 (102) fmol/mg	[89]
		21		318 (180) fmol/mg	
		19		119 (109) fmol/mg	
Albumin-BPDE	GSTM1+	10	ELISA	11.1 (9.0-29.5) fmol/mg	[90]
	GSTM1-	11		11.3 (6.0-18.4) fmol/mg	
	GSTM1+	11		12.0 (6.0-15.7) fmol/mg	
	GSTM1-	19		9.5 (6.0-18.9) fmol/mg	
Albumin-BPDE	mothers smokers	31	ELISA	0.35 ± 0.065 fmol/μg	[91]
	mothers non-smokers	56		0.17 ± 0.023 fmol/μg	
	household members smoking	32		0.18 ± 0.037 fmol/μg	
	no smoker in household	34		0.15 ± 0.022 fmol/μg	
	smokers	31		0.80 ± 0.15 fmol/μg	
	non-smokers	56		0.41 ± 0.057 fmol/μg	
	household members smoking	34		0.49 ± 0.079 fmol/μg	
	no smoker in household	32		0.31 ± 0.078 fmol/μg	
Albumin-BPDE	-	93	ELISA	0.356 ± 0.504 fmol/μg	[92]
		13		0.550 ± 0.369 fmol/μg	
Albumin-BPDE	non-smokers	44	ELISA	1.76 (0.51-3.07) fmol/mg	[93]
		45		1.35 ± 0.77 (0.11-3.45) fmol/mg	
Hb-BPDE	sample assessment in summers	50	GC/EC/NCI-HRMS	0.031 ± 0.22 fmol /mg	[94]
	sample assessment in winters	55		0.14 ± 0.38 fmol /mg	
Albumin-BPDE	high exposure	10	Sandwich ELISA	22.4–257 (336–3800) fmol/mg	[95]
	medium exposure	10		1.4–53.5 (21.0–801) fmol/mg	
	low exposure	10		0.5–15.3 (7.5–229) fmol/mg	
Albumin-BPDE	occupational exposure	207	HPLC	34.36 (10.69–64.48) fmol/mg	[96]
	control working in offices	102		21.90 (5.02–46.52) fmol/mg	
Albumin-BPDE	rural/suburban	44	ELISA	3.38 ± 1.35 fmol/mg	[97]
	city centers	56		2.81 ± 1.41 fmol/mg	
	-	101		4.01 ± 1.38 fmol/mg	

Adduct	Characteristics	Number of subjects	Technique used*	Protein adduct levels	References
Albumin-BPDE	all smokers	42	ELISA, HPLC	0.020 ± 0.005 fmol/mg	[98]
	non-smokers	23		0.019 ± 0.008 fmol/mg	
	passive smokers	19		0.021 ± 0.007 fmol/mg	
	smokers	27		0.042 ± 0.011 fmol/mg	
Hb-BPDE	all smokers	42		0.068 (0.014) fmol/mg	
	non-smokers	23		0.083 (0.024) fmol/mg	
	passive smokers	19		0.049 (0.007) fmol/mg	
	smokers	27		0.105 (0.020) fmol/mg	
Albumin-BPDE	high exposure	13	ELISA	30.7 (19-3) fmol/μg	[99]
	low exposure	35		24.5 (19-4) fmol/μg	
	nonexposed	45		11.2 (19 6) fmol/μg	
Albumin-BPDE	smokers	45	ELISA	0.55 (0.27-1.00) fmol/mg	[100]
	non-smokers	25		0.58 (0.17-1.15) fmol/mg	
	smokers	42		0.57 (0.16-1.45) fmol/mg	
	non-smokers	26		0.70 (0.19-1.55) fmol/mg	
Hb-BPDE	PAHs in air ≤4.0 μg/m ³	113	HPLC-FLD	24.3 (2.5) fmol/mg	[101]
	PAHs in air >4.0 μg/m ³	93		31.8 (2.3) fmol/mg	
	1-HOP in urine ≤2.0 μg/g creatinine	139		27.2 (2.4) fmol/mg	
	1-HOP in urine >2.0 μg/g creatinine	64		27.7 (2.5) fmol/mg	
Albumin-BPDE	smokers	23	GC-NCI-MS	0.026 ± 0.047 fmol/mg	[102]
	passive smokers	24		0.015 ± 0.040 fmol/mg	
	non-smokers	22		0.016 ± 0.029 fmol/mg	
Albumin-BPDE	smokers	27	GC-NCI-MS	0.042 (0.011) fmol/mg	[98]
	non-smokers	42		0.019 (0.008) fmol/mg	
	passive smokers	19		0.021 (0.007) fmol/mg	
Hb-BPDE	smokers	27		0.105 (0.020) fmol/mg	
	non-smokers	42		0.083 (0.024) fmol/mg	
	passive smokers	19		0.049 (0.007) fmol/mg	

* **Hb:** hemoglobin, **BPDE:** benzo[a]pyrene 7,8-dihydrodiol-9,10-epoxide, **GC/EC/NCI-HRMS:** gas chromatography/electron capture/negative chemical ionization high-resolution mass spectrometry, **GSTM1:** glutathione-S-transferase M1, **HPLC:** high-performance liquid chromatography, **ELISA:** enzyme-linked immunosorbent assay, **HPLC-FLD:** high-performance liquid chromatography with postcolumn fluorescence derivatization, **GC-NCI-MS:** gas chromatography negative chemical ionization mass spectrometry

1.3.2 Oxidative stress

It was believed for a long time that *anti*-diol epoxide-DNA adducts formed during B[a]P exposure are solely responsible for the mutagenic events in B[a]P-induced cancer, however, no mechanism could be provided for the formation of 8-hydroxy-dG and thymine glycol from diol epoxide. Soon it was realized that the cells were capable of converting B[a]P to redox-active *o*-quinones by the activity of dihydrodiol dehydrogenase and peroxidase [62, 103] (**Figure 5**). It was observed that these enzymes compete with CYPs for *trans*-dihydrodiol proximate carcinogens [104, 105]. In the presence of dihydrodiol dehydrogenase, diols undergo NADP^+ -dependent oxidation to form ketols that further undergo spontaneous rearrangement to catechols [62].

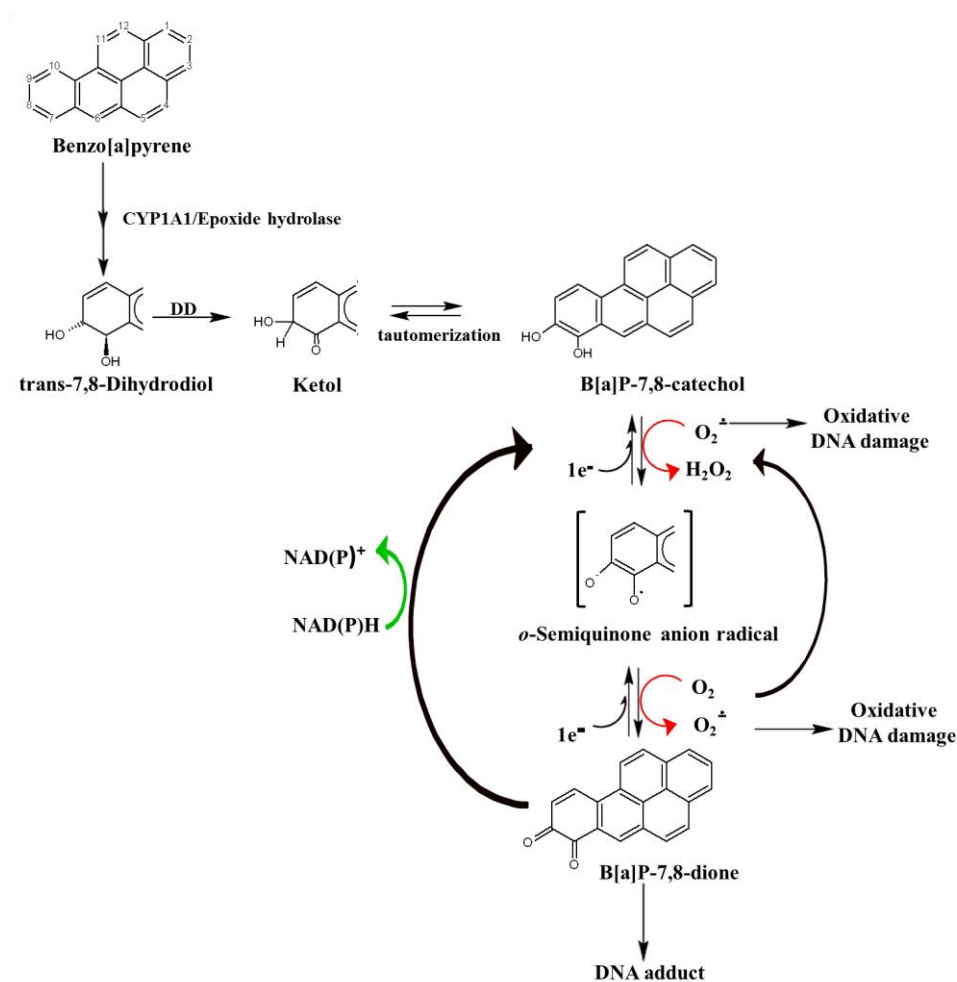


Figure 5: Generation of reactive oxygen species by B[a]P via *o*-quinone. Figure adapted from Xue et al., [74].

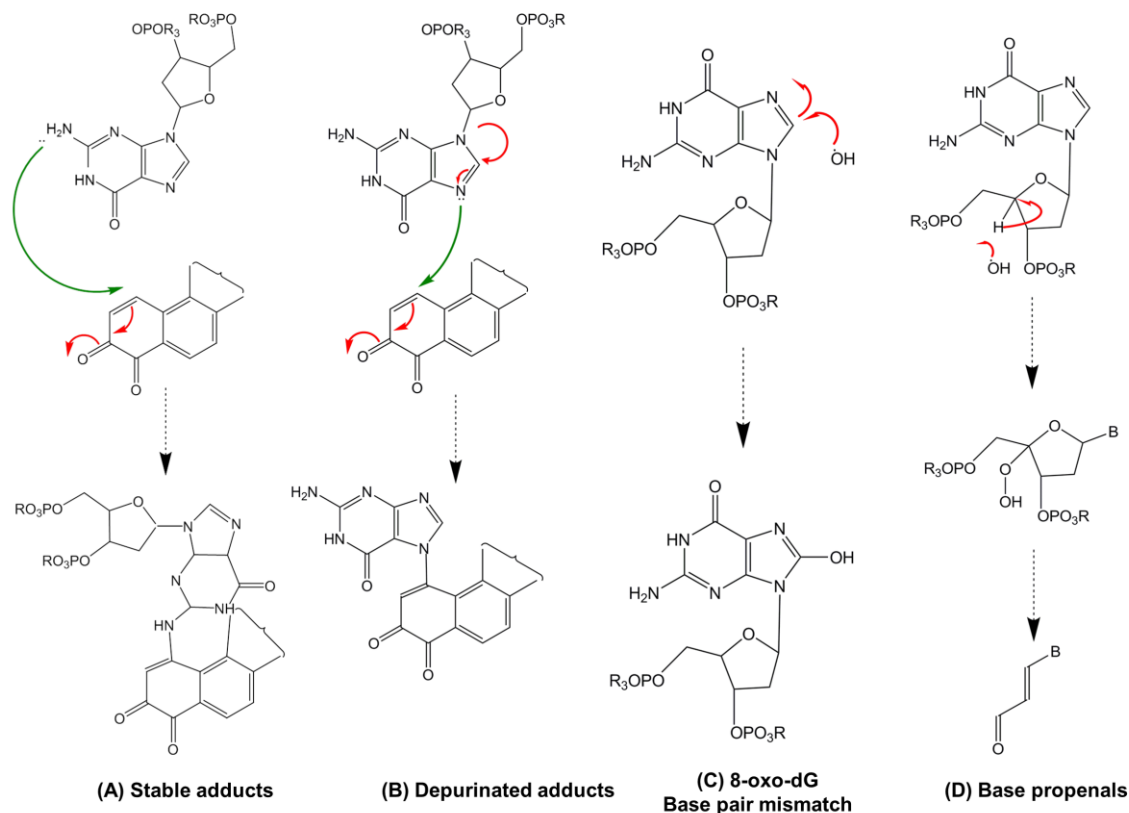


Figure 6: Generation of covalent and oxidative DNA adducts with *o*-quinones. (A, B) represent stable and depurinated adducts. (C, D) represent oxidative-DNA lesions. Figure adapted from Penning *et al.*, [106].

The catechols thus formed are itself unstable and undergo autoxidation in air. The first one-electron oxidation results in the formation of an *o*-semiquinone anion radical (SQ) and hydrogen peroxide. The second one-electron oxidation produces the fully oxidized *o*-quinone and superoxide anion ($O_2^{\bullet-}$) [36]. The resulting *o*-quinones are highly reactive and are capable of forming both stable and depurinated DNA adducts (**Figure 6**) [107, 108]. These adducts have the potential to give rise to the G \rightarrow T transversions as observed in ras and p53 gene mutations. Also, the *o*-quinone, by undergoing a two-electron non-enzymatic reduction, is capable of reforming the catechol or, by a one-electron enzymatic reduction, reforms the SQ. These events establish a futile redox cycle, which in turn leads to the amplification of ROS. The ROS thus generated are capable of forming 8-hydroxy-dG leading to G \rightarrow T transversions [109]. Moreover, ROS generation can promote lipid peroxidation and thus the generation of reactive mutagens [110]. Likewise, ROS generation can promote the production of mitogens and the activation of protein kinase C to enhance tumor promotion.

1.3.3 Disturbance of signal transduction pathways

Other than causing DNA damage, B[a]P is also known to interfere with signal transduction pathways, especially those involving calcium. Calcium, a universal second messenger, is involved in the regulation of a wide variety of cellular events, such as muscle contraction, gene expression, neurotransmission, fertilization, motility, hormone secretion, energy metabolism, cell growth, and cell death [111]. B[a]P has been shown to elicit an early and transient increase in intracellular calcium concentration (Ca^{2+})_i [112]. It has been proposed that the rise in (Ca^{2+})_i concentration is necessary for the AhR-mediated up-regulation of genes such as CYP or proinflammatory chemokines [113]. Other than that, it also affects cell proliferation and regulation by its profound effects on protein kinase C (PKC) [114]. PKC consists of a group of enzymes involved in controlling the functional activities of other proteins through phosphorylation of the hydroxyl groups of serine and threonine residues on these proteins [115]. B[a]P has been reported to inhibit these enzymes in a time- and concentration-dependent manner [116]. B[a]P is also known to interfere with epidermal growth factor (EGF) signaling cascades [117]. EGF is a membrane-bound tyrosine kinase receptor that primarily activates the Ras-MAPK signaling pathway following receptor autophosphorylation [118]. B[a]P is known to decrease EGF binding and hence affects proliferation and growth in placental cells and mouse fibroblasts [119, 120].

1.4 Objective

As one of the most frequently diagnosed urologic malignancies bladder cancer accounts for approximately ninety percent of cancers of the urinary collecting system (renal pelvis, ureters, bladder, and urethra). Depending upon its occurrence, bladder cancer is further divided into subcategories, such as transitional cell carcinomas, squamous cell carcinomas, adenocarcinomas, small cell carcinomas, and leiomyomas (Pauli et al. 1983). More than 90 % of all bladder cancers are transitional cell carcinomas arising from the cells lining the inside of the hollow organ (uroepithelium), roughly 10-20 % proliferate to the layers beyond the epithelium, thus impairing the prognosis [121]. Although many specific agents have been identified as causal factors of bladder cancer, epidemiological studies indicate that occupational and environmental chemicals are significant determinants in many of the cancer incidences. Cigarette smoking is one of the main known contributors to the development of urinary bladder cancer [122, 123]. Among the many components of cigarette smoke, B[a]P that occurs in amounts of twenty to forty nanogram per cigarette is among the best studied of these compounds, particularly because of its mutagenic and carcinogenic properties [124].

However, epidemiological analyses have not yet documented B[a]P or any other PAH as significant candidates for initiating bladder cancer development. Therefore, the risk that exposure to any of these compounds causes bladder cancer is still uncertain [121, 125, 126].

Thus, the overall objective of this thesis was to investigate the B[a]P-induced effects at the protein level in primary urinary bladder epithelial at non-toxic doses, in an effort to identify proteins and pathways involved in the cellular response to this potential bladder carcinogen.

For the studies primary urinary bladder epithelial cells (PUBEC) from pigs were chosen. These animals share many anatomical and physiological similarities with humans (**Table 3**) and have been one of the earliest animals used for research purposes.

Table 3: An overview on similarities between pigs and humans. Table taken from *Verma et al., Proteomics 2010, 11, 776–779*.

System	Comparative Anatomy*	Model system	References
Cardiovascular	coronary artery distribution		
	blood pressure higher in pigs: 145 - 160/105 mm Hg	cardioplegia ischemia	[127] [128]
	heart rate higher in pigs: 100 - 150 BPM	myocardial infarction	[129, 130]
	cardiac output	atherosclerosis	[131, 132]
	pulmonary pressure higher in pigs	cardiomyopathy	[61, 62]
Gastrointestinal	<i>torus pyloricus</i>	peptic ulcers	[133]
	branching of mesenteric vessels	intestinal transplant granulomatous enteritis (Crohn's disease)	[134] [135]
	spiral colon (ascending colon)	ileal bypass	[136]
Pulmonary	submucosal glands		
	striking similarities of glycoprotein composition of submucosal glands	chronic bronchitis	[137]
	lung size lung functional capacity	cystic fibrosis	[138]
Renal	cranial left kidney urine/plasma osmolal ratio creatinine reabsorption	embryonal nephroma (Wilms' tumor)	[139]
Immunologic	Peyer's patches		
	immunologically mature at 6 months	von Willebrand's disease porcine anaphylaxis	[140] [141]
	major histocompatibility complex (MHC)	rheumatoid arthritis	[142]
	clotting mechanism	malignant lymphoma	[143]

System	Comparative Anatomy*	Model system	References
Endocrine	–	segmental pancreatic transplants	[144]
		total pancreatectomy for type I diabetes	[145]
		type II diabetes	[146]
		GM2 gangliosidosis	[147]
		malignant hyperthermia	[148]
		obesity	[149]
Liver	blood supply metabolic function bile duct separate from pancreatic duct	liver transplantation	[150, 151]
			[152]
Reproductive	corkscrew fibromuscular penis accessory sex gland preputial diverticulum size of Fallopian tubes relaxin produced by ovaries	cryptorchidism	[153]
		training for laser and microsurgery	[41]
		maternal-fetal interaction	[154]
		sperms	[155]
		fetal surgery	[156]
		embryo development	[156, 157]

* Similar anatomy and physiology in pigs and humans unless otherwise specified.

However, factors such as size, cost, ethical, and societal implications often limit the use of this model organism. One cost-effective alternative for this limitation can be the use of organs from slaughtered pigs. Organs from slaughtered pigs represent an unlimited, reliable and inexpensive resource of viable cell material for all fields of applied research. The method for isolating primary bladder epithelia cells for our toxicoproteomic studies was adopted from Guhe *et al.* [158]. It was applied to achieve the following specific aims:

- To investigate the dynamics of B[a]P uptake and subcellular distribution in primary porcine urinary bladder epithelial cells (PUBEC) by using confocal laser scanning microscopy
- To quantify B[a]P and its metabolites in these cells by spectrofluorometry and gas chromatography-mass spectrometry (GC-MS)
- To establish proteome and phosphoproteome reference maps of PUBEC
- To investigate B[a]P toxicity at the protein level in PUBEC
- To analyze and compare protein complexes as downstream targets of AhR signaling in human bladder epithelial cells (RT4 cell line) exposed to B[a]P and TCDD

2. Material and Methods

2.1 Cell Culture

2.1.1 Pig urinary bladder epithelial cells (PUBEC)

Primary cultures of porcine urinary bladder epithelial cells were used for the experiments to minimize the heterogeneity of the cellular responses observed when using cell lines. Porcine urinary bladders were obtained immediately after slaughter from a local slaughterhouse. For the isolation of the cells, the method described by Guhe and Föllmann [158] was used with few modifications. For aseptic transfer bladders from slaughtered pigs were transferred in icecold phosphate-buffered saline solution, supplemented with 100 pg/mL streptomycin and 100 U/mL penicillin. Cells were isolated by scraping the inner wall of individual bladders with sterile glass slides. After washing the cells three times with PBS, cells derived from different bladders were pooled and resuspended in serum-free culture medium F-12, supplemented with 146 mg/mL glutamine, 100 U/mL penicillin, 100 µg/mL streptomycin, 1.25 µL/amphotericin B, 5 µg/mL transferrin, 10 µg/mL insulin, 0.1 mM non-essential amino acids, 2.7 mg/mL glucose, 1 µg/mL hydrocortisone, and 20 ng/mL epidermal growth factor.

Before culturing the cells, cell number and vitality were determined by the trypan blue exclusion assay. Trypan blue, a vital dye, is negatively charged and thus does not react with the cells, unless the cells are damaged. Therefore, the viable cells exclude the dye, and the dead cells are stained blue. For the assay, 20 µL of cell suspension were mixed with 500 µL of trypan blue solution plus 480 µL of PBS. The solution was thoroughly mixed, and 20 µL of the mixture were used for cell counting by using a hemocytometer plate. Cell numbers within four squares (1 mm³) were recorded. The total number was divided by four and multiplied by 50 (because of the dilution with trypan blue), then multiplied by 10,000 to obtain the number of cells per milliliter. The cell viability was calculated by dividing the total number of viable cells by the total number of viable plus dead cells and multiplying the result by 100. In all cell experiments, starting cultures contained at least 95 % viable cells. The volume of cell suspension corresponding to the number of required cells was calculated and added together with warm F12 medium and cultured in collagen-coated culture flasks for 72 h in a humidified incubator in an atmosphere of 95 % air and 5 % CO₂ at 37 °C before further use.

2.1.2 Evaluation of cell morphology and purity of PUBEC

Cell morphology of isolated epithelial cells was evaluated by using microscopic images. For the experiment 20,000 cells/chamber were seeded onto eight-well chamber slides (BD Falcon, Heidelberg, Germany). After five days of culture, the cells in the chamber slides were taken to prepare microscopic images by using a Leica microscope attached to a charged-coupled device (CDD) camera and the Leica application suite version 3.5.0 software (Leica Microsystems CMS GmbH, Switzerland). Cell purity was evaluated by immunostaining of the cells with the epithelial marker MCA1907T (AbD Serotec, Kidlington, Oxford, UK). MCA1907T is a pan cytokeratin reagent consisting of a cocktail of clone AE1 and clone AE3 that provides the broadest spectrum of reactivity to the 19 known human epidermal keratins and is known to produce positive staining in virtually all epithelial cells. For the analysis, the cells were fixed with icecold ethanol for 15 min at room temperature (RT). The cells were then washed 3 times with PBS (5 min each) and blocked by using 2 % BSA for 30 min at RT in a humidified chamber. After blocking, the cells were again washed three times with PBS for 5 min each. The cells were then incubated with 50 μ L mouse anti-keratin (2 μ g/mL/chamber) for 45 min at RT under humidified conditions. After the first incubation with the antibody the cells were again washed with PBS and incubated with the second antibody (50 μ L/chamber of a 1:50 diluted solution of rabbit antimouse IgG conjugated with Texas red) for another 45 min in a humidified chamber at RT, followed by three times washing with PBS and incubation for 1 min with 4',6-diamidino-2-phenylindole (DAPI) in the dark. The cells were again washed with PBS and placed on a glass slide with mounting medium for observation under the fluorescence microscope (DAPI: absorption at 358 nm, emission at 461 nm; Texas red: absorption at 589 nm, emission at 615 nm).

2.1.3 RT4 cell line

Cells of the human bladder urinary epithelial cell line RT4 were cultured in McCoy's 5A medium, supplemented with 10 % fetal bovine serum, 0.74 % L-glutamine, 100 units/mL penicillin, and 100 mg/mL streptomycin in a humidified incubator in an atmosphere of 95 % air and 5 % CO₂ at 37 °C.

2.2 Cell exposure

Shortly before starting cell exposure, cells were checked under the light microscope for normal growth, cell shape, and absence of contaminations. The medium in the flasks were then discarded, and the cells were washed once with warm PBS (37 °C). For cell exposure B[a]P or 2,3,7,8-tetrachlorodibenzo-*p*-dioxin (TCDD: used for comparative studies, see chapter 6) were dissolved in dimethyl sulfoxide (DMSO) and added to the fresh medium. Then, the cells were allowed to grow in this medium for another 24 h in a humidified incubator in an atmosphere of 95 % air and 5 % CO₂ at 37 °C.

2.3 Uptake and metabolism

2.3.1 Determination of the time course of B[a]P uptake and subcellular distribution by confocal laser-scanning microscopy

For fluorescence measurements 1.5x10⁶ cells/well were seeded onto collagen-coated glass coverslips (6.15 cm²) in six-well plates. After three days of culture, cells were exposed to 0.5 µM B[a]P dissolved in DMSO (<0.1 % of final volume) for different time intervals (2, 6, 12, 18, and 24 h). The same percentage of DMSO was used to expose controls in all experiments. At the time of measurement, pig epithelial cells were covered with 0.02 M HEPES-buffered H12 medium. B[a]P uptake and distribution were monitored with a laser-scanning microscope (LSM 510, Zeiss, Oberkochen, Germany) equipped with an argon laser. The objective lens was a 63 × NA 1.25 plan-neofluar. The pinhole was set at 136 µm, producing confocal optical slices of about 1.0 µm in thickness. Blue fluorescence of B[a]P, excited at 365 nm by using the UV laser power supply at 80 mW, was collected through a 389-470 nm long-pass filter. Three different areas from each chamber at all time periods were scanned by using the above settings. Single-cell fluorescence was determined by setting the region of interest (ROI) manually to the individual cells and for subcellular fluorescence to specific cellular compartments. Image processing and evaluation were performed by using the software of the LSM 510 imaging system. The intensity of B[a]P within the selected ROIs was evaluated and plotted over time. Experiments were carried out in triplicates with four different PUBEC pools prepared as described above.

2.3.2 Quantification of B[a]P uptake by spectrofluorometry

30x10⁶ cells in 50 mL culture medium were seeded in collagen-coated 175 cm² culture flasks. The cells were exposed to B[a]P after 72 h of cell culture at concentrations of 0.5 µM and

10 μM for 24 h. Cells at confluence were washed four times with PBS, and after every step PBS used for washing was stored for further analysis. Before harvesting the cells, care was taken to remove all of the residual PBS. The cells were collected by scraping them into a 2 mL Eppendorf tube, and the total volume of the cells (200 μL) was adjusted to 2 mL with icecold medium designed to simulate the composition of the cytosol [159].

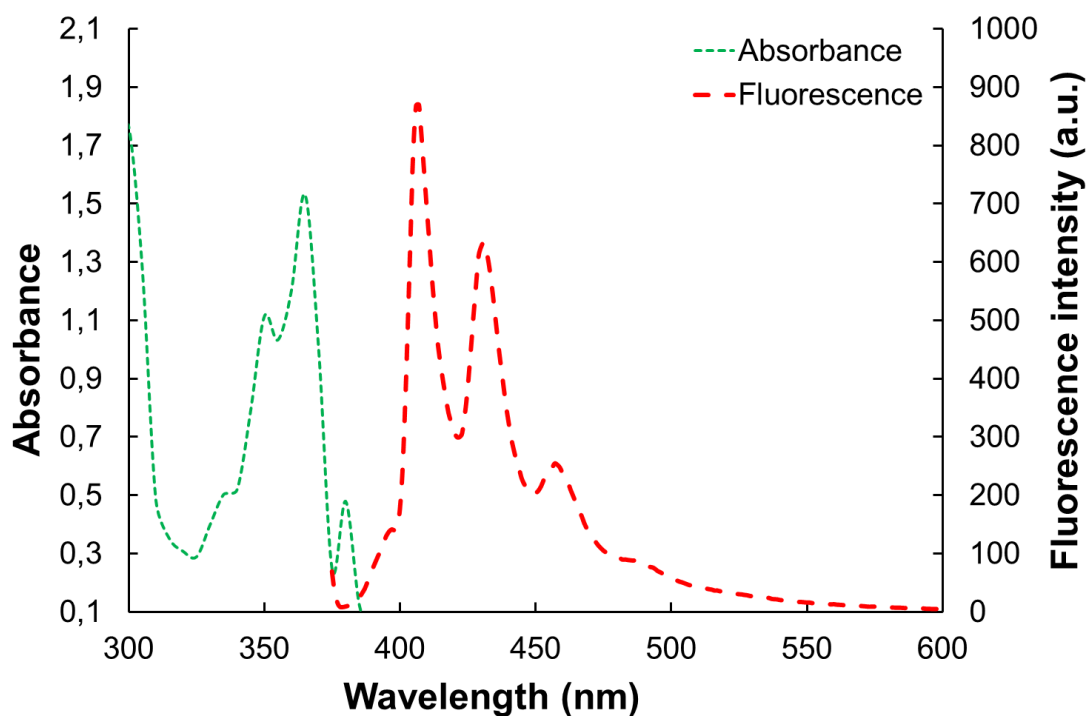


Figure 7: Spectral characteristics of B[a]P in cytosolic medium: absorbance (---) and emission spectrum (---) at 365 nm excitation for cell homogenate supernatant from B[a]P-loaded PUBEC (10 μM B[a]P, 24 h). Cytosolic medium served as blank. Figure taken from Verma *et al.*, *Archives of Toxicology* 2012, 32, 3600–3611.

The composition of “cytosolic medium” was: 40 % FCS, 100 mM KCl, 5 mM Na_2HPO_4 , 2 mM MgCl_2 , the full amino acid composition contained in Eagle’s minimum essential medium (MEM; from Sigma), 6.85 mM glucose, 1.5 mM lactate, 230 mM citrate, 138 mM pyruvate, 2.99 mM inorganic phosphate, 4 mM ATP, 4.5 mM glutathione (GSH) and 2 mM ascorbate (glutathione and ascorbate solutions freshly prepared), and 10 mM imidazole buffer, pH 7.2. Cells were then homogenized by using a mixer mill with steel grinding balls (MM200, Retsch, Haan, Germany) for 5 min at maximum frequency. After homogenization, the mixture was centrifuged (10 min at 30,000 g, 4 $^\circ\text{C}$), and the protein content of the supernatant was calculated by the Bradford assay. Fluorescence spectra of the homogenate supernatant (**Figure 7**) were recorded by using a spectrofluorometer (Varian Cary Eclipse, Varian, Palo Alto, CA).

B[a]P was quantified based on the UV excitation and fluorescence emissions at 365 and 405 nm, respectively, by using calibration curves (**Figure 8**) that were obtained under the same settings as for the sample measurements. The amount of B[a]P released from the cells, i.e., the intracellular B[a]P concentration, was calculated by considering a dilution factor of 10 (total cell volume of 200 μL plus 1,800 μL “cytosolic” medium). PBS used for washing the cultured cells was controlled for remaining B[a]P. A total of eight independent PUBEC pools were prepared for the experiment. Four PUBEC pools were exposed to 0.5 μM B[a]P and the other four to 10 μM B[a]P.

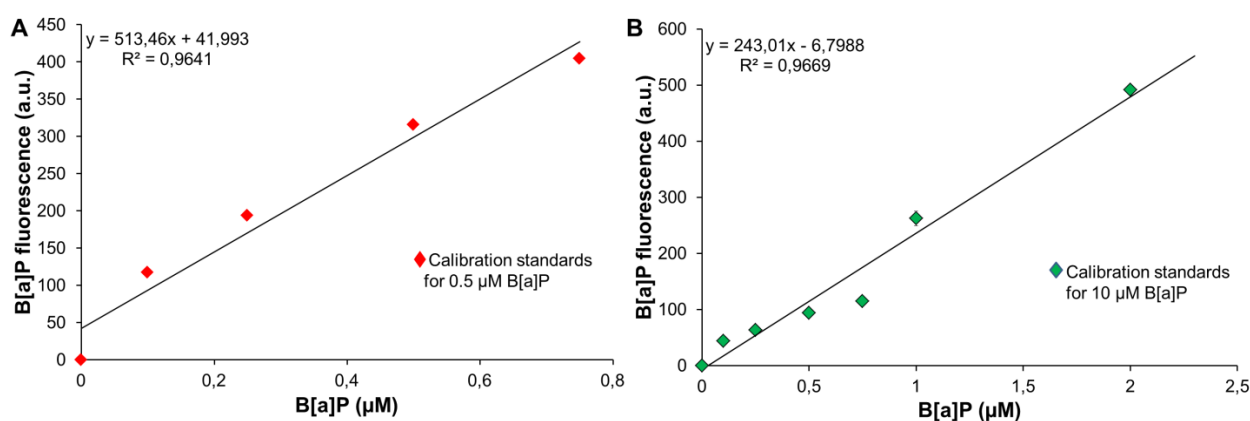


Figure 8: Calibration curves for the determination of intracellular B[a]P concentrations by spectrofluometry. [A] for cells exposed to 0.5 μM B[a]P; [B] For cells exposed to 10 μM B[a]P.

2.3.3 Quantification of B[a]P uptake by gas chromatography-mass spectrometry (GC-MS)

For GC-MS analysis a 30 m Optima 5 GC column (Macherey-Nagel, Düren, Germany) coupled to a quadrupole mass spectrometer (HP 6890/5973, Agilent Technologies, Waldbronn, Germany) was used. Following preparation of the samples as described above, aliquots of 100 μL each were spiked with 10 μL of a 100 ng/mL solution of B[a]P-d12 in toluene. To extract B[a]P, 100 μL of toluene were added, and the samples were shaken for one hour at room temperature. The organic layer was separated and used for analysis. The GC settings were as follows: injection of 1 μL of the analyte in the splitless mode: injector temperature 270 $^{\circ}\text{C}$: purge flow of 10 mL/min for 2 min: pressure 0.230 bar (23 kPa). The oven temperature was initially held at 80 $^{\circ}\text{C}$ for 10 min and then increased by 12 $^{\circ}\text{C}/\text{min}$ up to 250 $^{\circ}\text{C}$, where it was maintained for 8 min. After that, the oven was heated by 5 $^{\circ}\text{C}/\text{min}$ to 290 $^{\circ}\text{C}$ and kept at that temperature for another 10 min. The temperature of the quadrupole

was set at 150 °C and that of the ion source at 230 °C. A calibration curve (**Figure 9**) was prepared by spiking a set of B[a]P standard solutions (0.5, 1, 2.5, 5, 7.5, 10, 25 µg/mL), each with 10 µL of a 100 ng/mL solution of B[a]P-d12. The mass spectrometer was operated in the single ion monitoring mode recording the molecular ions at m/z 252 and 264 for the nondeuterated and deuterated B[a]P species, respectively.

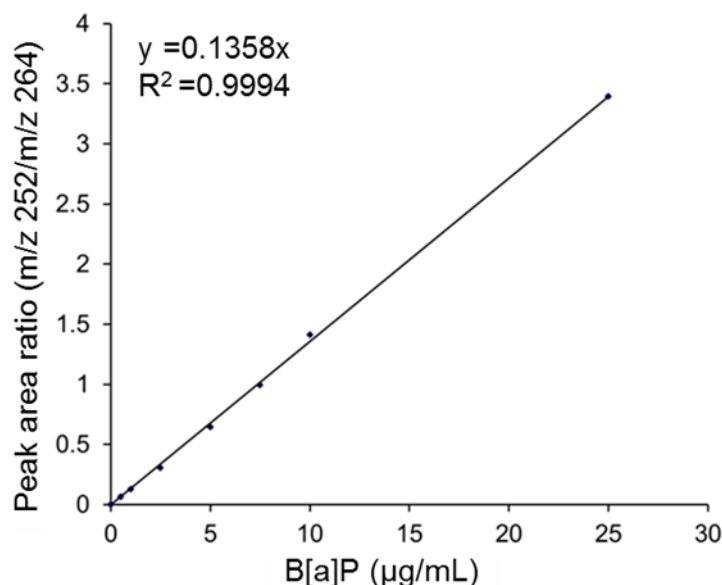


Figure 9: Calibration curve obtained from B[a]P standards (0.5, 1, 2.5, 5, 7.5, 10, 25 µg/mL) spiked with 10 µL of a 100 ng/mL solution of B[a]P-d12. The resulting ratios between the peak areas of the nondeuterated and deuterated B[a]P ($F = A_{\text{B[a]P}}/A_{\text{B[a]P-d12}}$) were used for the calculations.

2.3.4 Identification of 3-OH-B[a]P in PUBEC by GC-MS

3-OH-B[a]P, a major hydroxylated metabolite of B[a]P, was identified in PUBEC by using the analytical procedure described above for the quantification of the parent compound. A synthetic preparation of 3-OH-B[a]P (Campro Scientific GmbH) was used as reference compound. Following extraction, 90 µL of the derivatizing reagent *N,O*-bis(trimethylsilyl)-trifluoroacetamide (BSTFA) was added to 10 µL of the concentrated analyte. The solution was then heated at 80 °C for 30 min and, subsequently, the whole sample was injected into the GC-MS system for analysis. The mass spectrometer was operated in the single ion monitoring mode recording the molecular ion of the trimethylsilyl (TMS) derivative of 3-OH-B[a]P at m/z 340.

2.4 Proteomic analysis

2.4.1 2D gel electrophoresis

For 2D gel electrophoresis 30×10^6 cells were seeded in collagen-coated 175 cm² culture flasks in 50 mL culture medium. The cells were exposed to B[a]P after 72 h of cell culture at a concentration of 0.5 μ M. Cells at confluence were harvested and washed three times with ice-cold washing buffer containing 10 μ M Tris-HCl and 250 μ M sucrose (pH 7.0). The cell pellet was lysed by adding 1 mL of lysis buffer (8 M urea, 2 M thiourea, 2 % CHAPS, 1 % DTT, 0.8 % ampholyte, protease inhibitor cocktail). After ultracentrifugation at 30,000 rpm for 60 min at 4 °C, the supernatant was used for 2D gel electrophoresis. The protein concentration was determined by the Bradford assay. The separation of the proteins was carried out with a GE Health Care IPGphor IEF and an Ettan DALTsix electrophoresis system. 500 μ g of whole cell protein was mixed with 450 μ L of rehydration buffer (8 M urea, 10 % glycerol, 0.5 % CHAPS, 0.5 % ampholyte, and 0.002 % bromophenol blue). The rehydration step was performed with a precast 24 cm immobilized pH gradient (IPG) strip for 2 h, with subsequent active rehydration for 12 h at a voltage of 30 V. Isoelectric focusing (IEF) was run following a stepwise voltage increase procedure: After starting with 500 V and 1000 V for 1 h each, the voltage was linearly increased to 8000 V over a period of 8 h 20 min. After IEF, the IPG strips were subjected to a two-step equilibration in respective buffers (6 M urea, 30 % glycerol, 2 % SDS, 0.002 % bromophenol blue, and 50 mM Tris/HCl; pH 8) with 1 % DTT (w/v) for the first step, and 2.5 % iodoacetamide (w/v) for the second step. The separation in the second dimension was performed by using 1 mm thick 12.5 % polyacrylamide gels (35 x 45 cm). Electrophoresis was carried out overnight with running conditions of 2 W/gel for 14-16 h.

2.4.2 Precipitation of phosphoproteins

The whole cell lysates prepared for 2D gel electrophoresis were used for precipitation of pig phosphoproteins with a method developed in our laboratory [160]. The precipitation of phosphoproteins was carried out by the addition of 3 μ L LaCl₃ (1 M) to 1 mg/mL protein sample and 2 min of vortexing, followed by the addition of 3 μ L KH₂PO₄ (2 M). The mixture was vortexed and centrifuged at 2500 rcf at 4 °C for 1 min. The supernatant was decanted, and the pellet was resuspended in 300 μ L of a solution of 8 M urea and 1 % 3-[(3-cholamidopropyl)dimethylammonio]-1-propanesulfonate (CHAPS), followed by centrifugation for 30 s at 2500 rcf. The pellet was washed three times with 300 μ L mili-Q water to

remove urea and CHAPS. Finally, a mixture of 25 %/75 % 4 M imidazole/lysis buffer mixture was used to solubilize the pellet, and the supernatant containing the phosphoproteins was collected by centrifugation for 10 min at 18,000 rcf. The protein concentration was estimated, and 100 µg were used for 2DE gel separation analysis by applying to a 7 cm IPG strip in a stepwise procedure with increasing voltage: S1: step-n-hold 50 V, 50 Vhr; S2: gradient 150 V, 150 Vhr; S3: step-n-hold 300 V, 300 Vhr; S4: gradient 1000 V, 325 Vhr; S5: gradient 5000 V, 4500 Vhr; S6: step-n-hold 5000 V, 2500 Vhr. After IEF, the IPG strips were subjected to a two-step equilibration as described above. The separation in the second dimension was performed by using 1 mm thick 12 % polyacrylamide gels (10 cm x 10 cm) for 2 h.

2.4.3 Coomassie brilliant blue (CBB) staining of gels

Gels were stained according to the Coomassie staining protocol developed in our laboratory [161]. The staining solution was prepared by mixing 5 % aluminium sulfate 14–18 hydrate, 10 % ethanol, 0.02 % of CBB G-250, and 8 % phosphoric acid. The gels were stained for 3 h followed by destaining for 30 min in a solution containing 2 % phosphoric acid and 10 % ethanol. Gels were further allowed to destain in water overnight before being ready for further processing.

2.4.4 Image acquisition and analysis

The stained gels were scanned by using a ScanMaker 9800XL instrument (Microtek International, Inc., Willich, Germany). Spot detection, quantification (rel. % volume), and pattern matching were performed by using the Delta2D v4.0 software (Decodon, Greifswald, Germany). The background was removed from each gel, and image spots were matched, automatically detected, and then manually edited. The total density of each gel image was used to normalize the individual spot volumes to minimize variations between each gel. Each spot volume was normalized as relative percentage of the total volume of all spots present in a gel. To identify the protein spots with a consistent expression in the groups, only spots matching in at least 60 % of the gel images in a group were considered.

2.4.5 In-gel enzymatic digestion

Protein spots of interest were excised, and the gel pieces were washed and dehydrated by incubating them in 50 µL of pure acetonitrile (ACN, 100 %) for 5 min. Following the incubation the acetonitrile was removed, and the spots were digested with 30 µL of trypsin

solution (40 mM ammonium bicarbonate, 3 % ACN, 0.1 ng/mL trypsin) at 37 °C for three hours. The digestion was stopped by the addition of 20 µL of 1 % trifluoroacetic acid (TFA) and the digested peptides were purified by using C-18 Zip tips according to the manufacturer's protocol. The first step involved the activation of Zip tips with pure acetonitrile (two times), followed by two times washing with 0.1 % TFA solution. Finally, the samples were loaded onto the C18 column by pipetting the samples 7-10 times into these tips. The C18 tips with absorbed peptides were then washed twice with 0.1 % TFA solution, before the purified peptides were eluted with matrix solution (10 mg/mL α -cyano-4-hydroxycinnamic acid (CHCA) in 70 % ACN, 7 % water (Milli Q), and 0.3 % TFA) onto a MALDI target. The peptides were then allowed to dry for another 5-10 min before their analysis by MALDI-TOF-MS.

2.4.6 MALDI-TOF-MS analysis and protein identification

The protein analysis was performed on a Voyager-DETM STR MALDI-TOF mass spectrometer (Applied Biosystems, Foster City, CA, U.S.A.). Trypsin-digested samples were placed on a Mass-Spec-Turbo 192 CHCA Chip (Qiagen, Hilden, Germany). The mass spectrometer was operated in the positive-ion, delayed-extraction (200 ns delay time) reflector mode. The identification of the proteins was performed by peptide mass fingerprinting (PMF) using the Mass Spectrometry protein sequence DataBase (MSDB) and the National Center for Biotechnology Information (NCBI) protein databases with the special search engine Mascot (<http://www.matrixscience.com>). Raw data of the peptide masses were queried to the theoretical peptide mass of the entire database of MSDB and NCBI. The criteria for searching were set with assumptions that the peptides are monoisotopic, oxidized at methionine, and carboxyamidomethylated at cysteine residues. Only one missed trypsin cleavage and a peptide mass tolerance of 100 ppm was allowed for each peptide fragment. For the studies with pig epithelia cells the taxonomy was set to pigs, while for the studies with the RT4 cell line the taxonomy was set to humans. Probability-based molecular weight search (MOWSE) scores were estimated by comparison of the search result against an estimated random match population and was reported as $-10 \cdot \log_{10}(P)$, where P is the absolute probability. Scores greater than 65 were considered statistically significant ($p < 0.05$).

2.4.7 TdT-mediated dUTP-X nick end labeling (TUNEL) assay

Apoptosis, also known as programmed cell death, is a process involving a series of biochemical events leading to specific cell morphology characteristics and ultimately to the

death of cells. One of the peculiar characteristics of late stage apoptosis is the fragmentation of nuclear chromatin, which results in a multitude of 3'-hydroxyl termini of DNA ends. Terminal deoxynucleotidyl transferase-mediated biotinylated UTP nick end labeling (TUNEL) is a method that involves the identification of apoptotic cells by labeling the DNA breaks (3'-hydroxyl termini of DNA ends) with fluorescent-tagged deoxyuridine triphosphate nucleotides (F-dUTP). The enzyme terminal deoxynucleotidyl transferase (TdT) catalyzes a template-independent addition of deoxyribonucleoside triphosphates (dNTP) to the 3'-hydroxyl ends of double- or single-stranded DNA which generates DNA strands with exposed 3'-hydroxyl ends. The apoptotic cells can then be separated from non-apoptotic cells, as these cells do not incorporate much of the F-dUTP because of the absence of exposed 3'-hydroxyl DNA ends.

The assay was performed by using the *in situ* death detection kit TMR red (Roche Diagnostics GmbH, Germany) according to the manufacturer's instruction. Briefly, 20,000 cells/chamber were seeded onto eight-well chamber slides (BD Falcon, Heidelberg, Germany). After five days of culture, the cells were exposed to 0.5 μ M B[a]P for 24 h. The exposed epithelial cells were then fixed with 4 % paraformaldehyde in PBS (pH 7.4) for one hour at RT. The fixed cells were then washed three times with PBS for 5 min each. After fixation, the cells were permeabilized with freshly prepared 0.1 % Triton X-100 in 0.1 % sodium citrate. Cells were subsequently labeled with the TUNEL working solution. Apoptotic cells were identified as red fluorescent TUNEL-positive cells by fluorescence microscopy and are given in percentage of the total number of cells as determined by DAPI nuclear staining. The cells were treated with DNase as positive control. All experiments (n=6) were carried out in triplicates, and the level of statistical significance relative to control was calculated by using the one tailed t-test ($p < 0.05$).

2.4.8 Western blot

The differentially expressed proteins, screened with 2DE, were confirmed by immunoblotting. A total of 30 μ g of total protein was resolved in a 12 % polyacrylamide gel. These samples were then electrotransferred onto polyvinylidene fluoride (PVDF) membranes (Invitrogen GmbH, Germany). After blocking with 5 % nonfat dry milk, the membranes were immunoblotted with PMSD4, HSP27, HSP70, Hnrnpa1, VDAC2, and β -actin antibodies at dilutions recommended by the suppliers. Horse radish-conjugated secondary antibodies and a chemiluminescence kit (Invitrogen GmbH, Germany) were used for detection. Protein

expression was visualized by the Versa Doc Imaging System (Bio-Rad Hercules, CA, USA). The intensity of the bands normalized to the band of β -actin was measured by using the UNSCAN-IT automated digital system version 5.1 software (Orem, USA) and given in terms of calculated quantitative fold change with respect to control.

2.4.9 Comet assay

The comet assay, also known as single-cell gel electrophoresis, is a sensitive method for measuring DNA strand breaks in eukaryotic cells. The method involves the lysis of cells embedded in agarose on a slide with a detergent and a high amount of salt, which leads to the formation of nucleoids containing supercoiled loops of DNA, linked to the nuclear matrix. The supercoiled DNA is then electrophoresed at high pH, where looped DNA becomes free and moves towards the anode in structures resembling comets. These structures are then stained and observed by fluorescence microscopy. The intensity of the comet tail relative to the head reflects the number of DNA breaks.

The comet assay for the study was performed under alkaline conditions as previously reported [80]. Briefly, cells were exposed to different B[a]P concentrations (0.1 to 10 μ M) for 24 h. After exposure, the cells were washed twice and detached by trypsin/ethylenediamine tetraacetic acid (EDTA) treatment for 5 min. The cells were collected by centrifugation, and 20 mL of cell suspension (8000 cells) were mixed with 45 μ L of low-melting agarose and quickly pipetted into each of eight wells of a comet slide and allowed to set for 1 h at 4 °C in the dark. The slides were then immersed in prechilled lysis solution (10 mM Tris-HCl, 10 mM EDTA, 2.5 M NaCl, and 30 mM *N*-laurylsarcosine sodium salt, pH 10; 1 % Triton X and 10 % DMSO were added freshly) for overnight at 4 °C. Following the lysis, alkaline treatment in electrophoresis buffer (300 mM NaOH, 1 mM EDTA, and 10 mM Trizma; pH 13) was carried out for 30 min at 4 °C, and then electrophoresis was run for another 30 min at 4 °C (300 mA, 25 V). After neutralization (400 mM Tris-HCl, pH 7.5) for 60 min, the gels were dehydrated in absolute ethanol for 2 h and stored in the dark to dry completely. Just before image analysis, gels on each slide were stained with SYBR[®]-Green nucleic acid stain (Invitrogen, Darmstadt, Germany) in the dark for 20 min. A coverslip was placed over the moist gel, and the gels were examined by using the comet assay IV software (Perspective Instruments, UK) and a Leica microscope attached to a CDD camera. Values of the olive tail moment (OTM) were automatically calculated by the software. As a positive control, the cells were treated with 1 mg/mL *N*-ethyl-*N*-nitrosourea (ENU). All experiments were carried out in

triplicates, and the level of statistical significance relative to control was calculated by using the t-test ($p \leq 0.001$)

2.4.10 Detection of the mitochondrial membrane potential (MMP)

The mitochondrial potential of pig urinary epithelial cells was measured by use of the fluorescent dye Rhodamine123. Rhodamine123, a monovalent cationic dye, is used to monitor the mitochondrial function in living cells by its ability to distribute across the mitochondrial inner membrane according to the negative membrane potential [162]. The loss of potential due to early events during apoptosis results in a loss of the dye and, therefore, the fluorescence intensity.

For the determination of the mitochondrial potential, PUBEC at a concentration of 50,000 cells/well were plated in black 96-well plates with a clear bottom for 72 h, followed by exposure to 0.5 μM B[a]P for 2, 6, 12, and 24 h. Cells treated with normal cell culture medium were used as negative controls, while 100 μM of the ionophore valinomycin served as positive control. Following exposure, the cells were washed three times with warm PBS and exposed to 5 μM Rhodamine123 dye for 30 min at 37 °C. Measurements were obtained immediately at excitation and emission wavelengths of 488 and 535 nm by using the Tecan microplate reader (Tecan, Mainz, Germany).

2.5 Two-dimensional Blue Native/SDS-PAGE (2D BN/SDS-PAGE)

2.5.1 Sample preparation and subcellular fractionation of RT4 cells

For organellar enrichment ProteoExtract®, a commercially available subcellular fractionation kit (S-PEK), was applied. By using the kit control cells and cells exposed to B[a]P (0.5 μM) and TCDD (200 pM) were fractionated into four subcellular compartments: cytosol, membrane/organelle proteins, nuclear, and cytosolic fraction (**Figure 10**). Except for the cytosolic fraction, all other fractions were used for 2D BN/SDS-PAGE.

3.5×10^6 RT4 cells were seeded in 25 cm² culture flasks in 5 mL culture medium. Cells at confluence were harvested, mixed with 1 mL of cold extraction buffer 1 including protease inhibitors, and incubated at 4 °C for 10 min (all incubations were performed on an end-over-end shaker). Insoluble material was sedimented at 1000×g at 4 °C for 10 min, and the resulting supernatant, the cytosolic subproteome, was removed. Then, the whole procedure

was repeated. The pellet was mixed with 1 mL of cold extraction buffer 2 and incubated for 30 min at 4 °C. The insoluble material was sedimented at 6000×g at 4 °C for 10 min. The supernatant, the membrane/organelle subproteome, was removed, and the pellet was mixed with 500 µL of cold extraction buffer 3 including 1.5 µL benzoase to digest DNA. After 10 min of incubation, the insoluble material was sedimented at 7000×g at 4 °C for 10 min, and the supernatant, the nuclear fraction, was removed. The final fraction, the cytoskeletal subproteome, was obtained by resuspending the remaining pellet in 500 µL of extraction buffer 4. Fractions were aliquoted and stored at -80 °C until further use. The buffer composition for the subcellular fractionation, as provided in the kit, was sufficient. Therefore, no external detergent was added to these buffers. To enrich the subcellular fractions and to avoid the large carryover of proteins from one fraction to another, the enrichment step on each fraction was repeated up to three times. These enriched fractions were then used for 2D BN/SDS-PAGE.

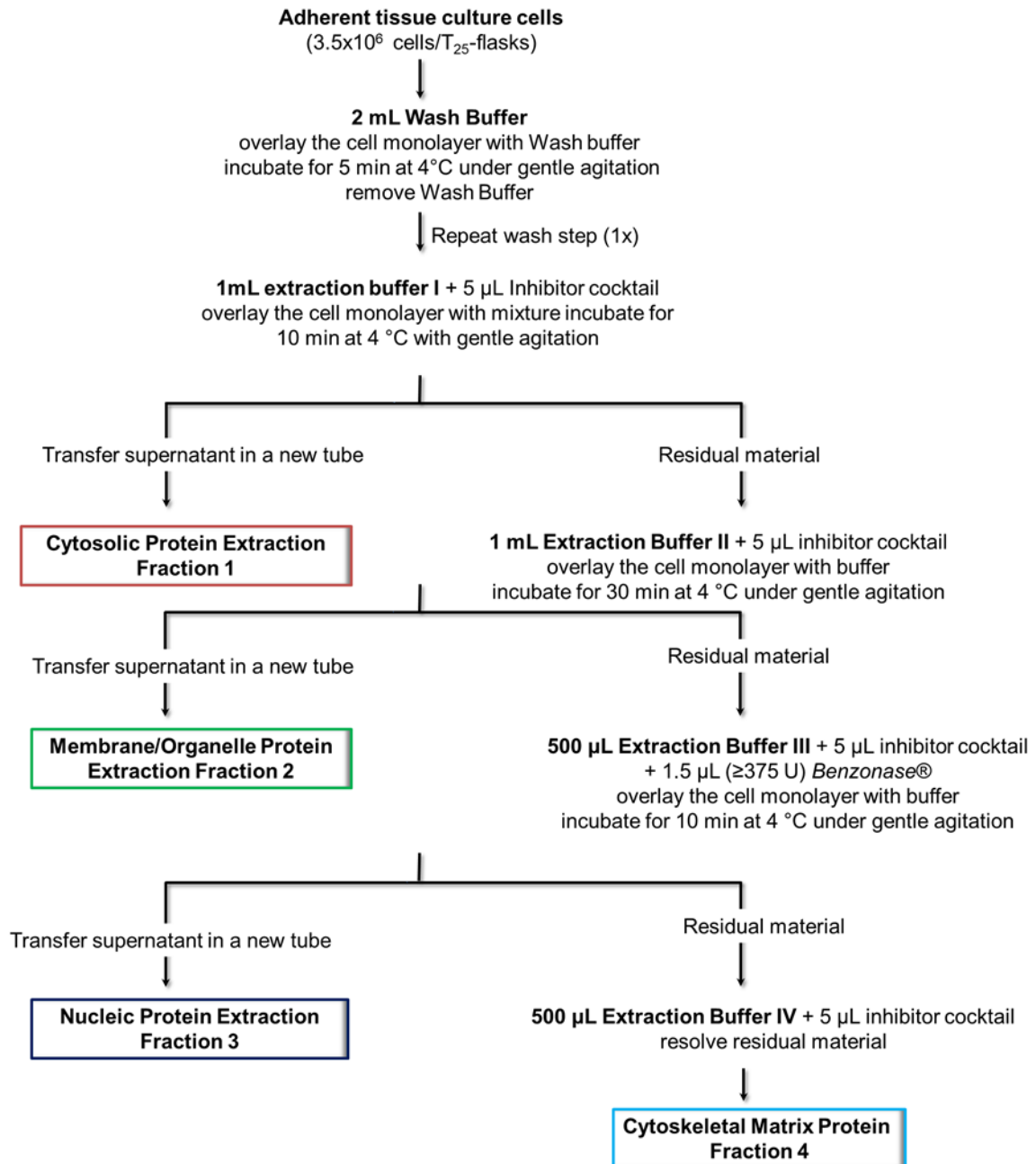


Figure 10: Pictorial representation of subcellular extraction by using S-PEK.

2.5.2 2D BN/SDS-PAGE

Blue Native/SDS-PAGE is a kind of native electrophoresis that helps in high-resolution separation of enzymatically active protein complexes from tissue homogenates or cell fractions. The separation principle relies on binding of CBB G250, which provides negative charges, to the surface of the protein. During migration to the anode, protein complexes are separated according to their molecular mass and/or size, and high resolution is obtained by the decreasing pore size of a polyacrylamide gradient gel. These complexes are then separated

into the subunits by usual SDS gel electrophoresis (**Figure 11**). Thus, this technique allows the separation of multiprotein complexes in their native forms.

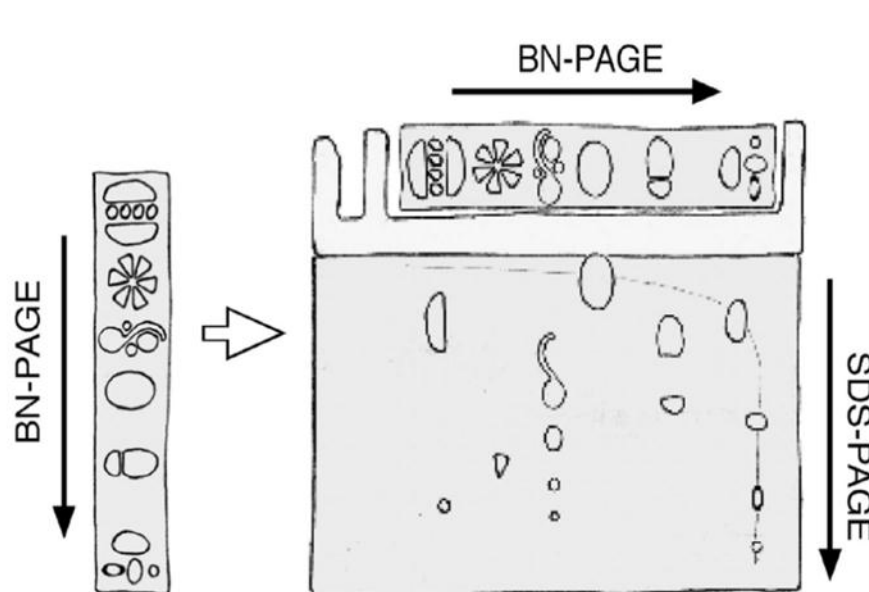


Figure 11: Principle of 2D BN/SDS-PAGE. Figure adapted from **Camacho *et al.*, [163]**.

50 mg of protein sample were mixed with 5 μ L of sample buffer (750 mM aminocaproic acid and 5 % (w/v) CBB G-250) and centrifuged at 14,000 rpm for 10 min at 4 $^{\circ}$ C. The supernatant was then separated on a 4–16 % Bis-Tris polyacrylamide native gradient gel by using the Invitrogen electrophoresis system. The outer chamber was filled with icecold anode buffer (50 mM Bis-Tris, pH 7.0) and the inner chamber with icecold blue cathode buffer (15 mM Bis-Tris, pH 7.0, 50 mM tricine, and 0.02 % CBB G-250). Electrophoresis was performed at 20 mA, 200 V and 10 W for approximately 4 h at 4 $^{\circ}$ C and stopped when the tracking line of the CBB G-250 dye had left the edge of the gel. The lanes from the first dimension were cut into individual strips, and before the separation in the second dimension, the strips were equilibrated in denaturation buffer (1 % SDS and 1 % iodoacetaamide (IAA)) for 30 min at RT and placed into a 12 % Bis-Tris polyacrylamide gel of the same thickness. The second-dimension run was performed at 150 V, 75 mA, and 5 W, until the blue front migrated out. At the end of the run, the gel was stained with Coomassie, and the spots were picked up for mass spectrometry by applying the protocol described above.

2.5.3 Determination of intracellular chelatable iron by Phen GreenTM SK

Phen GreenTM SK (PG SK), a metal-sensitive probe, was used for measuring the cellular labile iron content of the cells. The dye can be swiftly loaded into cells via its nonfluorescent acetomethoxy precursor PG SK-AM. Once inside the cell, the lipophilic blocking groups are cleaved by nonspecific esterases, resulting in a charged form that leaks out of cells far more slowly than its parent compound. The PG SK-loaded cells have a fluorescence component (ΔF) that is quenched by intracellular iron and can be revealed by the addition of a chelator, e.g., phenanthroline. The rise in fluorescence is equivalent to the change in PG SK concentration or to the amount of cellular iron originally bound to PG SK. Thus, the change in PG SK fluorescence intensity is directly proportional to the labile iron pool. (**Figure 12**)

For the determination of chelatable iron with PG SK, the protocol described by Petrat et al. was used [159]. 2×10^6 cells/well were seeded onto collagen-coated glass coverslips (6.15 cm^2) in six-well plates. After two days of culture, the cells were exposed to $0.5 \text{ }\mu\text{M}$ B[a]P or 200 pM TCDD dissolved in DMSO ($<0.1 \%$ of final volume) for 24 h. The same percentage of DMSO was used to expose controls in all experiments. The experiment was repeated four times in duplicates. The cells after exposure were washed twice with Hanks balanced salt solution (HBSS; 137 mM NaCl, 5.4 mM KCl, 1 mM CaCl₂, 0.5 mM MgCl₂, 0.4 mM KH₂PO₄, 0.4 mM MgSO₄, 0.3 mM Na₂HPO₄, and 25 mM Hepes, pH 7.4).

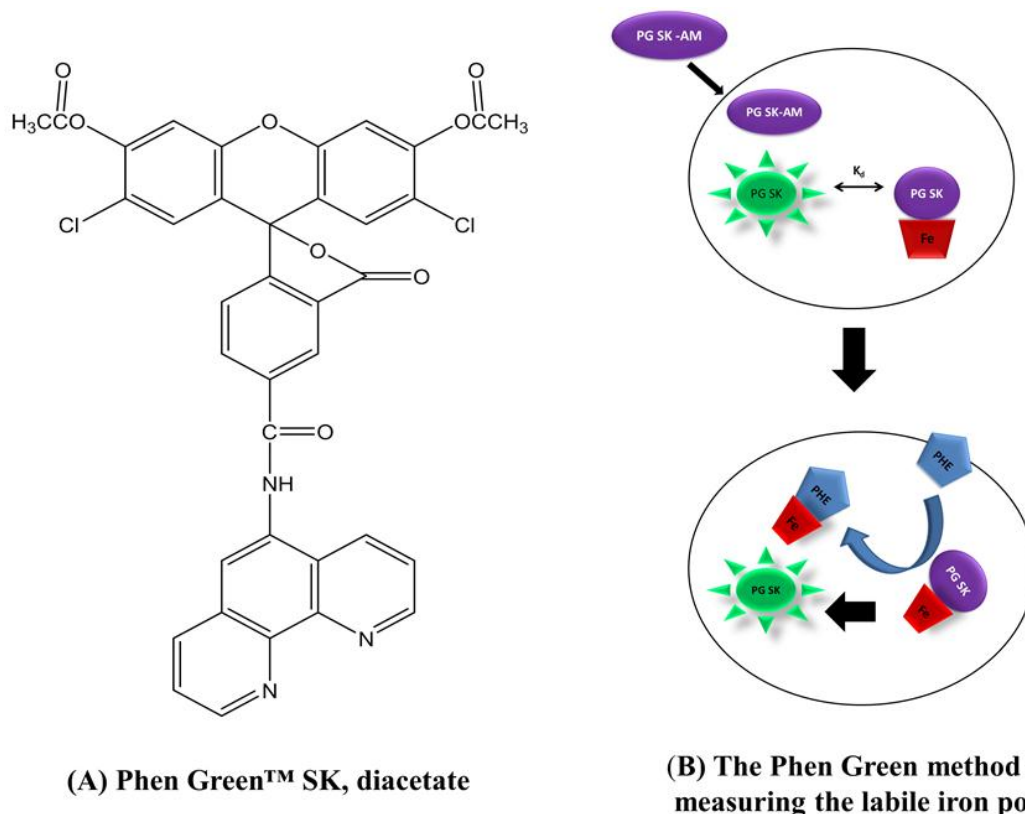


Figure 12: Measurement of the labile iron pool by using the Phen Green™ SK molecular probe. (A) PG SK-AM, the acetomethoxy derivate of Phen Green™ SK, is a nonfluorescent and membrane-permeable dye. (B) Upon entry into the cells, PG SK-AM is hydrolyzed to give the fluorescent PG SK that is quenched upon binding of iron (Fe). Phenanthroline (PHE), a strong iron chelator, evokes the fluorescence dequenching by competing with PG SK-bound iron. Thus, the rise in fluorescence is equivalent to the change in PG SK concentration or to the amount of cellular iron originally bound to PG SK. Figure adapted from **Kakhlon *et al.***, [164].

The cells were loaded with PG SK (20 μM) for 10 min at 37 °C in a CO₂ incubator. After the incubation the cells were washed three times with HBSS buffer and again incubated in 5 mL HBSS buffer at 37 °C in a CO₂ incubator for another 10 min. A laser scanning microscope (LSM 510; Zeiss, Oberkochen, Germany), equipped with an argon laser and a helium/neon laser, was used to perform the fluorescence measurements. The objective lens was a 63 \times NA 1.25 plan-neofluar. The green fluorescence of PG SK, excited at 488 nm by using the argon laser at a power rating of 6.75 mW, was collected through a 505 nm longpass filter. Confocal images (scanning time 30 s) were collected with the power of the argon laser set at 0.7 % after 3 min of PG SK loading. After establishing baseline fluorescence, cellular chelatable iron was removed from PG SK by adding the cell-permeant iron chelator 1,10-phenanthroline (2 mM) to the supernatant, and the images were collected first after 2 min of addition and then after every 10 min for the next 50 min. Full image scans of the cells were determined. Image processing and evaluation were performed by using the software of the

LSM 510 imaging system. Experiments were carried out in triplicates with RT4 cells prepared as described above.

2.5.4 Determination of NO with the Griess test

Nitric oxide (NO) is a key biosignaling molecule produced by a family of enzymes known as nitric oxide synthases (NOSs). The Griess method involves the determination of nitrite and nitrate (as a measure of nitric oxide) by formation of a red azo dye upon treatment of a NO_2^- containing sample with the Griess reagent (**Figure 13**). The reagent is an acidic solution of sulfanilamide and alpha-naphthylamine that undergoes a diazotization reaction with nitrites, forming a red azo dye.

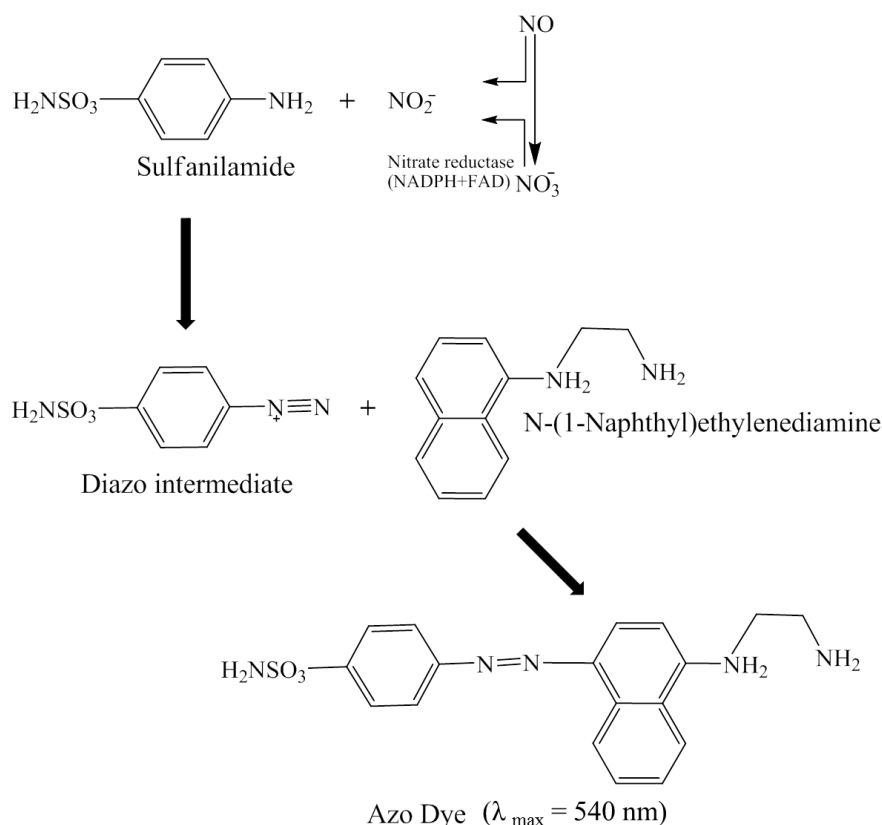


Figure 13: Mechanism of nitrite detection by using the Griess reagent. Figure taken from Sun *et al.*, [165].

The production of NO was determined by measuring the total nitrite/nitrate ($\text{NO}_2^-/\text{NO}_3^-$) concentration by means of the Griess reaction [165], using a commercially available photometric nitrate test (R-Biopharm, Darmstadt, Germany) with some modifications. 4.0×10^6 RT4 cells were seeded in 3 mL culture medium into a 6-well plate. Cells at confluence were exposed to 750 μL of medium containing B[a]P (0.5 and 5 μM) or TCDD

(200 pM and 1 nM) for 24 h. The medium used for exposure was filtered (Vivaspin 500, MW 30,000, Sartorius Stedim Biotech, Göttingen, Germany) by centrifugation (15,000×g, 60 min, 4 °C) subsequent to a wash step of the filters with distilled water to remove possible contaminating nitrate. 50 µL of the undiluted filtered sample was mixed with 50 µL phosphate buffer (50 mM, pH 7.4), and after adding 50 µL of a NADPH/FAD solution and 5 µL of nitrate reductase solution (both from the nitrate test kit of R-Biopharm) the mixture was incubated for 20 min at RT. Afterwards, 5 µL of sodium pyruvate solution (12 mg/mL distilled water) and 5 µL lactate dehydrogenase solution (Roche, Mannheim, Germany, diluted 1:10 with distilled water.) were added to this mixture and incubated for another 20 min at RT. Finally, 200 µL of Griess reagent (1 % sulfanilamide plus 0.1 % *N*-(1-naphthyl) ethylenediamine dihydrochloride, 1:1) was added to the mixture, and after 10 min of incubation the absorption was determined at 542 nm. Concentrations in micromoles were then assessed from calibration curves performed from standard solutions of NaNO₂ (10–1000 µM).

2.5.5 Determination of intracellular calcium concentration

Based upon the same principle as the Phen Green molecular probe, Fluo-4/AM and Rhod-2/AM are fluorescence indicators for calcium (**Figure 14**). Having an absorption spectrum that is compatible with an excitation at 488 nm by argon ion laser sources, Fluo4 exhibits a high calcium-binding affinity and selectivity and a very large increase (>100-fold) of fluorescence intensity in response to calcium binding ($K_d = 345$ nM). Rhod-2/AM, on the other hand, is a cationic dye with a strong affinity for mitochondria, and thus acts as a selective indicator for mitochondrial calcium. It has its fluorescence excitation and emission maxima at 552 nm and 581 nm, respectively, and upon calcium binding the fluorescence intensity has been reported to increase up to more than 100-fold ($K_d = 540$ nM).

To study $[Ca^{2+}]_i$ modulations by B[a]P and TCDD, two Ca^{2+} -sensitive dyes were used: Fluo-4/AM (1.4 µM) to observe changes of $[Ca^{2+}]_i$, and Rhod-2/AM (3,6 µM) to determine the changes of Ca^{2+} within the calcium stores. 2×10^6 cells/well were seeded onto collagen-coated glass coverslips (6.15 cm²) in six-well plates. After two days of culture, cells were exposed to 0.5 µM B[a]P or 200 pm TCDD dissolved in DMSO (<0.1 % of final volume) for 24 h. The same percentage of DMSO was used to expose controls in all experiments. The experiment was repeated four times in duplicates. The cells after exposure were washed twice with HBSS (137 mM NaCl, 5.4 mM KCl, 1 mM CaCl₂, 0.5 mM MgCl₂, 0.4 mM KH₂PO₄,

0.4 mM MgSO₄, 0.3 mM Na₂HPO₄ and 25 mM Hepes, pH 7.4). Afterwards, the cells were incubated with a HBSS solution containing Fluo-4/AM (1.4 μM) and Rhod-2/AM (3.6 μM) for 30 minutes at RT, followed by incubation for another 30 min at 37 °C. The dye solution was then removed and the cells were incubated for additional 30 min at 37 °C in 3 mL HBSS buffer supplemented with 2.5 mM probenecid (500 mM stock solution in 1 N NaOH).

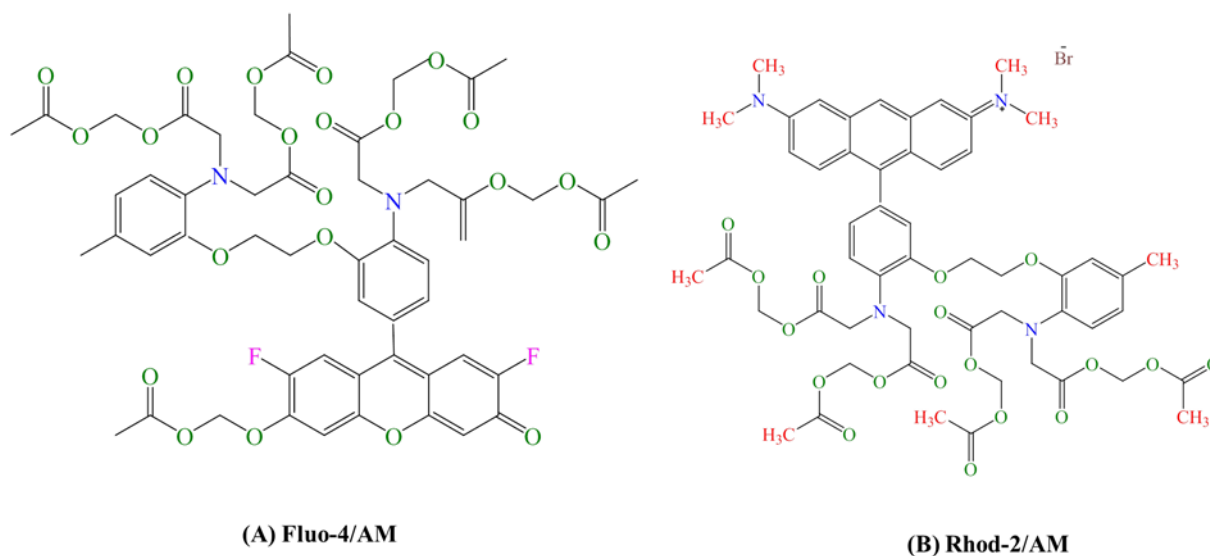


Figure 14: Chemical structures of intracellular calcium staining dye Fluo-4 and calcium store staining dye Rhod-2/AM.

For measurement, the coverslips were washed once with warm HBSS (37 °C) and placed in a coverslip holder. The cells were overlaid with 3 mL probenecid-supplemented HBSS buffer, and the fluorescence was measured on a confocal laser scanning microscope equipped with an argon laser and a helium/neon laser. The green fluorescence of Fluo-4/AM was excited at 488 nm by using the argon laser and was collected through a 505 nm longpass filter, whereas the red fluorescence of Rhod-2/AM, excited at 543 nm (by using the helium/neon laser), was collected through a 560 nm longpass filter. Three different areas from each chamber at all time periods were scanned by using the above settings. Full image scans of cells were determined. Image processing and evaluation were performed by using the software of the LSM 510 imaging system. All experiments were carried out in triplicates.

2.6 Bioinformatic analysis

The Protein Analysis Through Evolutionary Relationships database (PANTHER) was used to elucidate the molecular function, biological process, and signaling pathway associated with each individual protein (<http://panther.appliedbiosystems.com/>) [166]. The subcellular location annotation of the proteins was predicted by using the clustering program (<http://david.abcc.ncifcrf.gov/>) called Database for the Annotation Visualization and Integrated Discovery (DAVID) [167].

3. Exposure of PUBEC to B[a]P: *In vitro* uptake, intracellular concentration, and biological response[†]

3.1 Objective

A requirement for B[a]P to mediate its carcinogenic potential is the ability of the particular tissue to incorporate the chemical and to subsequently metabolize it to reactive intermediates. Although a basic phenomenon, the simple mechanism behind B[a]P uptake is still largely unknown. Moreover, the presence of B[a]P metabolites in urine has been used as gauge for PAH exposure in environmental toxicology for a long time, yet no information is available on the ability of bladder tissue for B[a]P uptake. Investigations in humans and in animal models suggest that the urothelium may be exposed to B[a]P both by its diffusion from the capillaries in the *lamina propria* and by its uptake from urine.

Therefore, the aim of the present study was to investigate the dynamics of B[a]P uptake and its subcellular distribution in bladder epithelial tissue. To analyze these processes in a cell type that closely reflects the native function within the living system, the experiments were performed with primary urinary epithelial cells from pigs (PUBEC). As an eutherian mammal, pigs share many similarities with humans. PUBEC have previously been used for many *in vitro* studies and are known to maintain all functions specific to bladder epithelial cells [80, 168-173].

3.1.1 Morphologies and purity of PUBEC

Isolated porcine urothelial cells maintain all morphological structures typical of the urothelium. Microscopic images were made after five days of cell culture to evaluate the morphology of isolated epithelial cells from pig bladders. The cultured cells formed a monolayer with many morphological polarities resembling the epithelium *in vivo* (**Figure 15A**). Moreover, immunostaining of isolated cells with MCA1907T, a pan cytokeratin reagent, also confirmed the epithelial characteristics of these cells (**Figure 15B**).

[†] Verma *et al.*, *Archives of Toxicology*, 2012, (doi 10.1007/s00204-012-0899-y)

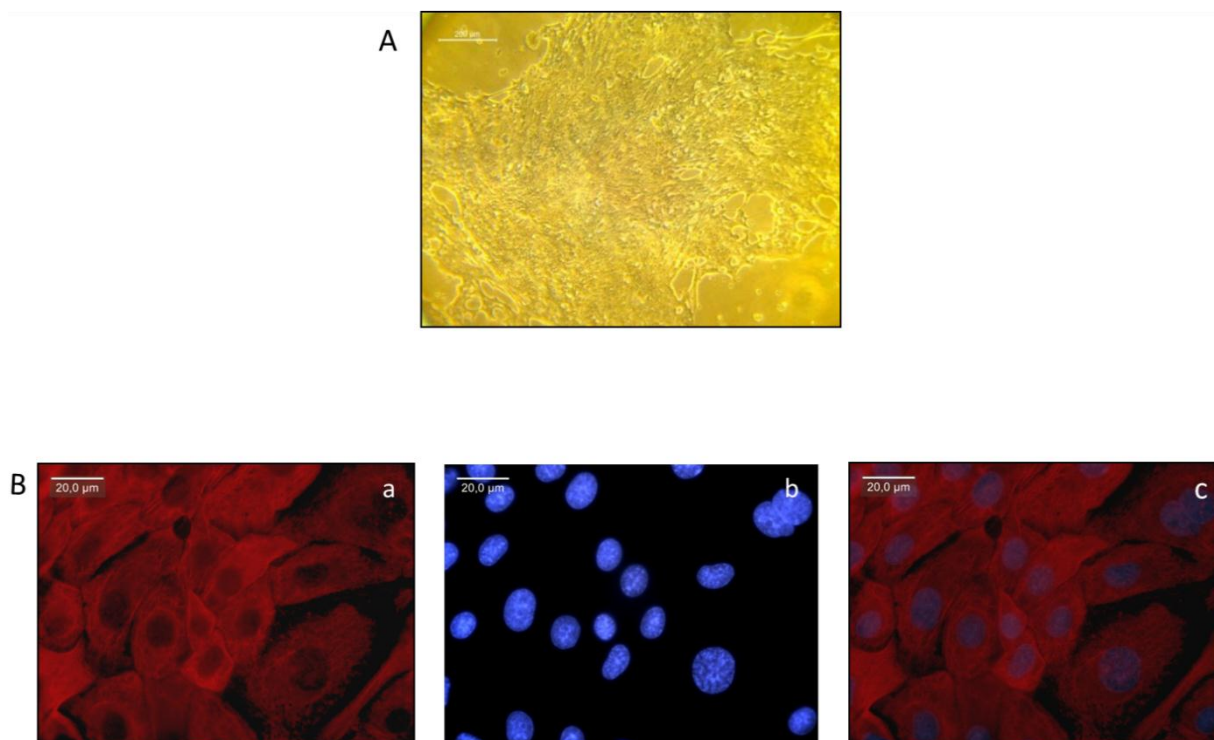


Figure 15: Establishment and characterization of porcine bladder epithelial cell culture: (A) Pig bladder epithelial cells were seeded onto collagen-coated plates and cultured for seven days. The cultured cells formed a monolayer and showed many morphological structures typical of urothelial cells. (B) Epithelial cell marker expression of cultured bladder epithelial cells for cell morphology and purity. (a) Positive staining shown in red; (b) DAPI was used to stain nucleus blue; (c) merged image of positively stained epithelial cells and DAPI-stained nucleus. Figure taken from *Verma et al., Electrophoresis 2011, 32, 3600–3611*.

3.1.2 Analysis of B[a]P uptake and its subcellular distribution

The time-dependent increase of the intracellular amount of B[a]P was monitored by using confocal laser scanning microscopy. (Figure 16) demonstrates the uptake of PUBEC expose to 0.5 μM B[a]P for different time intervals. As compared to nonexposed control cells, a time-dependent increase in the cellular fluorescence intensity of B[a]P-exposed cells was observed, however, no significant uptake was measured during the initial 2 h of exposure. Only after six hours of exposure an initial cellular uptake of B[a]P occurred, which increased linearly with time but with substantial variation among the different cell pools.

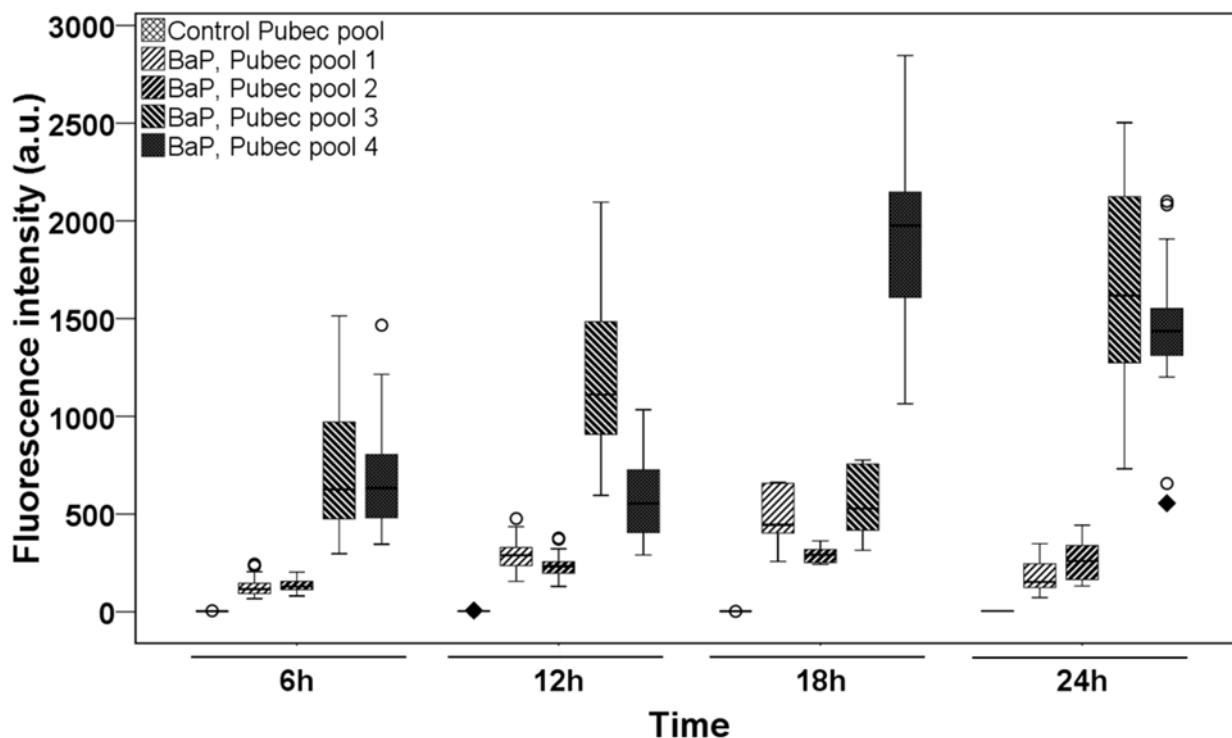


Figure 16: Box plots representing the time-dependent increase in B[a]P fluorescence of different PUBEC pools exposed to 0.5 μM B[a]P. The fluorescence was monitored by using laser-scanning microscopy ($\lambda_{\text{excitation}} = 365 \text{ nm}$; $\lambda_{\text{emission}} = 389\text{-}405 \text{ nm}$). The boxes encompass the 25th and 75th percentiles. Horizontal bars inside the box represent the median. Whiskers extend to the highest and lowest levels that are not outliers. (○) Outliers representing 1.5 box lengths from the 25th or 75th percentile. (◆) Outliers representing 3 box lengths from the 25th or 75th percentile. Figure taken from Verma *et al.*, *Archives of Toxicology* 2012.

Analysis of the subcellular distribution revealed a substantial B[a]P uptake by the plasma membrane as compared to other cellular compartments. A significant increase of cell membrane fluorescence intensity was recorded over the time period of 24 h (**Figure 17A, B**). In addition, a slight but significant increase in fluorescence intensity was observed in the cytosol and nucleus (**Figure 17C, E**).

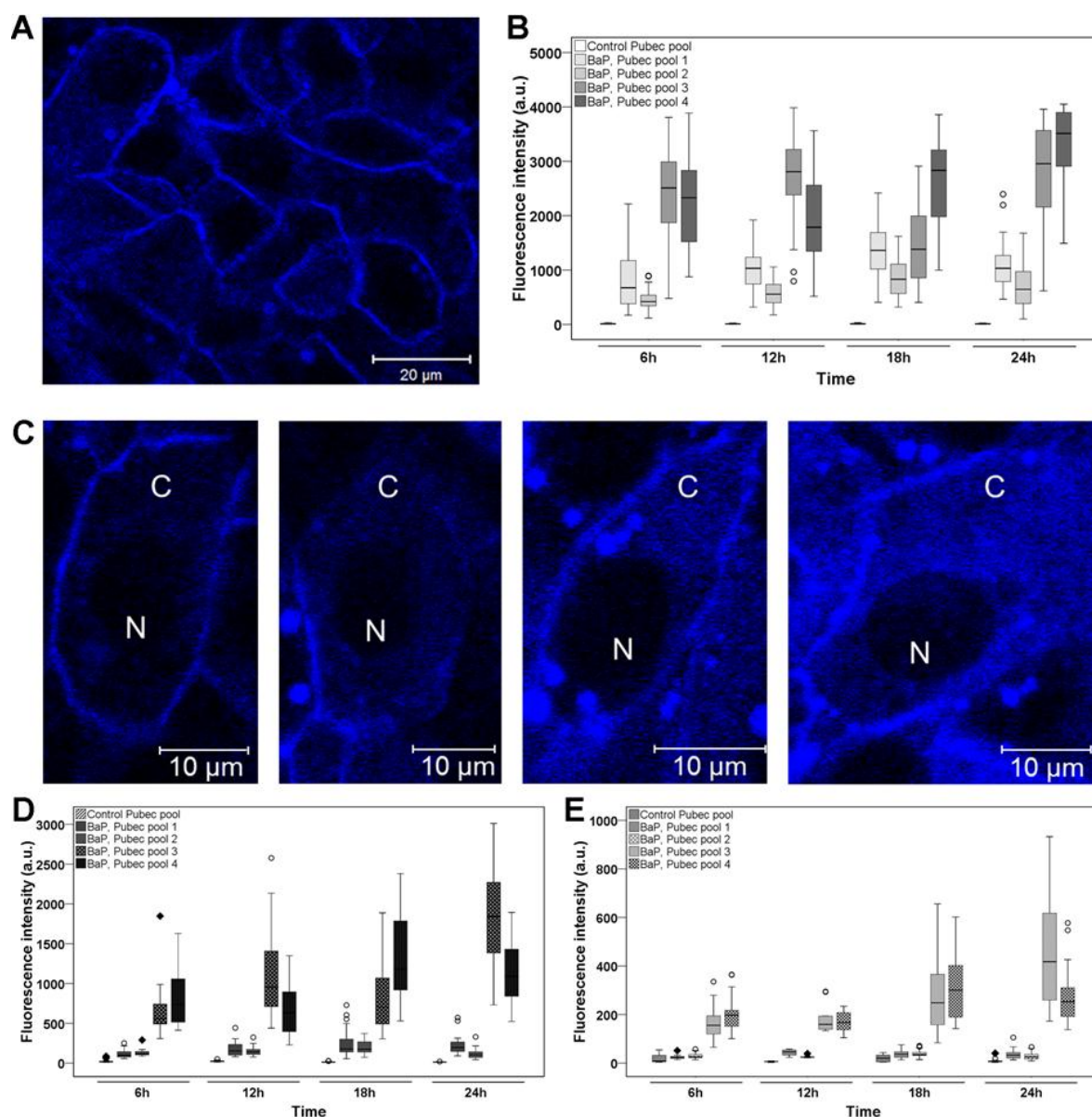


Figure 17: Subcellular distribution of B[a]P in PUBEC. Cells were cultured on collagen-coated glass coverslips and exposed to 0.5 μM B[a]P for up to 24 h. The fluorescence was recorded by using a laser-scanning microscope ($\lambda_{\text{excitation}} = 365$; $\lambda_{\text{emission}} = 389\text{-}470$ nm). (A) Intracellular distribution of B[a]P fluorescence in the plasma membrane after 24 h of incubation. (B) The box plot shows the time-dependent increase in B[a]P fluorescence in the plasma membrane of different PUBEC pools. (C) Single-cell images of the subcellular distribution of B[a]P fluorescence in the cytosol and nuclei of PUBEC (6-24 h). (D, E) The box plots show the time-dependent increase in B[a]P fluorescence in cytosol and nuclei of different PUBEC pools, respectively. C, cytosol; N, nucleus. Figure taken from Verma *et al.*, *Archives of Toxicology* 2012.

3.1.3 Quantification of intracellular B[a]P concentration by spectrofluorometry and GC-MS

By exploiting the fluorescence properties of B[a]P, the quantification of the intracellular concentration was carried out by spectrofluorometry, and the results were further verified by GC-MS. By using an *ex situ* calibration method, the intracellular B[a]P concentration was

determined spectrofluorometrically as a function of the released fluorescence in pig epithelial cells exposed to 0.5 mM or 10 μ M B[a]P for 24 h. For the *ex situ* calibration B[a]P concentrations were plotted vs. their fluorescence. The emission intensity linearly depended on the B[a]P concentration. The intracellular concentration of PUBEC pools (n = 4) exposed to 0.5 μ M B[a]P ranged from 7.28 μ M to 35.70 μ M, whereas the concentration of B[a]P in cells (four other PUBEC pools) exposed to 10 μ M B[a]P ranged from 29.90 μ M to 406.64 μ M. At both exposure concentrations considerable variation in intracellular B[a]P accumulation was observed (**Table 4**).

Table 4: Spectrofluorometric quantification of B[a]P concentrations in pig urinary bladder epithelial cells. PUBEC pools were incubated with 0.5 μ M (A) and 10 μ M B[a]P (B) for 24 h, respectively, and then homogenized. B[a]P standards (0.1–2.5 μ M) were dissolved in cytosolic medium (pH 7.2, 37 °C), designed to simulate the composition of the cytosol as described in the text. Measurements were performed by using an excitation wavelength of 365 nm and an emission wavelength of 405 nm. Figure obtained from Verma *et al.*, *Archives of Toxicology* 2012.

Sample	Exposure concentration (μ M)	Intracellular concentration (μ M)	Accumulation factor (%)
PUBEC pool 5	0.5	7.28	14.6
PUBEC pool 6	0.5	10.75	21.5
PUBEC pool 7	0.5	23.17	46.3
PUBEC pool 8	0.5	35.70	71.4
PUBEC pool 9	10	29.95	2.9
PUBEC pool 10	10	48.31	4.8
PUBEC pool 11	10	373.72	37.4
PUBEC pool 12	10	406.64	40.7

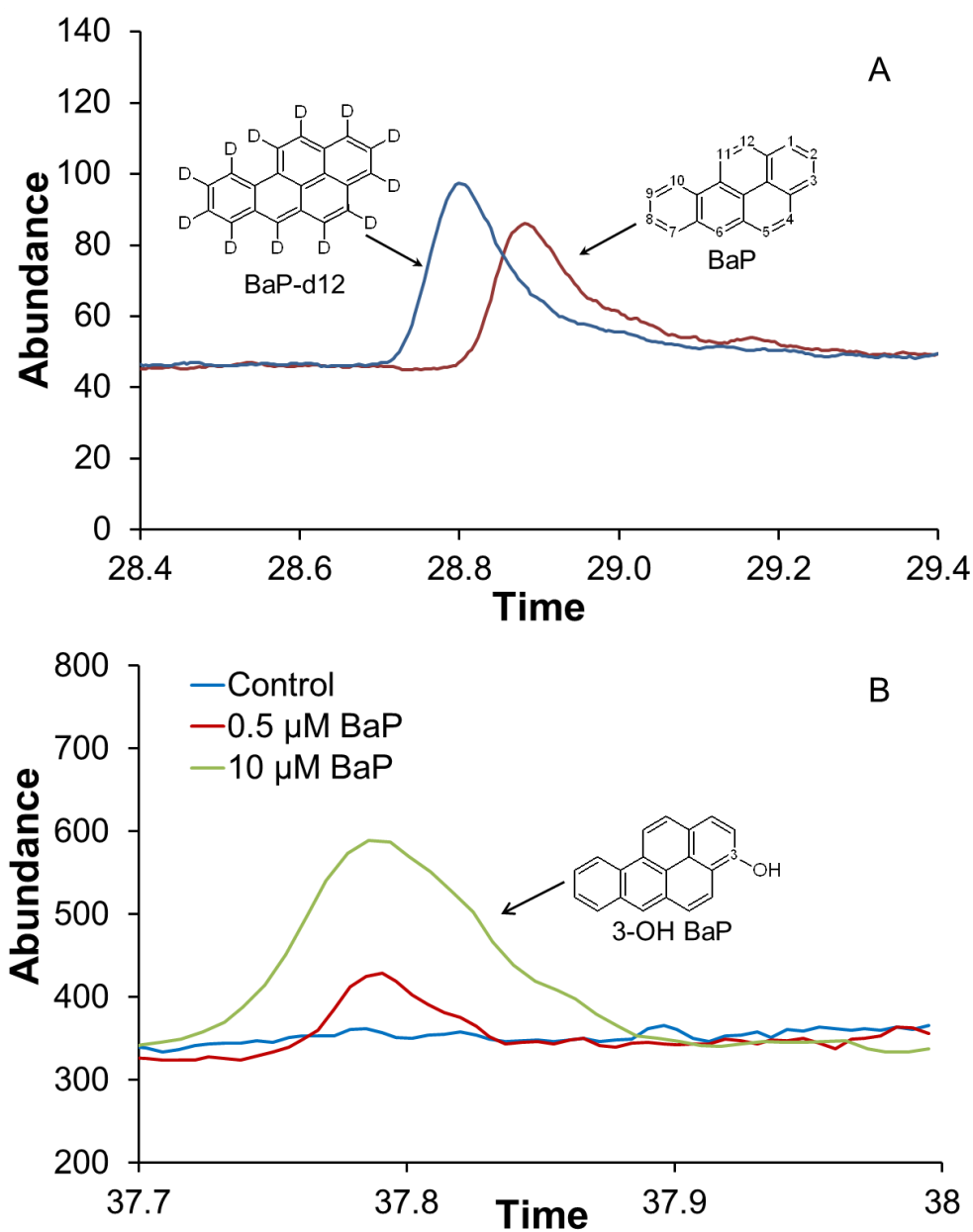


Figure 18: (A) A representative single ion chromatogram obtained from the supernatant of a PUBEC pool exposed to 0.5 μM B[a]P for 24 h. The deuterated B[a]P (—) elutes earlier than the non-deuterated compound (—). (B) GC-MS separation of the B[a]P metabolite 3-OH-B[a]P in unexposed samples (—) and cells exposed to 0.5 μM (—) and 10 μM (—) B[a]P for 24 h (retention time 37.80 min). Figure obtained from Verma *et al.*, *Archives of Toxicology* 2012.

By using B[a]P d-12 as internal standard, the intracellular B[a]P concentrations of the individual PUBEC pools as obtained by spectrofluorometry were further verified by GC-MS analysis. The intracellular B[a]P concentrations were measured by means of a calibration curve prepared by measuring the B[a]P standards in the presence of a constant B[a]P-d12 amount. The deuterated and the non-deuterated B[a]P differ from each other in their elution time: B[a]P eluted after 28.87 min and B[a]P d-12 after 28.78 min (**Figure 18A**). The resulting ratios between the peak areas of the nondeuterated and deuterated B[a]P ($F = \text{AB[a]P} / \text{AB[a]P-d12}$) were used for the mathematical calculations. Thus, as observed from the experiment based on laser scanning microscopy, also these experiments point at distinct batches of PUBEC with strongly different properties in B[a]P uptake.

3.1.4 Formation of 3-OH-B[a]P in PUBEC

In PUBEC, the expression of CYP involved in the metabolism of B[a]P has recently been demonstrated [172]. To prove the actual formation of B[a]P metabolites in PUBEC, cells exposed to 0.5 and 10 μM B[a]P were analyzed by GC-MS. By using a commercially available standard of 3-OH-B[a]P, this major phenolic BaP intermediate could indeed be identified for the first time (**Figure 18B**). However, because of the unavailability of a deuterated reference compound, it could not be quantified. Nevertheless, it appeared from the peak areas of the metabolite in the exposed samples that a considerably larger quantity of 3-OH-B[a]P was formed in PUBEC exposed 10 μM B[a]P as compared to PUBEC exposed to 0.5 μM B[a]P.

4. Proteome and phosphoproteome maps of PUBEC[‡]

4.1 Objective

The majority of bladder cancers is transitional cell carcinomas and is thought to be caused to a significant part by the exposure to chemical carcinogens. In recent years, major advances in the culture of urinary bladder-derived cells have been achieved, and various urothelial *in vitro* models have been developed. Since culturing primary human tissues is still a difficult task, often because of an insufficient availability of cells required to perform large-scale studies, the culture of animal urothelial cells is used as an alternative. Beyond that, cell lines derived from transformed cells may be applied in specific investigations. With the advent of high-throughput and multiplex proteomic technologies in recent years, a variety of cell models and transformed cell lines have been utilized in an effort to achieve a better understanding of bladder biology, in particular of bladder carcinogenesis. However, information regarding the expression of proteins in normal bladder tissue is essentially missing as yet. Therefore, the aim of the present study was to develop a 2D map of proteins expressed in normal bladder cells that can be used as a reference map for studying alterations in urothelial biology.

4.2 2DE analysis and identity assignment

Inasmuch as the porcine model bears some remarkable similarities with humans, it is important to recognize that there are some differences between the two species, too, which may lead to a divergent response to a certain experimental regime. For reducing the variability and interindividual differences, pooling of PUBEC from several pigs has been suggested [171]. To reduce the effects of polymorphism as often observed in pigs, cells from a minimum of 30 pig bladders were pooled. The cells were cultured, and the extracted proteins were used for subsequent 2DE separation. The experiment was repeated eight times (n=8), and the gel triplicates of eight different protein extracts representing eight different groups were used for establishing the proteome map. The expression of more than 1000 spots with molecular masses ranging from 10 to 150 kDa and pI values ranging from 4 to 10 were observed. To determine the significantly expressed proteins in the groups, the gels were compared by using the Delta2D v4.0 software. Only protein spots with an expression variance of no more than ± 1.2 in the samples (eventually 150 proteins) from different gels were further

[‡] Verma *et al.*, *Electrophoresis* 2011, 32, 3600–3611

considered for inclusion in the proteome map. A representative fused gel image obtained after matching eight different protein lysates is shown in (Figure 19) in which all spots identified as consistently expressed are marked by numbered arrows.

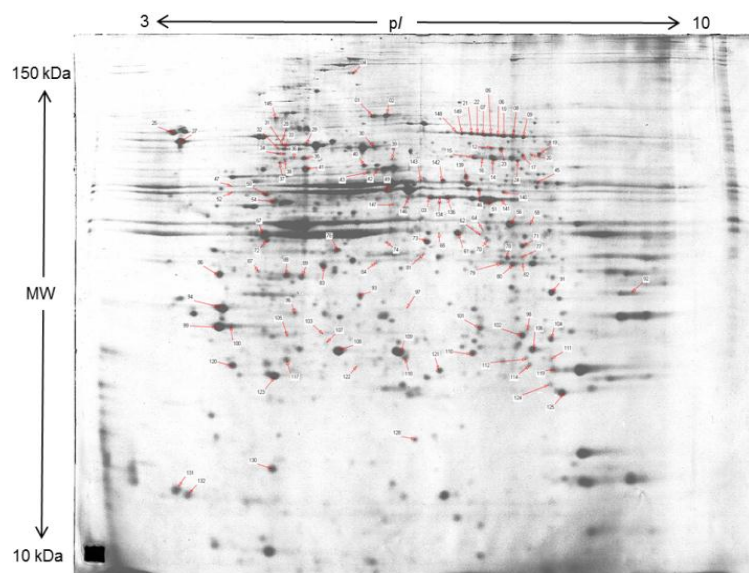


Figure 19: Representative 2DE gel image of PUBEC. 450 μg of proteins from a whole cell extract were separated and stained with Coomassie brilliant blue. Numbered spots were identified by mass spectrometry after in-gel digestion of proteins by trypsin. Figure taken from Verma *et al.*, *Electrophoresis* 2011, 32, 3600–3611.

For assigning the identity of significantly expressed proteins as analyzed by MALDI-TOF-MS, protein peptide mass matching was performed on Mascot by searching the MSDB and NCBI nr protein databases with the taxonomy pig. Out of the total of 150 proteins the identity could only be assigned to 61 % (92 proteins) of the protein spots analyzed (Table 5). 39 % of the spots remained unidentified, although utilizable MS data were collected. To overcome the problem of poor sequence representation for proteomic identification, the pig proteins were matched against the protein equivalents of other species such as human, rat, and mouse. By that approach the rate of identification was considerably increased, and the identity of another 28 spots could be clarified, making the total of identified proteins to 80 % (120 proteins). Twenty percent of spots remained unidentified, which might be due to common technical problems such as spot overlapping or incorrect mass identification.

Table 5: Summary of the proteins of primary cultured PUBEC identified by 2DE separation and peptide mass fingerprinting. Table taken from Verma *et al.*, *Electrophoresis* 2011, 32, 3600–3611.

Spot no	Protein name	Gene name	Theoretical molecular weight / pI	Experimental molecular weight / pI	Score	Peptides matches	Sequence coverage (%)	GRAVY values	Reference organism
1	Gelosin*	GSN	85,06/5.93	85,10/5.54	61	17	23	-0,155	<i>Sus scrofa</i>
2	Gelosin*	GSN	85,06/5.93	86,33/5.56	119	17	23	-0,155	<i>Sus scrofa</i>
3	Beta-enolase	ENO3	47,44/8.05	47,89/6.32	71	11	28	-0,209	<i>Sus scrofa</i>
4	Keratin 9	KRT9	62,19/5.14	123,38/5.23	104	12	31	-0,626	<i>Homo sapiens</i>
5	Lamin-A/C*	LMNA	74,40/6.73	77,30/7.09	219	26	40	-0,677	<i>Sus scrofa</i>
6	Lamin-A/C*	LMNA	74,40/6.73	77,50/6.94	134	16	31	-0,677	<i>Sus scrofa</i>
7	Lamin-A/C*	LMNA	74,40/6.73	76,89/6.87	99	17	27	-0,677	<i>Sus scrofa</i>
8	Lamin-A/C*	LMNA	74,40/6.73	76,89/7.33	231	29	39	-0,677	<i>Sus scrofa</i>
9	Lamin-A/C*	LMNA	74,40/6.73	76,89/7.45	188	24	32	-0,677	<i>Sus scrofa</i>
10	Lamin-A/C*	LMNA	74,40/6.73	77,50/7.22	218	28	40	-0,677	<i>Sus scrofa</i>
12	WD repeat-containing protein 1	WDR1	58,59/6.41	71,37/6.99	70	9	28	-0,238	<i>Homo sapiens</i>
14	Lamin-A/C*	LMNA	74,40/6.73	67,75/7.00	189	22	43	-0,677	<i>Sus scrofa</i>
15	Lamin-A/C*	LMNA	74,40/6.73	67,75/6.79	184	24	47	-0,677	<i>Sus scrofa</i>
16	Lamin-A/C*	LMNA	74,40/6.73	67,26/6.88	60	11	35	-0,677	<i>Sus scrofa</i>
19	Purinergic receptor	P2RY12	39,35/9.59	70,48/7.53	55	7	43	0,384	<i>Sus scrofa</i>
20	Heterogeneous nuclear ribonucleoprotein L	HNRNPL	64,13/8.46	69,44/7.46	66	20	23	-0,649	<i>Homo sapiens</i>
21	Lamin-A/C*	LMNA	74,13/6.57	77,09/6.81	129	20	32	-0,677	<i>Sus scrofa</i>
22	Lamin-A/C*	LMNA	74,13/6.57	77,30/6.81	64	12	21	-0,677	<i>Sus scrofa</i>
23	Cingulin	CGN	136,58/5.46	71,37/7.09	55	16	15	-1,071	<i>Sus scrofa</i>
24	Lamin-A/C*	LMNA	74,13/6.57	66,93/7.31	80	14	27	-0,677	<i>Sus scrofa</i>
25	Involucrin	IVL	36,18/4.39	73,33/3.18	64	9	19	-1,914	<i>Sus scrofa</i>
26	Calreticulin	CALR	48,42/4.32	73,57/3.29	212	19	52	-0,33	<i>Sus scrofa</i>
27	GRP78 precursor	HSPA5	72,18/5.03	73,76/4.49	147	23		-0,545	<i>Homo sapiens</i>
28	Heat shock cognate 71 kDa protein isoform 1*	HSPA8	70,89/5.37	71,91/4.79	183	19	43	-0,456	<i>Homo sapiens</i>
29	Heat shock 70 kDa protein 1B	HSPA1B	71,08/5.30	70,30/5.60	153	23	40	-0,376	<i>Sus scrofa</i>
30	Heat shock cognate 71 kDa protein isoform 1*	HSPA8	71,082/5.37	70,30/4.54	138	18	48	-0,859	<i>Homo sapiens</i>
32	LMNB1 *	LMNB1	38,28/5.37	70,13/4.45	82	11	37	-0,859	<i>Homo sapiens</i>
33	LMNB1 *	LMNB1	38,28/5.37	70,30/4.55	88	12	36	-0,859	<i>Homo sapiens</i>
34	GRP 78 precursor	HSPA5	72,40/5.07	68,25/4.52	188	22	32	-0,545	<i>Homo sapiens</i>
35	Heterogeneous nuclear ribonucleoprotein K	HNRNPK	47,75/5.46	66,61/4.77	104	15	34	-0,705	<i>Homo sapiens</i>
36	Heat shock 70kDa protein 5, partial	HSPA1A	73,93/5.68	68,25/4.70	84	13	25	0.005	<i>Sus scrofa</i>

Spot no	Protein name	Gene name	Theoretical molecular weight / pI	Experimental molecular weight / pI	Score	Peptides matches	Sequence coverage (%)	GRAVY values	Reference organism
37	Transitional endoplasmic reticulum ATPase	VCP	70,43/5.41	64,87/4.48	102	13	31	-0.348	<i>Homo sapiens</i>
38	Heterogeneous nuclear ribonucleoprotein K isoform a variant	HNRNPK	49,00/5.48	65,97/4.54	98	13	34	-0.701	<i>Homo sapiens</i>
39	T-complex protein 1 subunit alpha	TCP1	60,83/5.71	64,87/5.85	92	14	25	-0.038	<i>Sus scrofa</i>
40	F-actin-capping protein subunit beta	CAPZB	31,58/5.47	63,80/5.51	60	9	42	-0.558	<i>Sus scrofa</i>
41	Heat shock 60 kDa protein 1	HSP60	61,04/5.71	63,09/4.80	224	25	51	-0.165	<i>Sus scrofa</i>
42	Muscle and heart F-box protein 40	FBXO40	61,33/7.02	62,16/5.65	45	4	19	-0.473	<i>Sus scrofa</i>
43	Cell division protein kinase5	CDK5	33,72/4.57	61,29/5.56	51	6	26	-0.286	<i>Sus scrofa</i>
44	Stratifin	SFN	28,03/4.78	30,03/5.00	198	26	61	-0.617	<i>Sus scrofa</i>
45	D-3-phosphoglycerate dehydrogenase	PHGDH	57,51/6.44	59,33/7.39	103	16	30	0.102	<i>Sus scrofa</i>
46	RuvB-like 1 (49 kDa TATA box-binding protein-interacting protein)	RUVBL1	50,22/6.02	56,28/6.90	109	11	41	-0.251	<i>Sus scrofa</i>
47	Centrin 2	CETN2	56,41/4.00	56,54/4.01	48		28	-0.768	<i>Sus scrofa</i>
49	Keratin, type II cytoskeletal 7	KRT7	51,41/5.40	55,27/5.81	107	13	23	-0.472	<i>Homo sapiens</i>
50	Mitochondrial ATP synthase, H ⁺ transporting F1 complex beta subunit	ATP5J	47,06/4.99	54,64/4.42	221	28	62	0.015	<i>Sus scrofa</i>
51	Beta-enolase	ENO3	47,44/8.05	54,15/7.09	85	13	33	-0.209	<i>Sus scrofa</i>
54	Heterogeneous nuclear ribonucleoprotein F isoform 2	Hnmpf	45,98/5.31	52,35/4.46	99	12	44	-0.470	<i>Sus scrofa</i>
56	NADP-Isocitrate dehydrogenase	IDH1	46,65/6.53	47,25/7.32	67	7	42	-0.085	<i>Sus scrofa</i>
58	Beta actin	ACTB	45,16/5.29	47,36/7.54	116	14	54	-0.200	<i>Homo sapiens</i>
61	Ig heavy chain variable region	IGHD	42,25/8.31	44,60/6.70	54	5	33	-0.555	<i>Homo sapiens</i>
62	Poly(rC)-binding protein 1	cpcG1	31,93/9.25	44,50/6.98	72	8	20	-0.505	<i>Homo sapiens</i>
64	Paralemmin 2	PALM2	42,18./5.04	45,60/7.01	41	7	15	-0.830	<i>Sus scrofa</i>
65	Keratin, type I cytoskeletal 19*	KRT19	44,07/5.04	44,41/6.52	67	10	22	-0.532	<i>Homo sapiens</i>
67	Keratin, type I cytoskeletal 19*	KRT19	44,10./5.05	44,41/6.52	100	10	22	-0.532	<i>Homo sapiens</i>
70	Short-chain specific acyl-CoA dehydrogenase, mitochondrial precursor	ACADS	45,22/8.36	43,72/7.06	111	16	38	-0.067	<i>Sus scrofa</i>
71	Sialic acid synthase	SAS	40,58/6.44	42,38/7.50	143	15	51	-0.334	<i>Sus scrofa</i>
72	Tropomodulin-3	TMOD3	39,72/4.98	42,38/4.43	82	11	35	-0.583	<i>Sus scrofa</i>
73	Serine proteinase inhibitor, clade B, member 5	Serpina4	43,35/6.73	42,01/6.35	86	12	37	-0.143	<i>Sus scrofa</i>
74	Keratin, type II cytoskeletal 1	KRT1	66,03/8.75	41,92/5.87	59	10		-0.626	<i>Homo sapiens</i>
76	Cytoskeletal beta actin	ACTB	45,16/5.55	40,54/5.30	65	9	35	-0.200	<i>Sus scrofa</i>
77	LOC100130354 protein	LOC100130354	15,92/8.70	39,73/7.51	65	4	53	-0.802	<i>Homo sapiens</i>
78	Pyruvate kinase 3 isoform 2	PK2	58,50/6.14	39,56/7.34	157	13	2	-0.245	<i>Sus scrofa</i>

Spot no	Protein name	Gene name	Theoretical molecular weight / pI	Experimental molecular weight / pI	Score	Peptides matches	Sequence coverage (%)	GRAVY values	Reference organism
79	Annexin A2*	ANXA2	38,79/6.49	38,42/7.28	133	16	46	-0.509	<i>Sus scrofa</i>
80	Annexin A2, isoform CRA_c*	ANXA2	38,79/6.49	38,16/7.40	70	11	37	-0.509	<i>Homo sapiens</i>
81	Dehydrogenase, glyceraldehydephosphate	ANX2							
82	Annexin A2, isoform CRA_c*	GAPDH	36,05/8.57	39,12/6.28	81	8	34	-0.108	<i>Sus scrofa</i>
83	Chain B, tubulin alpha-beta dimer, electron diffraction	ANXA2	38,79/6.49	38,42/7.54	130	14	51	-0.524	<i>Homo sapiens</i>
84	Annexin A2, isoform CRA_c*	-	48,31/5.17	37,15/5.14	148	21	38	-0.390	<i>Sus scrofa</i>
86	Tropomyosin alpha-4 chain isoform 2	ANXA2	38,79/6.49	37,91/5.79	159	18	34	-0.524	<i>Homo sapiens</i>
87	Immunoglobulin heavy chain variable region	TPM4	28,62/4.67	34,94/3.96	90	11	36	-1.021	<i>Sus scrofa</i>
88	Splicing factor, arginine/serine-rich 1 isoform 1*	IGHD	42,25/8.30	36,24/4.34	62	9	20	-0.555	<i>Homo sapiens</i>
89	Splicing factor, arginine/serine-rich 1 isoform 1*	SRSF1	27,84/10.37	35,26/4.72	178	19	52	-1.152	<i>Sus scrofa</i>
91	Voltage-dependent anion-selective channel protein 2	SRSF1	27,84/10.37	34,94/4.90	117	13	54	-1.152	<i>Sus scrofa</i>
92	Voltage-dependent anion-selective channel protein 1	VDAC2	32,08/7.49	32,91/7.94	105	9	50	-0.288	<i>Sus scrofa</i>
94	Tropomyosin alpha-3 chain isoform 2	VDAC2	30,82/8.62	33,14/8.98	177	15	67	-0.288	<i>Sus scrofa</i>
96	Chloride intracellular channel protein 1	TPM4	29,24/4.75	28,83/4.05	200	21	50	-1.021	<i>Sus scrofa</i>
98	Valacyclovir hydrolase precursor	CLIC1	27,17/5.09	28,83/4.87	78	7	36	-0.284	<i>Homo sapiens</i>
100	14-3-3 protein sigma	BPHL	32,54/9.20	28,28/7.68	50	4	20	-0.242	<i>Homo sapiens</i>
101	Endoplasmic reticulum protein 29	SFN	28,03/4.78	25,87/4.13	127	17	51	-0.599	<i>Sus scrofa</i>
102	Phosphoglycerate mutase 2	ERP29	29,32/6.85	26,59/7.09	105	12	49	-0.297	<i>Sus scrofa</i>
103	14-3-3 protein ζ/δ	PGAM2	28,90/6.67	25,61/7.62	163	18	59	-0.530	<i>Sus scrofa</i>
104	Enoyl-CoA hydratase, mitochondrial	YWHAZ	26,43/5.00	25,67/5.22	70	10	50	-	<i>Homo sapiens</i>
105	Actin, beta	ECHS1	31,55/8.81	25,29/8.02	86	11	34	-0.056	<i>Sus scrofa</i>
106	Triosephosphate isomerase 1	ACTB	41,32/5.56	24,90/4.89	68	9	48	-0.070	<i>Homo sapiens</i>
107	Gamma-actin	TPI1	26,87/6.54	23,52/7.77	243	21	76	-0.148	<i>Sus scrofa</i>
108	Heat shock protein beta-1*	ACTG	26,14/5.65	25,22/5.21	89	9	65	-0.199	<i>Homo sapiens</i>
109	Heat shock protein beta-1*	HSPB1	22,98/6.23	21,29/6.27	98	7	30	-0.556	<i>Sus scrofa</i>
110	Heat shock protein beta-1*	HSPB1	22,98/6.23	22,24/6.61	150	10	51	-0.556	<i>Sus scrofa</i>
111	Mesoderm development candidate 2	HSPB1	22,98/6.23	22,84/7.05	155	12	51	-0.556	<i>Sus scrofa</i>
114	Proteasome subunit alpha type-2	-	21,22/4.80	22,36/8.04	61	6	56	0.023	<i>Sus scrofa</i>
117	Cathepsin B	PSMA2	25,99/6.92	21,34/7.75	93	10	43	-0.129	<i>Sus scrofa</i>
118	Growth factor receptor-bound protein 2 isoform 1	CTSB	37,87/5.81	21,23/4.80	60	9	21	-0.304	<i>Sus scrofa</i>
119	Chain A, structure of porcine class Pi Glutathione S-transferase	GAB1	25,30/5.89	21,34/6.27	57	6	21	-0.777	<i>Sus scrofa</i>
120	Tumor protein, translationally-controlled 1	GSTP1	23,72/8.07	20,93/8.08	151	9	53	-0.334	<i>Sus scrofa</i>
121	Parkinson disease protein 7	TPT1	19,69/4.84	20,30/4.17	98	14	58	-0.427	<i>Sus scrofa</i>
		PDDC1	20,09/6.33	20,24/6.67	141	16	79	0.178	<i>Sus scrofa</i>

Spot no	Protein name	Gene name	Theoretical molecular weight / pI	Experimental molecular weight / pI	Score	Peptides matches	Sequence coverage (%)	GRAVY values	Reference organism
122	BAG family molecular chaperone regulator 2	BAG2	23,77/6.25	20,64/5.67	69	13	37	-0.592	<i>Homo sapiens</i>
123	Thioredoxin peroxidase 1	PRDX2	14,27/4.70	19,10/4.71	97	6	36	0.078	<i>Sus scrofa</i>
124	Glutathione S-transferase P	GSTP1	23,71/8.07	19,05/8.06	74	8	36	-0.334	<i>Sus scrofa</i>
125	Neuropolypeptide H3	PEBP1	16,06/8.81	17,72/8.22	74	7	45	-0.652	<i>Homo sapiens</i>
128	BTF3L4 protein	BTF3L4	16,46/5.41	11,20/6.46	71	8	69	-0.548	<i>Homo sapiens</i>
130	Protein unidentified	-	-	80,24/4.78	38		85	-	<i>Sus scrofa</i>
131	Myosin light chain isoform LC17b	MYL6	16,99/4.46	58,00/3.63	86	12	74	-0.389	<i>Sus scrofa</i>
132	Myosin light polypeptide 6 isoform 1	MYL6	16,99/4.46	58,00/3.77	87	11	72	-0.389	<i>Sus scrofa</i>
134	Beta-enolase*	ENO3	47,44/8.05	53,65/6.54	76	9	32	-0.209	<i>Sus scrofa</i>
136	Beta-enolase*	ENO3	47,44/8.05	53,91/6.70	96	12	35	-0.209	<i>Sus scrofa</i>
139	T-complex protein 1 subunit beta	CCT2	57,75/6.09	57,98/6.76	196	22	53	-0.015	<i>Sus scrofa</i>
140	Temporarily assigned gene name family member	-	52,59/9.28	56,15/7.20	54	16	15	-	<i>Sus scrofa</i>
141	Beta-enolase	ENO3	47,44/8.05	53,91/7.36	87	13	36	-0.209	<i>Sus scrofa</i>
142	Proteasome subunit beta type 3	PDDC1	29,50/ 5.69	58,51/6.48	57	15	61	0.107	<i>Sus scrofa</i>
143	Keratin, type II cytoskeletal 8	BAG2	53,70/5.52	58,24/6.25	70	4	27	-0.297	<i>Sus scrofa</i>
145	Valosin-containing protein isoform 3	VCP	89,93/5.31	83,42/4.38	300	32	32	-0.346	<i>Sus scrofa</i>
146	Beta-enolase*	ENO3	47,44/8.05	53,54/6.88	74	11	30	-0.209	<i>Sus scrofa</i>
147	Heat shock 60 kDa protein 1	HSPD1	61,04/5.71	50,97/5.95	76	12	30	-0.165	<i>Sus scrofa</i>
148	Lamin-A/C*	LMNA	74,40/6.73	76,89/6.56	80	5	25	-0.677	<i>Sus scrofa</i>
149	Lamin-A/C*	LMNA	74,40/6.73	76,89/6.63	188	24	40	-0.677	<i>Sus scrofa</i>

Gene name, protein name, GRAVY value, theoretical molecular weight and pI entries in Uniprot Database for each protein identified by MALDI-TOF-MS.

Sequence coverage, peptide matches, score, and reference organism entries in the Mascot search engine.

If multiple spots were identified as the same protein, the protein is marked with an asterisk (*)

4.3 Physicochemical properties of identified proteins

For the 120 proteins identified, physicochemical properties such as hydrophobicity (GRAVY value), pI , and molecular weight were examined. The analysis of pI distribution revealed that the pI of the identified proteins varied between 4 and 10. Proteins with theoretical pI values higher than 9.6 were not detected. The molecular mass of 70 % of the identified proteins varied between 20 kDa and 80 kDa. Only one protein with a molecular mass higher than 100 kDa was identified (**Figure 20**). One of the most likely limitations for the identification of low-molecular proteins is associated with the staining method. Yet with the staining method developed in our laboratory that is able to stain protein in amounts as low as 2 ng [161], a few lower molecular mass proteins could also be stained and identified (spot no-130-132).

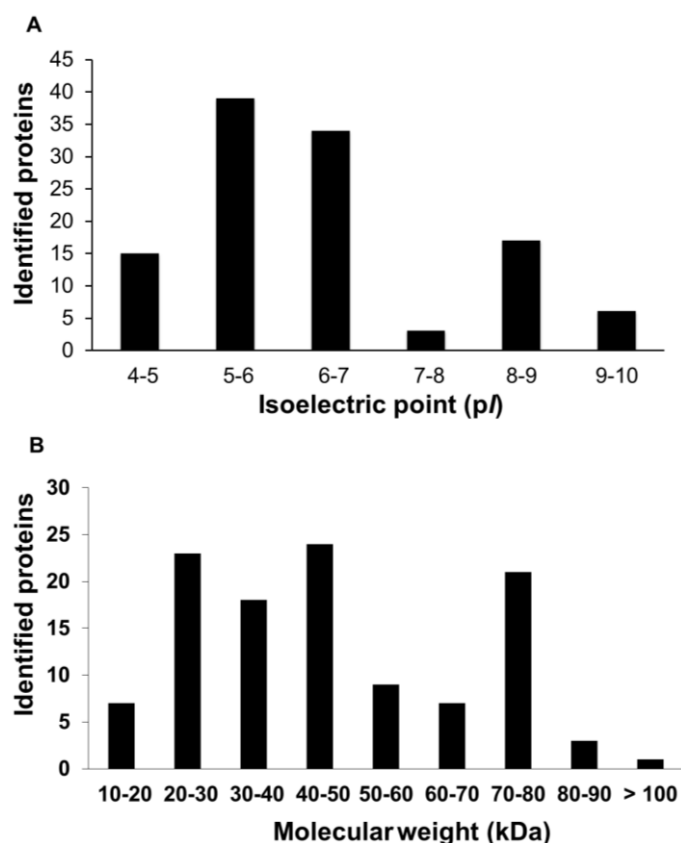


Figure 20: Theoretical isoelectric point (pI) (A) and molecular weight (MW) distribution (B) of proteins from pig bladder epithelial cells in relation to the number of identified proteins. Figure taken from **Verma *et al.*, Electrophoresis 2011, 32, 3600–3611.**

For displaying the hydrophobic character of a protein, grand average of hydropathy values (GRAVY) as annotated in the Swiss-Prot database were determined according to the method described by Kyte and Doolittle [174]. For the 120 proteins identified, the GRAVY values ranged from -1.021 to + 0.107. In the range from +2 to -2, a positive GRAVY score indicates

a hydrophobic nature of the protein, while a negative GRAVY score points to a hydrophilic property. Most of the proteins of the proteome map were hydrophilic, which is expected as the proteins identified by use of 2DE gels are generally hydrophilic. However, four protein spots with positive values were also observed (heat shock 70 kDa protein 5, partial (spot no-36), D-3-phosphoglycerate dehydrogenase (spot no-45), mitochondrial ATP synthase, H⁺ transporting F1 complex beta subunit (spot no-50), and proteasome subunit beta type 3 (spot no-142).

4.4 Functional and subcellular annotation of proteins

The identified proteins represent multiple gene families and functions. To get an initial overview on the structural, trophic, metabolic, and signaling conditions of the tissue, the identified proteins were analyzed with the PANTHER classification system. This system grouped the identified proteins into four different functional annotations, namely biological functions, molecular functions, protein pathways, and protein classes (**Figure 21**). The molecular classification of these proteins revealed that they were involved in twelve different metabolic pathways: ion channel activity (4 %), transporter activity (1 %), translation (1 %), transcriptional regulatory activity (2 %), enzyme regulatory activity (5 %), catalytic activity (26 %), motor activity (3 %), receptor activity (4 %), antioxidant activity (1 %), structural molecular activity (23 %), and binding activity (30 %). The identified proteins were grouped into twenty-two different pathways by the annotation software: ATP synthesis (2 %), apoptosis signaling pathway (7 %), angiogenesis (2 %), Alzheimer disease-presenilin pathway (4 %), integrin signaling pathway (4 %), inflammation mediated by chemokine and cytokine signaling pathway (4 %), EGF receptor signaling pathway (7 %), Parkinson's disease (11 %), PI3 kinase pathway (2 %), cytoskeleton regulation by Rho GTPase (7 %), PDGF signaling pathway (2 %), nicotinic acetylcholine receptor signaling pathway (4 %), cadherin signaling pathway (4 %), serine glycine biosynthesis (2 %), Huntington's disease (7 %), p53 pathway (2 %), VEGF signaling pathway (2 %), glycolysis (7 %), FGF signaling pathway (4 %), TCA cycle (4 %), and ATP synthesis (2 %).

The analysis of biological functional annotation revealed that the identified proteins were involved in diverse arrays of processes including 14 proteins (20.3 %) in cell communication, 28 proteins (40.6 %) in cellular processes, 11 proteins (15.9 %) in transport, 13 proteins (18.8 %) in cellular component organization, 2 proteins (2.9 %) in apoptosis, 8 proteins (11.6 %) in system processes, 1 protein (1.4 %) in reproduction, 11 proteins (15.9 %) in

responses to stimuli, 16 proteins (23.2 %) in developmental processes, 3 proteins (4.3 %) in the generation of precursor metabolites and energy, 4 proteins (5.8 %) in cell cycle, 13 proteins (18.8 %) in immune system processes, 2 proteins (2.9 %) in cell adhesion, and a maximum of 36 proteins (52.2 %) in metabolic processes.

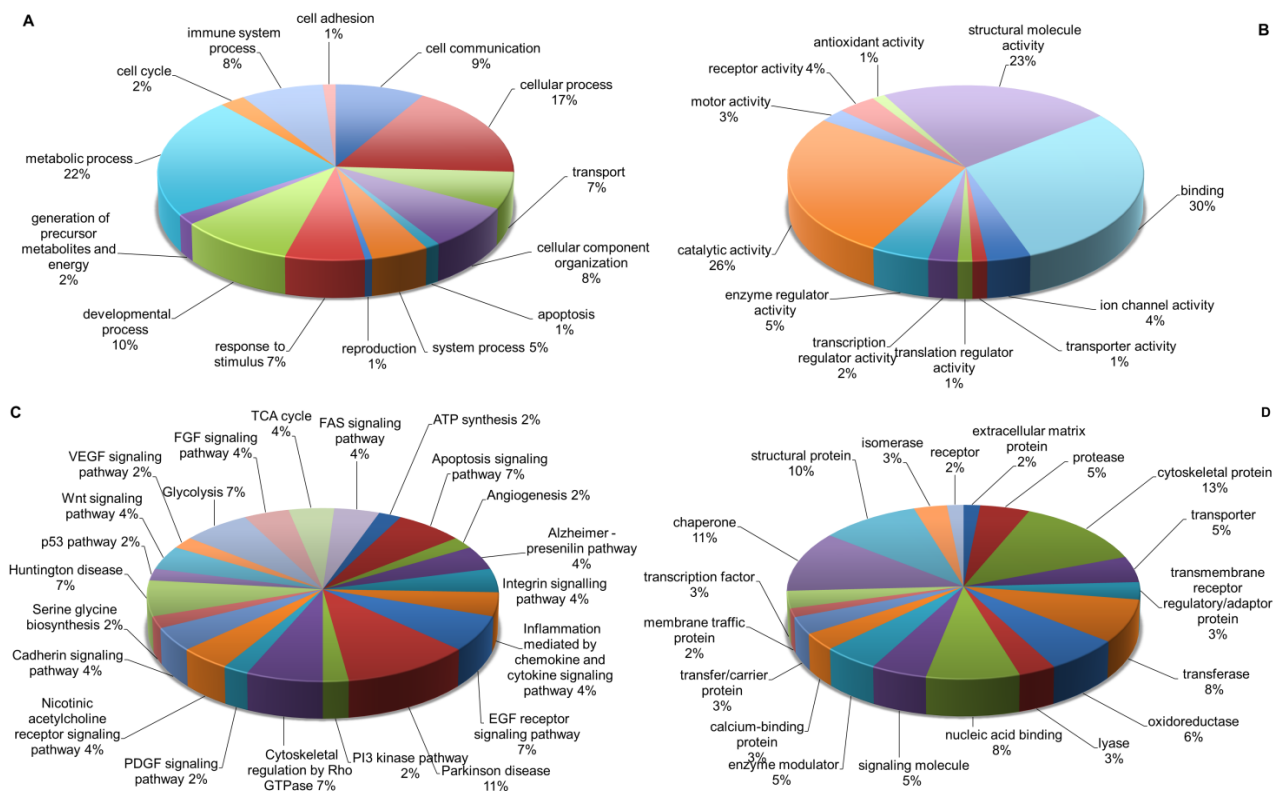


Figure 21: Ontological classification of the identified proteins according to the PANTHER prediction (4A). The proteins were classified according to their (A) biological functions, (B) molecular functions, (C) pathways, and (D) protein classes. Figure taken from **Verma et al., Electrophoresis 2011, 32, 3600–3611**.

Meanwhile, the protein classes' annotation categorized the proteins into nineteen different groups, among which 13 % of proteins were grouped as cytoskeleton proteins, 5 % as transporter proteins, 3 % as transmembrane receptor regulatory/adaptor proteins, 8 % as transferases, 6 % as oxidoreductases, 3 % as lyases, 8 % as nucleic acid binding proteins, 5 % as signaling molecules, 5 % as enzyme modulators, 3 % as calcium-binding proteins, 3 % as transfer/carrier proteins, 2 % as membrane traffic proteins, 11 % as chaperons, 10 % as structural proteins, 3 % as isomerases, 2 % as receptor proteins, 2 % as extracellular matrix proteins, and 5 % as proteases.

For detailed subcellular annotation of the identified proteins, a functional annotation database clustering program (<http://david.abcc.ncifcrf.gov/>) called Database for the Annotation Visualization and Integrated Discovery (DAVID) was used [167] (**Figure 22**). According to

the program 31.6 % of proteins were grouped as cytosolic, 22.8 % as cytoskeleton-related, 12.3 % as mitochondrial, 12.3 % as cytoplasmic/membrane-associated, 12.2 % as ribonucleo-protein complex, 5.2 % as endoplasmic, and 3.5 % as nuclear proteins.

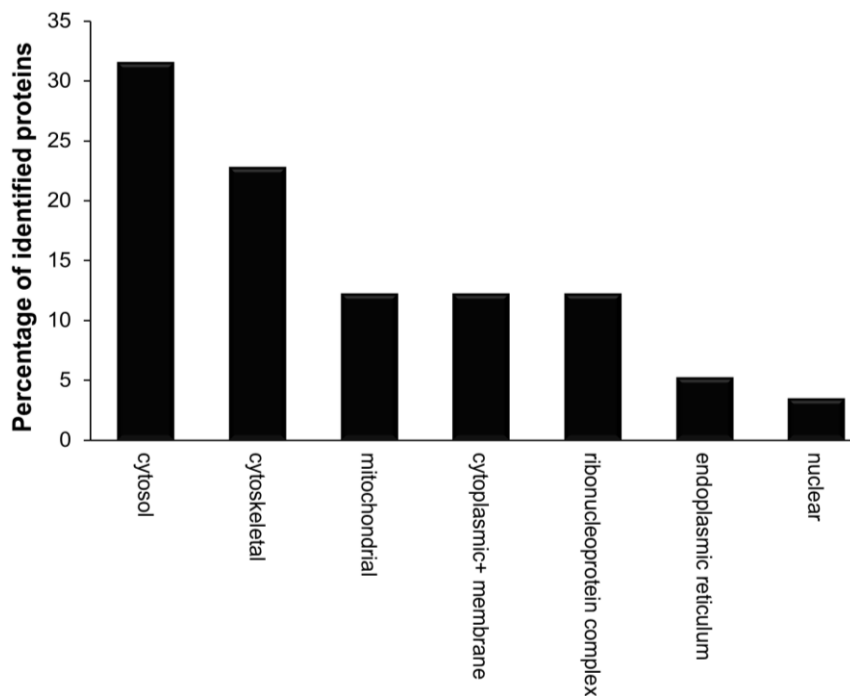


Figure 22: Subcellular location of the identified proteins according to DAVID prediction. Figure taken from Verma *et al.*, *Electrophoresis* 2011, 32, 3600–3611.

4.5 Phosphoproteome profiling of PUBEC

By using the lanthanum precipitation method for phosphoprotein enrichment, 33 phosphoproteins were identified, with minimal contamination by non-phosphopeptides (Table 6). The identified phosphoproteins exhibited many single or multiple phosphorylation sites.

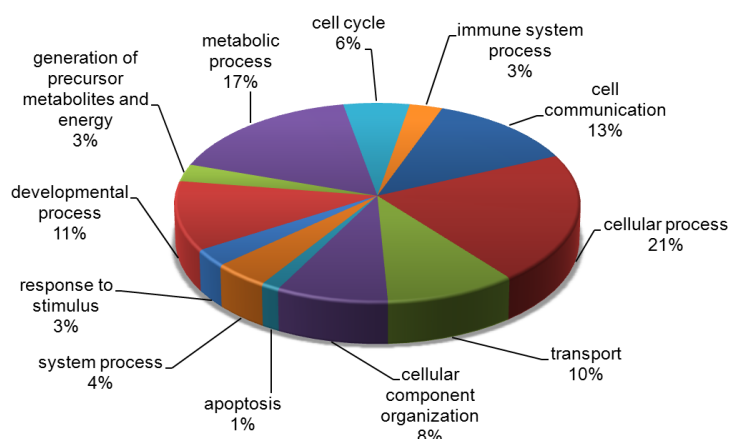


Figure 23: Classification of the identified phosphoproteins from PUBEC based on their predicted biological function Figure taken from Verma *et al.*, *Electrophoresis* 2011, 32, 3600–3611.

Gene ontology examination of the phosphoproteins revealed 21 % proteins associated with cellular processes, 17 % involved in metabolic processes, 13 % in cell communication, 10 % in transport, 8 % in cellular component organization, 11 % in developmental processes, 4 % in system processes, 3 % in responses to stimuli, 3 % in immune system processes, 6 % in cell cycle, 3 % in generation of precursor metabolites and energy, and 1 % in apoptosis (Figure 23).

Table 6: List of phosphoproteins identified in PUBEC after precipitation by La³⁺ ions. Table taken from Verma *et al.*, *Electrophoresis* 2011, 32, 3600–3611.

Accession number ^a	Protein Name	Gene name	Phosphorylation sites ^b	Phosphorylated amino acid ^c
O75369	Filamin-B	FLNB	18	S, T, Y
P63104	14-3-3 protein zeta/delta	YWHAZ	5	S, T
P06753	Tropomyosin alpha-3 chain isoform 2	TPM3	3	S, T, Y
Q6QAAQ1	Actin, cytoplasmic 1	ACTB	8	T, Y
P08758	Annexin A5-like, partial	ANXA5	1	Y
P83686	NADH-cytochrome b5 reductase 3-like	CYB5R3	2	S, T, Y
P19620	Annexin A2	ANXA2	11	S, T, Y
P05787	Keratin, type II cytoskeletal 8	KRT8	33	S, T, Y
P04175	NADPH-cytochrome P450 reductase	POR	1	Y
Q14974	Importin subunit beta-1-like	KPNB1	1	S
O43707	Alpha-actinin-4-like	ACTN4	1	Y
Q52NJ1	Ras-related protein Rab-11A*	RAB11A	5	S, T, Y
Q00610	Clathrin heavy chain 1	CLTC	6	S, T, Y
P83686	NADH-cytochrome b5 reductase 3	CYB5R3	1	Y
P04574	Calpain small subunit 1*	CAPNS1	1	S
O75665	Oral-facial-digital syndrome 1 protein-like	OFD1	2	S
P16949	stathmin isoform a	STMN1	7	S
P06753	Tropomyosin 3	TPM3	3	S, T, Y
P80230	Enhancer of rudimentary homolog*	ERH	3	S, T, Y
P84103	Serine/arginine-rich splicing factor 3	SRSF3	9	S
P08758	Annexin A5-like, partial	ANXA5	1	Y
Q3YLA6	Serine/arginine-rich splicing factor 1 isoform 1	SRSF1	10	S, Y
O43852	Calumenin isoform 1	CALU	3	S, T
P02543	Vimentin-like	VIM	31	S, T, Y
P28491	Calreticulin*	CALR	1	Y
P34935	78 kDa glucose-regulated protein	HSPA5	1	Y
P26234	Vinculin	VCL	9	S, T, Y
P31943	Heterogeneous nuclear ribonucleoprotein H	HNRNPH1	8	S, T, Y
P38646	Stress-70 protein, mitochondrial-like	HSPA9	2	S, Y
P31946	14-3-3 protein beta/alpha isoform 1	1433B	2	S
P60174	Triosephosphate isomerase 1	TPI1	2	S

^aUniprot accession number^bPhosphorylation site and phosphorylated amino acid entries in Uniprot Database for each protein identified by mass spectrometry.

Proteins marked with an asterisk (*) with entries for phosphorylation site and phosphorylated amino acids (S: serine, T: thymine, Y: tyrosine) in GeneCards V3 Database.

5. Toxicoproteomic analysis of apoptotic pathway in B[a]P- exposed PUBEC

5.1 Objective

Epidemiologic studies have indicated that, in addition to genetic factors and chronic irritation, occupational and environmental chemicals are significant determinants in many of the incidences of bladder cancer. In most populations tobacco smoking is the main known contributor to this malignancy: Among the many components of cigarette smoke, B[a]P which occurs in amounts of twenty to forty nanograms per cigarette is by far the best studied of these compounds and is known for its mutagenic and carcinogenic properties. However, epidemiological analyses have not yet documented B[a]P or any other PAH as significant candidates for initiating bladder cancer development. Therefore, the risk that exposure to any of these compounds causes bladder cancer is still uncertain. While genomic studies have helped in understanding the role of gene expression changes induced by B[a]P, the analysis at the protein level is a must to reveal the impact of these changes on cellular functions. The prime aim of this study was to analyze the early protein expression changes induced by B[a]P at low doses by using 2DE and MALDI-TOF-MS analysis in order to identify proteins/pathways involved in the cellular response to B[a]P-mediated toxicity. This is the first proteomic study using primary urinary epithelial cells for investigating the effects of B[a]P exposure on urothelial cell biology.

5.2 2DE analyses of protein expression in control and B[a]P-exposed cells

To closely reflect the epithelial cell conditions *in vivo*, cultured PUBEC derived from pigs were used to study the effects on B[a]P-induced toxicity, particularly in respect to its potential role in bladder cancer development. Proteins from five whole cell lysates obtained from each group of B[a]P-exposed and control cells were subjected to 2DE. Over 1000 protein spots were quantitatively identified by using the image analysis software Decodon 4.0. The comparison between the B[a]P-exposed and control groups indicated a more than twofold expression change of 40 proteins. Representative fused gels of control and B[a]P-exposed cell extracts are shown in

(**Figure 37, see annex I**) in which all spots identified as consistently differentially regulated are marked by numbered arrows. Due to the “poor” peptide mass database for pigs, only 25 proteins could be identified by MALDI-TOF-MS (**Table 7**). Among these 13 proteins (52 %) were up-regulated while 11 proteins (44 %) were down-regulated. Next, the biological networks of the identified proteins were examined by using the search tool STRING 9 (Search Tool for the Retrieval of Interacting Genes/Proteins). The identified proteins were searched with the corresponding Swiss-Prot access number for their exact gene counterpart in STRING 9. The gene counterparts were uploaded to the STRING pathway analysis software. Interestingly, the software associated the differentially expressed proteins with a network that contains three nodes of interest involving TP53, XPC, and splicing genes (**Figure 24**).

5.3 Induction of DNA repair proteins and determination of DNA damage

Xeroderma pigmentosum, complementation group C, also known as XPC, is a protein that is involved in the recognition of bulky DNA adducts in nucleotide excision repair. One of the metabolite of B[a]P, 7,8-dihydrodiol-9,10-epoxide (BPDE), is known to form such adducts. Biological network pathways analysis using the STRING pathway analysis software showed significant correlations between four differentially regulated proteins (RAD23A, RAD23B, PMSD5, and PMSD4) and the XPC protein system. The up-regulation of these proteins points towards DNA damage in the urothelial cells during exposure to B[a]P for 24 h and is in agreement with the results obtained by the comet assay (see section-5.4)

Table 7: Proteins with altered expression (≥ 2) after B[a]P exposure compared to controls.

ID ¹	Accession No. ²	Gene name ²	Protein name ²	MOWSE score ³	Peptide matches ³	Regulation ⁴
ID01	P10775	RNH1	Ribonuclease inhibitor	122	18	up-regulated
ID02	Q32YV9	PMSD4	Proteasome 26S subunit non-ATPase 4	95	13	up-regulated
ID03	A1BPP7	ACTB	Beta actin	69	22	up-regulated
ID04	F1SGG2	KRT8	Keratin 8	178	13	up-regulated
ID05	Q6W6X2	PMSD5	Proteasome 26S subunit, ATPase, 5	213	34	down-regulated
ID09	Q9MZ15	VDAC2	Voltage-dependent anion selective channel protein 2	177	10	up-regulated
ID11	A3EX84	LGALS3	Lectin galactoside binding soluble 3	75	14	down-regulated
ID16	Q3MI39	HNRPA1	Heterogeneous nuclear ribonucleoprotein 1	123	14	down-regulated
ID18	Q29561	CMPK	UMP-CMP kinase	70	8	up-regulated
ID19	Q5S1U1	HSP27	Heat shock protein beta-1	155	12	down-regulated
ID20	P00795	CTSD	Cathepsin D	171	18	up-regulated
ID21	P54725	RAD23A	UV excision repair protein RAD23 homolog A	169	35	up-regulated
ID22	Q06A98	SFRS2	Serine/arginine-rich splicing factor 2	178	19	up-regulated
ID23	Q3YLA6	SFRS1	Serine/arginine-rich splicing factor 1	117	13	up-regulated
ID24	F1SP32	RAD23B	UV excision repair protein RAD23 homolog B	101	27	up-regulated
ID29	P03974	VCP	Transitional endoplasmic reticulum ATPase	88	17	down-regulated
ID35	Q08094	CNN2	Calponin 2	108	14	down-regulated
ID37	P34935	HSPA5	Heat shock 70 kDa protein 5	140	17	down-regulated
ID38	P34935	HSPA5	Heat shock 70 kDa protein 5	199	24	down-regulated
ID39	P36871	PGM1	Phosphoglucomutases	187	23	down-regulated
ID40	Q1KYT0	ENO3	Enolase 1	108	14	down-regulated
ID41	P15311	EZR	Ezrin	145	21	up-regulated
ID42	P28768	SOD2	Superoxide dismutase 2	103	10	up-regulated
ID43	Q29371	TPI1	Triosephosphate isomerase 1	152	14	down-regulated
ID44	P42639	TPM1	Tropomyosin 1	114	14	up-regulated

1 Internal ID number, 2 Gene name and protein name in Uniprot Database for the each protein identified by MALDI-TOF-MS, 3 Peptides matches and entries in the Mascot search engine, 4 Protein scores greater than 66 are considered significant ($p < 0.05$)

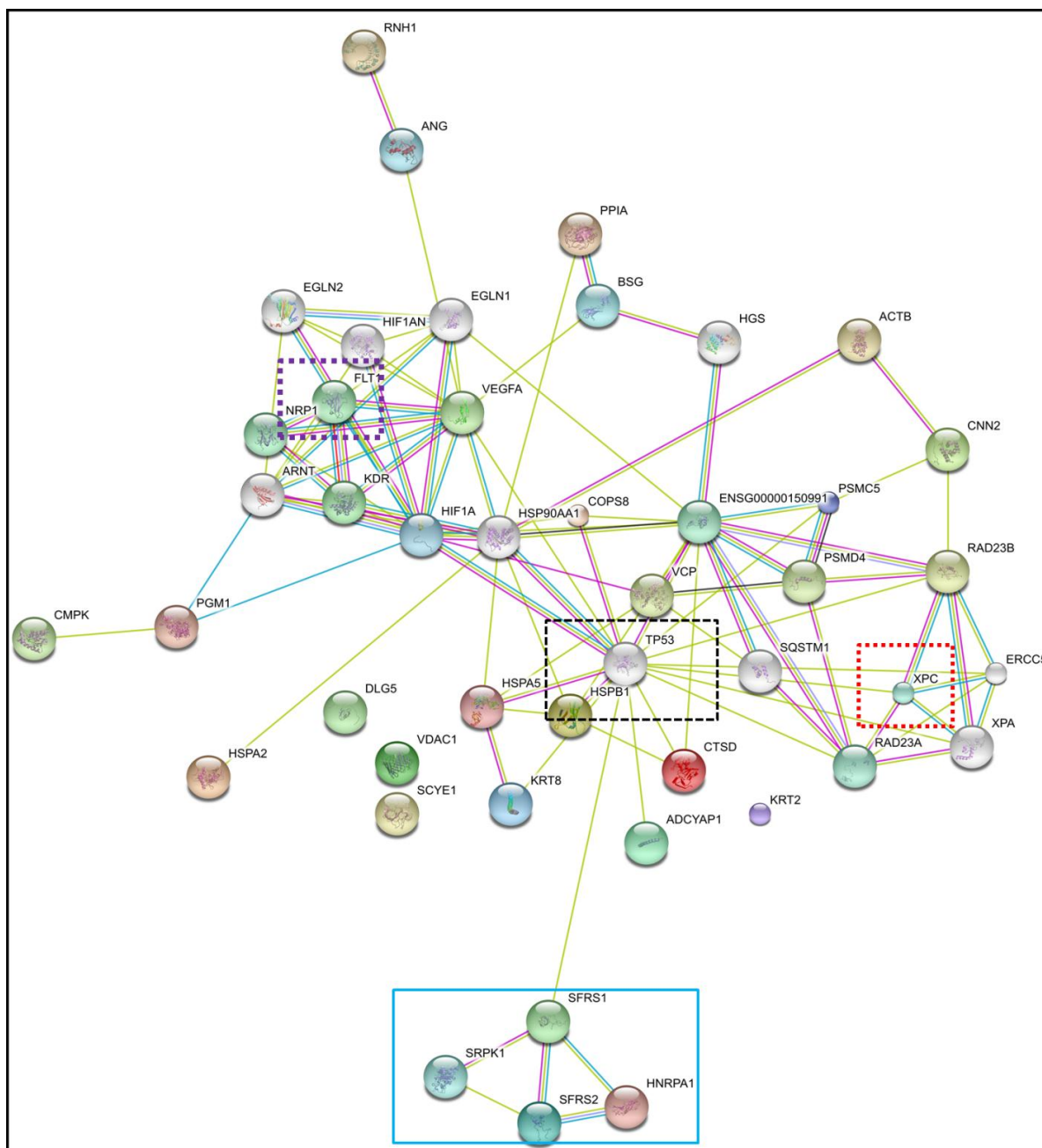


Figure 24: Potential protein-protein interactions of all differentially expressed protein species ($p < 0.05$) associated with B[a]P exposure as suggested by the STRING 9 database and web resources. Uniprot gene names were loaded into the STRING tool (<http://string-db.org/>) and analyzed by using the standard settings (medium confidence, network depth 1, no additional white nodes). The color of the connecting lines between two protein species encodes the source of the information: experimental data (rose), databases (light blue), co-expression data (black), co-occurrence data (dark blue), and text mining. (green) The nodes of interest are marked in colored boxes.

5.4 Verification of DNA damage in PUBEC exposed to 0.5 μM B[a]P

Results obtained by the comet assay indicating DNA damage in B[a]P-treated pig epithelial cells are shown in (Figure 25). The cells in culture were exposed to B[a]P in concentrations ranging from 0.1 to 10 μM for 24 h. The experiments were repeated three times with different PUBEC pools. The application of the comet assay revealed the presence of nuclear DNA forming tail-like structures in a concentration-dependent manner. The mean value of the olive tail moment (OTM) of the control cells was 0.35 ± 0.03 after 24 h of B[a]P exposure, while the mean values of the OTMs of the cells exposed to higher concentrations (5 or 10 μM B[a]P) were 1.72 ± 0.07 ($p < 0.001$) and 1.13 ± 0.08 ($p < 0.001$), respectively, indicating a significant level of DNA damage. The mean values of the OTMs of the bladder epithelial cells exposed to 0.5 μM B[a]P also showed a statistically significant increase when compared to control cells.

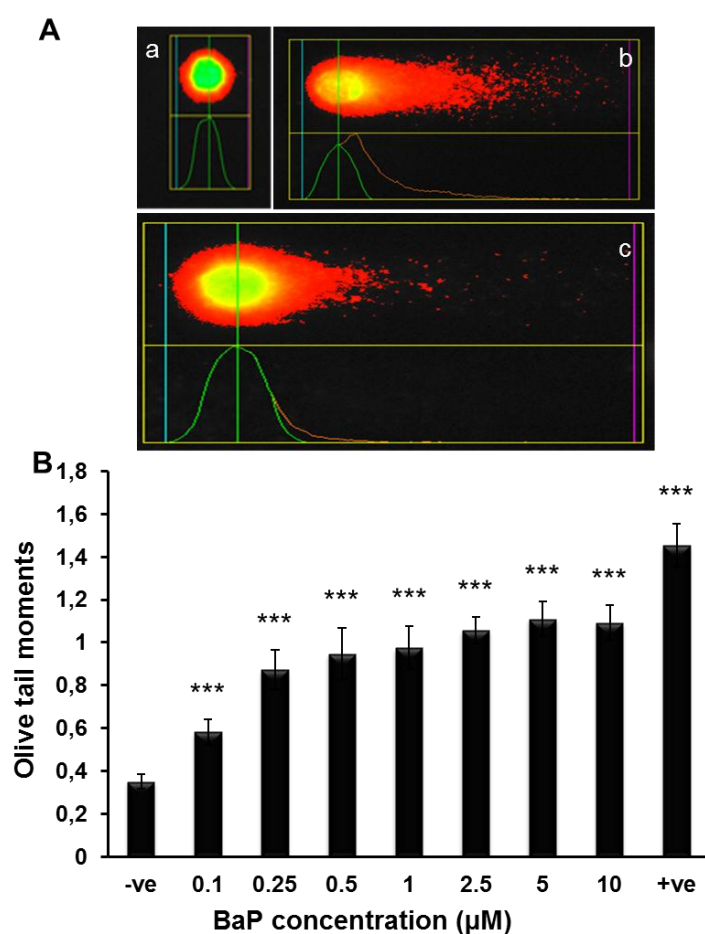


Figure 25: Concentration-dependent increase in B[a]P-induced DNA damage evaluated with the comet assay. (A) Alkaline comet assay images of individual bladder epithelial cells with various degrees of DNA damage: a) unexposed cells, b) positive control (1 mg/ml *N*-ethyl-*N*-nitrosourea (ENU), c) 0.5 μM B[a]P. (B) PUBEC pools were incubated with increasing concentrations of B[a]P (0.1-10 μM) for 24 h, and ENU was used as positive control. As indicator for DNA strand breaks, the olive tail moment is expressed as mean \pm standard deviation obtained in three independent experiments with pooled PUBEC cultures. The level of significance relative to controls was determined by using the t-test (***) $p < 0.001$.

5.5 B[a]P induced changes expression of proteins involved in apoptosis

Notably, many of the identified proteins were associated with another very interesting network involving TP53 (**Figure 24**). Other than its role in genome stability, senescence, DNA repair, and cell cycle arrest, TP53 is known to play a major role in the induction of apoptosis. PUBEC exposed to B[a]P showed a differential expression of Cathepsin D, VDAC 2, HSP27, and HSP70, proteins known to be involved in the intrinsic mitochondrial death receptor pathway. To find out whether B[a]P exposure indeed induced mitochondria-associated apoptosis, changes in mitochondrial potential were assessed and the TUNEL test was employed.

5.6 Analysis of mitochondrial alterations following B[a]P exposure

In order to validate whether the mitochondrial dysfunction was involved in B[a]P-induced apoptosis, the mitochondrial membrane potential (MMP) was measured in PUBEC by using Rhodamine 123. As indicated by the decrease of fluorescence intensity of Rhodamine 123 (**Figure 26**), the MMP was significantly impaired at a B[a]P concentration of 0.5 μM after exposure times of 2, 6, and 12 h, with the maximum impairment being observed after 2 h ($p < 0.001$ in all experiments). However, the MMP was nearly reconstituted after 24 h of exposure.

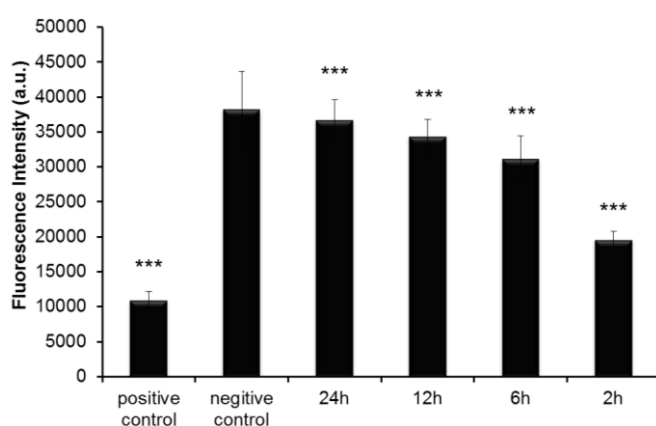


Figure 26: Determination of the MMP of PUBEC by using the monovalent cationic dye Rhodamine 123. Cells were cultured on collagen-coated 96-well plates with a clear bottom and were exposed to 0.5 μM B[a]P for different time periods (2, 6, 12, and 24 h). Valinomycin (100 μM) was used as positive control, while as negative control cells were only exposed to cell culture medium. Rhodamine 123

(5 μM) was applied for 30 min. The measurements were performed by using an ELISA plate reader ($\lambda_{\text{excitation}} = 488$; $\lambda_{\text{emission}} = 535$ nm). A significant decrease in MMP in a time-dependent manner was observed. The data were presented as mean \pm standard deviation of three independent experiments with pooled PUBEC cultures. The level of significance relative to the positive control was determined by using the t-test (*** $p < 0.001$).

5.7 Application of western blot and TUNEL assay for analysis of apoptosis in PUBEC

Next, the validation of the p53-regulated apoptotic proteins modulated in response to B[a]P exposure was sought. The TUNEL assay and immunochemical quantification were used to confirm these findings. The percentage of apoptotic PUBEC was determined by counting the number of positively stained pig epithelial cells and total epithelial cells in a ten-field (**Figure 27A**). The number of TUNEL-positive cells noticeably increased in the presence of 0.5 μM B[a]P ($n = 6$ independent experiments, $p < 0.05$), whereas apoptotic cells were barely detectable in control epithelial cells (**Figure 27B**).

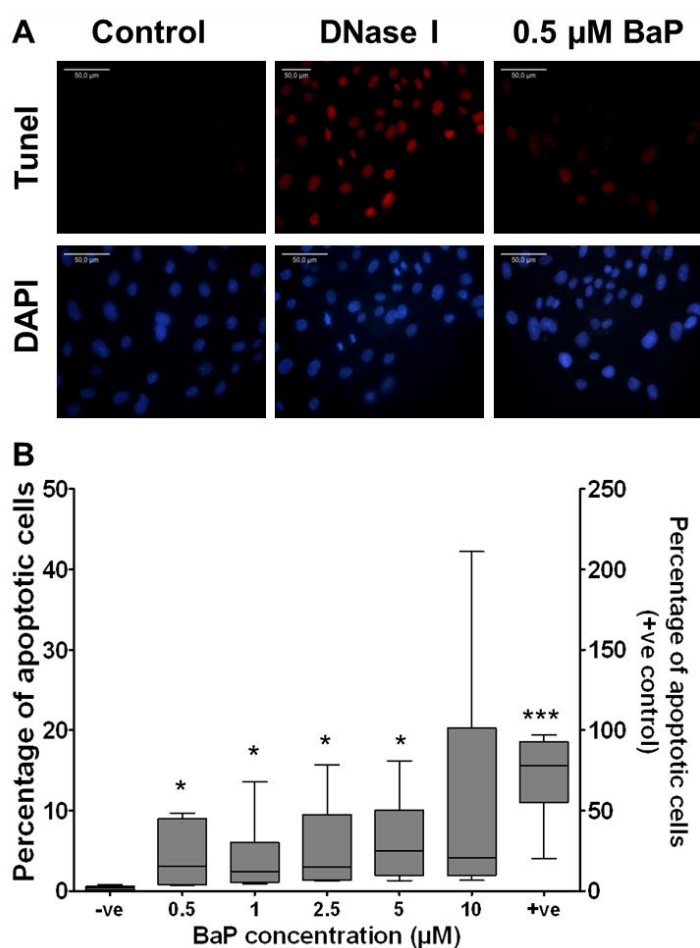


Figure 27: Analysis of pig urinary epithelial cell apoptosis by the TUNEL assay. Control and B[a]P-exposed (0.5 to 10 μM) PUBEC pools ($n = 6$) were subjected to the TUNEL assay. (A) A TUNEL-positive control was obtained by incubation with DNase I. In control cells exposed to DMSO (<0.1 %), apoptotic cells were hardly detected. However, a marked increase in TUNEL-positive cells was observed in B[a]P-exposed (0.5-10 μM , 24 h) epithelial cells. The white bars represent 50 μm . (B) Box plots (median and interquartile range) show the level of apoptosis in PUBEC pools exposed for 24 h to different concentrations of B[a]P compared to controls. -ve represents PUBEC unexposed to B[a]P, while +ve represents positive controls obtained by incubation of PUBEC with DNase I. The level of significance relative to control was

determined by using the t-test (** $p < 0.001$, * $p < 0.05$).

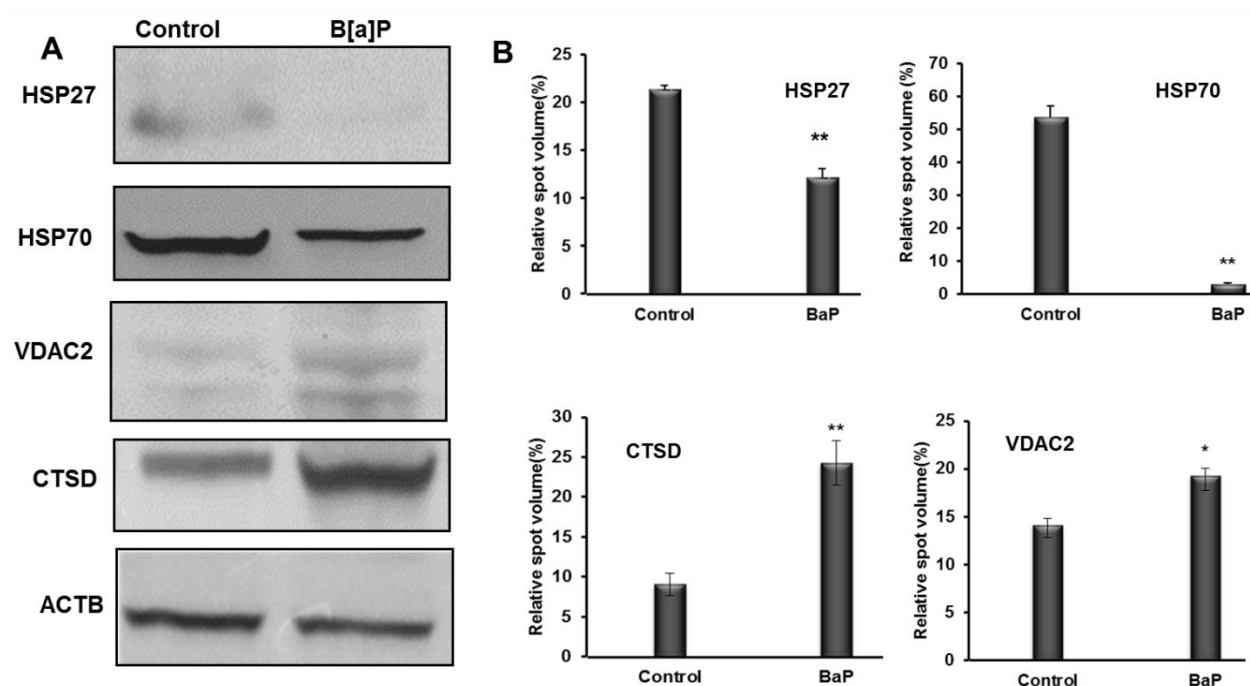


Figure 28: Immunoblot analysis of differentially expressed proteins. (A) Western blot analysis of total protein extracts (30 mg of protein) from three independent lysates from PUBEC exposed to 0.5 μM B[a]P and from controls was carried out on a 12 % SDS gel. Actin was used as loading control. (B) Densitometric analysis of gel bands after western blot analysis. The bars represent the mean of three SEM of gel band density determined in B[a]P-exposed and control PUBEC. The level of significance relative to control was determined by using the t-test (** $p < 0.001$, * $p < 0.05$).

The expression of apoptosis-related proteins identified by MALDI-TOF-MS was determined by using immunoblot analysis. CTSD, VDAC 2, HSP27, and HSP70 were chosen for analysis, as these proteins play a key role in the intrinsic mitochondrial apoptotic pathway. The analysis confirmed the increased abundance of Cathepsin D and VDAC 2 and a decreased expression of proteins such as HSP27 and HSP7 in PUBEC exposed to 0.5 μM B[A]P when compared to control cells. These findings are consistent with the results obtained by 2DE and MALDI-TOF-MS (**Figure 28**).

6. Blue Native PAGE analysis of B[a]P- and TCDD-exposed cells

6.1 Objective

Multiprotein complexes are vital supramolecular assemblies involved in the regulation of various intracellular processes and signaling pathways. Most molecular processes in the cell result from interactions of different protein complexes. Therefore, a complete understanding of the composition and interactions of these complexes is crucial for the understanding of the molecular mechanisms mediated by these complexes. As detailed in the introduction, B[a]P is a ligand for the aryl hydrocarbon receptor complex (AhR). The same holds true for 2,3,7,8-dibenzo-*p*-dioxin (TCDD), another environmental contaminant. AhR is a cytosolic receptor complex involved in the transcriptional modulation of cell growth and differentiation and, most importantly, in the transcriptional regulation of drug metabolizing enzymes such as cytochrome P450 (CYP). These enzymes help in the detoxification of PAH and other xenobiotics and are also known to affect other cellular processes by interaction with other protein complexes. While a lot of information is available on the interaction of these xenobiotics with the AhR complex, much less is known in regard to their possible effects on other protein complexes.

The understanding of these complexes and the possible interactions between them can shed some light into the possible mechanism of B[a]P-mediated toxicity. Therefore, the present work was carried out to identify and characterize multiprotein complexes by using Blue Native PAGE (2D BN/SDS-PAGE) to elucidate the network of protein-protein interactions that regulate protein functions and hence the toxicity of B[a]P and TCDD. 2D BN/SDS-PAGE permits the separation of multiprotein complexes under native conditions and thus maintains the intact complex. For the enrichment of the complex, subcellular fractionation was performed. 2D BN/SDS-PAGE and subcellular fractionation form an ideal partnership when it comes to the enrichment and analysis of intracellular organelles and of low-abundant multiprotein complexes. Nevertheless, the concurrent study on the effects of B[a]P and TCDD was performed to find out whether the protein expression profiles are similar or different in response to two different classic inducers of the AhR pathway.

6.2 Subcellular fractionation and 2D BN/SDS-PAGE analyses of fractionated samples for proteome map generation

For organellar enrichment, the commercially available subcellular fractionation kit ProteoExtract[®] (Calbiochem, Darmstadt, Germany) was applied. By using this kit, the control cells and cells exposed to B[a]P (0.5 μ M) or TCDD (200 pM) were fractionated into four subcellular compartments: cytosol, membrane/organelle proteins, nuclear, and cytosolic fraction. The method was able to enrich proteins to a certain degree, but a few carryovers from one fraction to another were observed. The proteins from these fractionated samples were then used for 2D BN/SDS-PAGE electrophoresis.

To have an overview about the protein complexes of the RT4 cell line, a suborganellar proteome map was generated by analyzing the complexes of unexposed cells of different fractions by 2D BN/SDS-PAGE analyses. In the gels obtained from five different preparations approx. 200 protein spots per fraction were detected, among which only those spots were identified by MALDI-TOF-MS which showed a significant expression of ± 1.3 in all gels. A total of 64 protein spots were identified in the cytosolic fraction, 65 protein spots for the membrane and organelle fraction and 55 protein spots for the nuclear fraction (**Table 9-11, see annex II**). Interestingly, the identified proteins were enriched; however, some proteins were carried over between the fractions, but with very low inter-experimental variation.

6.2.1 Protein complexes of cytosolic fraction

As discussed for 2D-BN/SDS-PAGE gels [163], the resulting gels showed typical patterns for BN-PAGE experiments, i.e. monomeric proteins within a certain hyperbolic diagonal field, whereas the components of stable protein complexes (subunits of the same protein) arranged in an vertical line under this diagonal field.

By using the above mentioned criteria, MALDI-TOF-MS analysis of this fraction revealed among others many typical cytosolic proteins (**Table 9, see annex II**), such as proteins of the proteasome complex (including both α and β subunits, **Figure 29**, protein spots ID-5 to ID-18), proteins of the lactate dehydrogenase (LDH) enzyme complex (**Figure 29**, protein spot ID 24-29), and the dimeric enzyme complex phosphoglycerate mutase (PGAM, **Figure 29**, protein spot ID 61-63). LDH consists of A and B chains, both of which were identified in the cytosolic fraction. Along with these proteins many proteins involved in glucose metabolism

(phosphoglycerate kinase, isocitrate dehydrogenase, glyceraldehyde-3-phosphate dehydrogenase, UDP-glucose 6-dehydrogenase) were also identified.

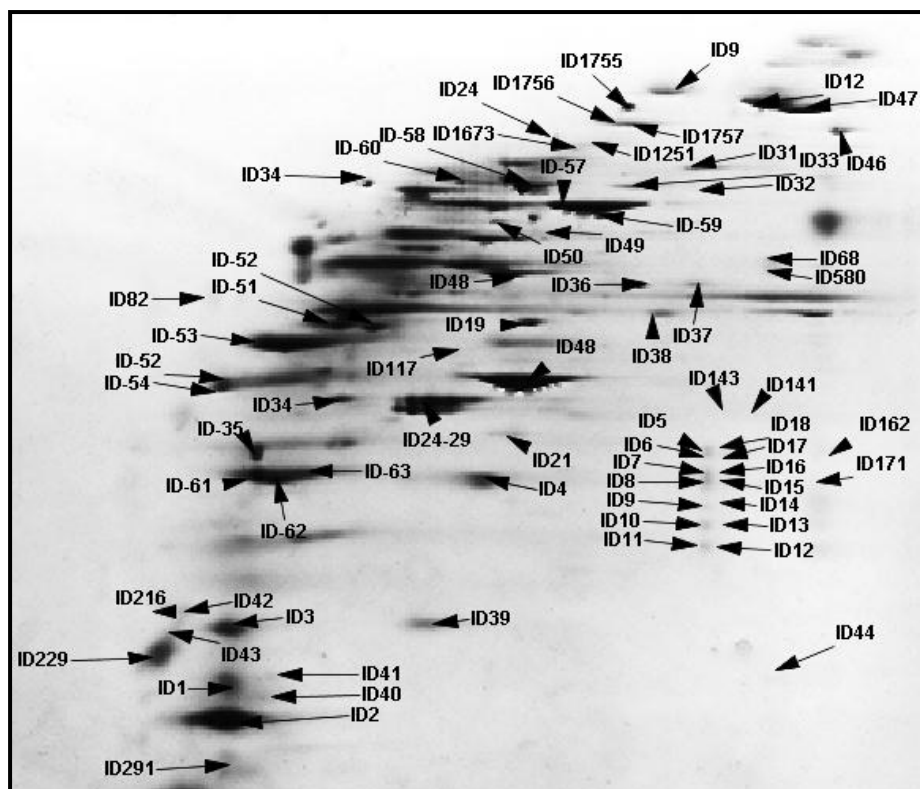


Figure 29: Representative 2D BN/PAGE gel of the cytosolic fraction of RT4 cells. The gels were stained with Coomassie brilliant blue after 4-12 % BN-PAGE and 12 % SDS-PAGE separation followed by identification of the protein spots by MALDI-TOF-MS. The ID number, protein name, molecular weight, Mascot score, and peptide match is listed in **Table 9**.

6.2.2 Protein complexes of the membrane/organelle fraction

The 2D BN/SDS-PAGE analyses of this fraction revealed many mitochondria-related proteins, which include proteins of the respiratory chain ATP synthase complex (alpha and beta subunits of F₁-ATP synthase, **Figure 30**, protein spot ID 60-62) and the alpha and beta subunits of the electron transfer flavoprotein complex (ETF_A and ETF_B). Also, many mitochondrial enzymes, such as mitochondrial malate dehydrogenase 2, NADPH:adrenodoxin oxidoreductase, mitochondrial glutamate dehydrogenase 1, mitochondrial 60 kDa heat shock protein, and NADP(+)-dependent isocitrate dehydrogenase, were also identified. Other than mitochondrial complexes, a few proteins of the endoplasmic reticulum (cyclophilin B complexed with cyclosporine and calreticulin (**Figure 30**, protein spot ID 24-25) and of the cytoskeleton (actin-binding ARP2/3 complex, **Figure 30**, protein spot ID no 7-12) were also detected (**Table 10**, see annex II).

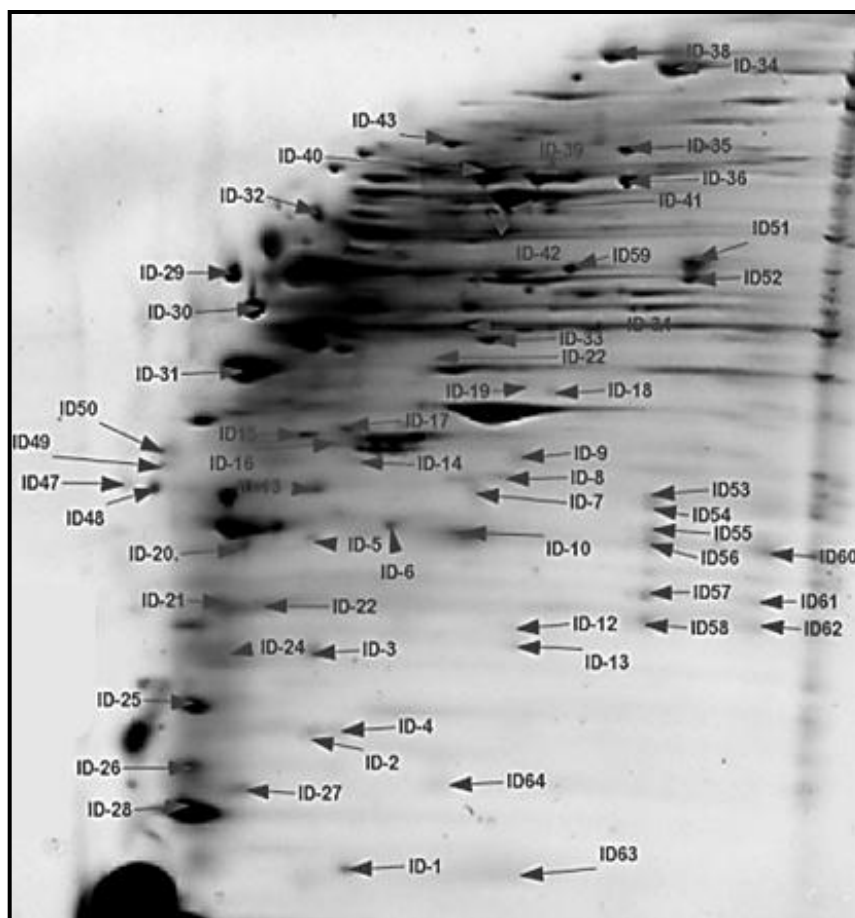


Figure 30: Representative 2D BN/PAGE gel of the membrane/organelle fraction of RT4 cells. The gels were stained with Coomassie brilliant blue after 4-12 % BN-PAGE and 12 % SDS-PAGE separation followed by identification of the protein spots by MALDI-TOF-MS. The ID number, protein name, molecular weight, Mascot score, and peptide match is listed in **Table 10**.

6.2.3 Protein complexes of the nuclear fraction

In the nuclear fraction several proteins belonging to the nuclear matrix (lamins), nucleosome (histone core complex proteins), and proteins related to DNA processing (DNA polymerase α , HnRNPs) were detected (**Table 11, see annex II**). Lamins exist as a homodimer consisting of lamin A and lamin C. Of these two, lamin A along with a wide range of cytoskeletal proteins (cytokeratin 19, 7, 8, and 17) were identified. Other than structural proteins, proteins of the histone core complex were found. This complex exists as an octamer occurring at the center of a nucleosome core particle. It consists of two copies of each of the four core histone proteins (H2A, H2B, H3, and H4), and as tetramer of two copies of both H3 and H4 complexed with two H2A/H2B dimers. In the samples both monomers and dimers of histone proteins were found separated in close proximity to each other. Additionally, many proteins

involved in DNA processing, such as subunits of Pol I complex, HnRNP/splicing factor (Heterogeneous nuclear ribonucleoprotein, Serine/arginine-rich splicing factor 9, and Heterogeneous nuclear ribonucleoproteins A2/B1 isoform A2), ribosomal protein (60s ribosomal protein L10a), DNA/RNA-binding proteins (ATP-dependent RNA helicase A, RNA-binding protein 4 isoform 3, DNA topoisomerase 2-beta, and DNA2-like helicase), and transcription factors (Homeobox B7) were also identified.

6.3 2D BN/SDS-PAGE analyses of fractionated samples of B[a]P-and TCDD-exposed cells

After establishing the proteome map of protein complexes in our cell model (RT4 cell line), 2D BN/SDS-PAGE analyses was applied to reveal alterations in these complexes after exposure to B[a]P or TCDD. The cells exposed to 0.5 μ M B[a]P or 200 pM TCDD and control cells were fractionated as described in the Materials and Methods chapter. After fractionation 2D BN/SDS-PAGE analyses of cytosolic, membrane/organelle, and nuclear fraction were carried out for B[a]P- and TCDD-exposed and for control cells. To reveal differential expressions of protein complexes in control cells and cells exposed to B[a]P or TCDD, gels from five different experiments for all three fractions were compared by using the Decodon software (as described in the Materials and Methods chapter). Only those proteins were considered significant which showed an expression change of ± 2 . The entire process of analysis with the Decodon software was repeated individually for all three fractions exposed to B[a]P or TCDD and the control samples. In total, more than 200 spots were found in each fraction, with a differential expression of 19 proteins in the cytosolic fraction, of 23 proteins in the membrane/organelle fraction, and of 8 proteins in the nuclear fraction for TCDD-exposed cells, while 15 proteins in the cytosolic fraction, 21 proteins in the membrane/organelle fraction, and 18 proteins in the nuclear fraction were differentially expressed in the B[a]P-exposed cells (**Table 11.1-11.6, see annex III**). Representative images of 2D BN/SDS-PAGE of all three fractions are shown in (**Figure 36-38, see annex IV**). Protein spots identified as proteins with statistically significant expression differences between control and exposed cells were marked.

6.4 Alterations in calcium- and iron-containing proteins

MALDI-TOF-MS analysis of the differentially expressed proteins yielded many proteins involved in calcium and iron homeostasis in both TCDD- and B[a]P-exposed cells (**Table 8**).

Table 8: List of calcium- and iron-associated proteins with altered expression (≥ 2) after B[a]P or TCDD exposure compared to controls

Identified calcium-containing proteins differentially regulated in control and TCDD-exposed RT4 cells. Representative images of 2D BN/SDS-PAGE marked with differentially expressed proteins are shown in **Figure 37** and **Figure 38, annex IV**

Spot ID no	gene name	protein name	subcellular fraction	regulation
ID 231	CALM1	calmodulin	cytosol	2.13139
ID203	S100A2	protein S100-A2	cytosol	3.8684
24	ANXA10	annexin A10	membrane/organelle proteins	1.02979
25	ANXA5	annexin A5	membrane/organelle proteins	1.34865
16	GSN	gelsolin isoform b	membrane/organelle proteins	1.08039

Identified calcium-containing proteins differentially regulated in control and B[a]P-exposed RT4 cells. Representative images of 2D BN/SDS-PAGE marked with differentially expressed proteins are shown in **Figure 38, annex IV**

Spot ID no	gene name	protein name	subcellular fraction	regulation
31	PPIB	cyclophilin B	membrane/organelle proteins	1.74984
43	PPIA	cyclophilin A	membrane/organelle proteins	3.41278
30	ANXA10	annexin A10	membrane/organelle proteins	-3.95467
19	CALR	calreticulin	membrane/organelle proteins	2.15407

Identified iron-containing proteins differentially regulated in control and TCDD-exposed RT4 cells. Representative images of 2D BN/SDS-PAGE marked with differentially expressed proteins are shown in **Figure 37** and **Figure 38, annex IV**

Spot ID no	gene name	protein name	subcellular fraction	regulation
ID172	HEBP2	heme-binding protein 2	cytosol	2.03805
ID1755	FTH1	ferritin	cytosol	-2.68431
ID5,6	TFRC	transferrin receptor protein 1	membrane/organelle proteins	1.35857

Particularly in the TCDD-exposed cells a unique cluster of three protein spots was observed (**Figure 31**) that was missing on the gels of the B[a]P- and the nonexposed cells. Two out of three protein spots were identified as calmodulin and protein S100-A2. Modulations of calcium- and iron-containing proteins upon exposure to TCDD or B[a]P have been reported before, however, none of the studies till date has suggested that a possible interaction between these two protein systems might exist.

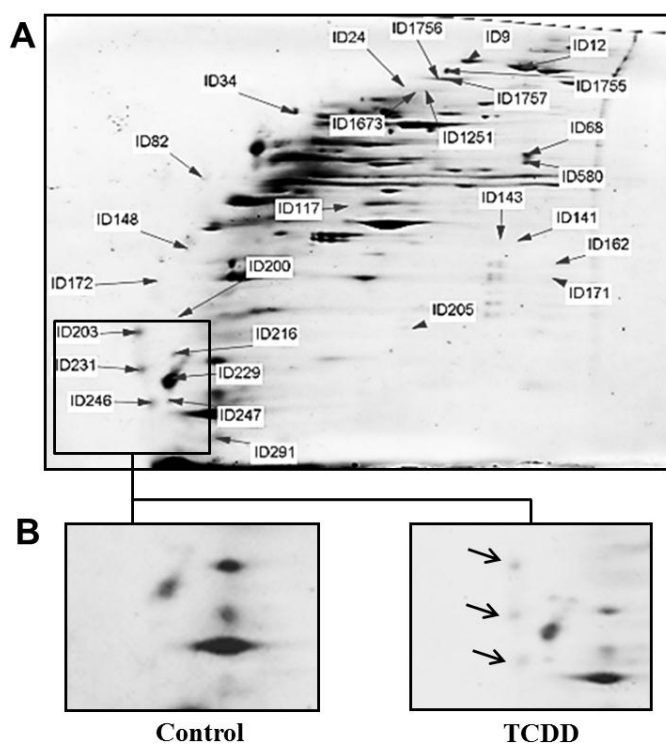


Figure 31: Protein complexes differentially expressed in control and TCDD-exposed RT4 cells. [A] BN-PAGE gel from cytosolic fraction of TCDD-exposed cells subjected to SDS-PAGE in the second (vertical) dimension. Control and TCDD-exposed samples were separated and compared by using the Delta2D v4 software. [B] Arrows represent the gel image region of differential expression of three protein spots only in TCDD-exposed samples. Protein spots of interest were excised, trypsin-digested, and subjected to analysis by MALDI-TOF-MS. The identified proteins with ID no are listed in **Table 11 1**, annex III.

In a few recent studies the role of calmodulin (CaM) in AhR-dependent and -independent genomic responses after exposure to these compounds have been indicated. Other researchers reported a TCDD-mediated impairment of cellular iron homeostasis due to a changed ferritin content associated with transferrin (TfR-1) induction. Based upon these studies and the expression of both calcium- and iron-containing proteins observed in the TCDD- and B[a]P-exposed samples, it is hypothesized that these two protein systems might interact *via* the nitric oxide synthase enzyme. Accordingly, a rapid increase in intracellular calcium ion concentration occurs upon exposure to TCDD or B[a]P, which activates the major calcium sensor CaM. CaM further activates the nitric oxide synthase, which in turn modulates the labile iron pool through nitric oxide production (details of this hypothesis is given in the discussion section of the thesis). The following experiments were carried out to prove this hypothesis.

6.5 Analysis of intracellular calcium changes after B[a]P and TCDD exposure

To monitor whether exposure to B[a]P or TCDD for 24 h alters the intracellular calcium concentration the fluorescence indicators Fluo-4 and Rhod-2 were used. The fluorescence measurement with Fluo-4 revealed an increase of intracellular calcium by 21 % in the B[a]P-exposed cells, whereas an elevated level of 27 % was found in the TCDD-exposed cells. The

determination of calcium in internal calcium stores with Rhod-2 showed significantly raised levels for both exposure groups. The B[a]P-exposed cells exhibited a 12 % higher calcium level than that of controls, while in the TCDD-exposed group an increase of 30 % was observed compared to control cells (**Figure 32**). In some studies a transient increase in $[Ca^{2+}]_i$ that occurs 2–5 min after the addition of an apoptosis-inducing agent have been observed. However, such an increase in both B[a]P- or TCDD-exposed cells was not found in the present experiments.

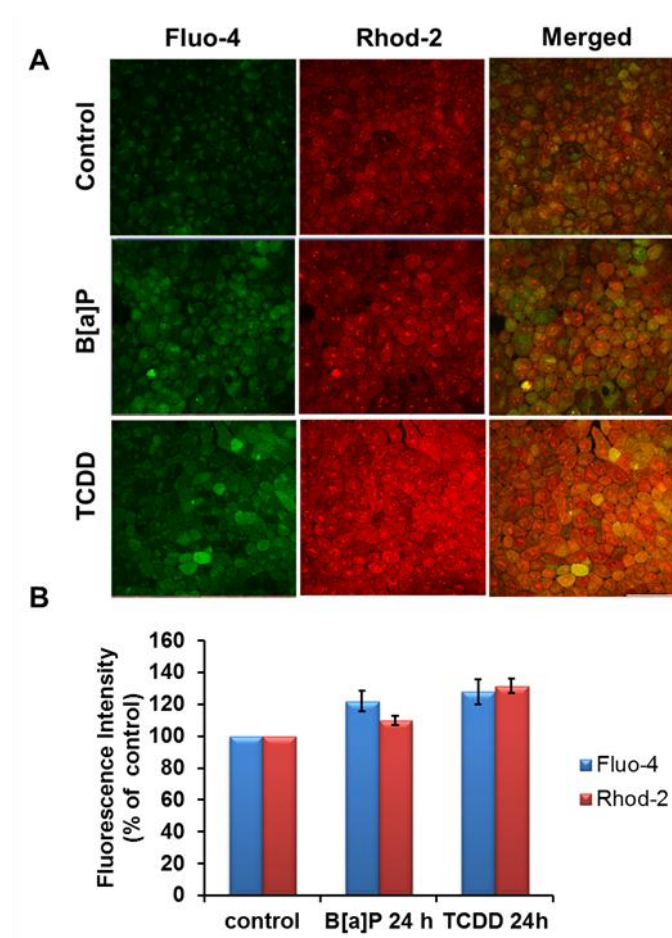


Figure 32: Alterations of cellular calcium homeostasis after exposure to B[a]P or TCDD. Cells were cultured on collagen-coated glass coverslips and loaded with Fluo-4/AM (1.4 μ M) and Rhod-2 AM (3.6 μ M) for 30 minutes at room temperature, followed by incubation for another 30 min at 37 $^{\circ}$ C after exposure to 200 pM TCDD for 24 h. The fluorescence was recorded by using a laser-scanning microscope (Fluo 4/AM, $\lambda_{excitation}$ = 488; $\lambda_{emission}$ = 505 nm, Rhod-2/AM, $\lambda_{excitation}$ = 543; $\lambda_{emission}$ = 560 nm). [A] Fluorescence images of control, TCDD- and B[a]P-exposed cells loaded with Fluo-4 and Rhod-2. [B] Statistical analysis of intracellular calcium levels following treatment of RT4 cells with 0.5 μ M B[a]P or 200 pM TCDD. Data are expressed as percentage of calcium levels found in unexposed cells, arbitrarily set to 100 %. The results correspond to the mean \pm S.D of four independent experiments. The

white bar represents 50 μ m.

6.6 Effects of B[a]P and TCDD on the labile iron pool (LIP) and the possible role of calcium

To prove whether the changes in the expression of proteins involved in iron homeostasis led to alterations in the LIP, the chelatable iron pool of the RT4 cell line was determined by using the fluorescent probe Phen GreenTM SK (PG SK). Control cells and the cells exposed to 0.5 μ M B[a]P or 200 pM TCDD for 3 h and 24 h, respectively, were loaded with PG SK for the analysis. In the cells exposed to TCDD for both 3 h and 24 h, the LIP increased moderately compared to control cells (about 7 % and 13 %, respectively), whereas no effect on the cellular LIP was observed in B[a]P-exposed cells (**Figure 33**). To analyze whether the calcium sensor protein calmodulin (CaM) was responsible for the TCDD-induced increase in LIP, the cells were blocked with the CaM antagonist W-7 (10 μ M), followed by treatment of the cells with 200 pM TCDD for 3 h and 24 h. During the initial three hours, W-7 inhibited the TCDD-mediated increase of LIP, and to a lesser extent this effect was also observed in the cells exposed for 24 h. These results demonstrated that CaM was activated by TCDD and that it was somehow modulating the iron content of the cells.

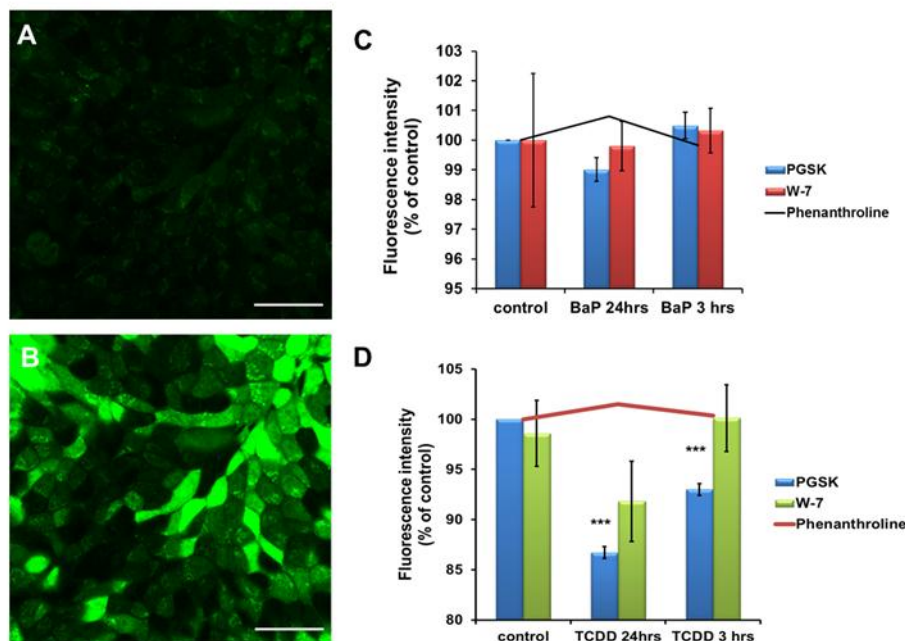


Figure 33: Measurement of the chelatable iron pool by PG SK. For confocal images cells were cultured on glass coverslips and loaded with 20 mM PG SK (10 min, 37 °C) after exposure to 200 pM of TCDD for 24 h. Cellular fluorescence was excited at 488 nm by using a laser scanning microscope (LSM 510) equipped with an argon laser. For emission, a 505 nm longpass filter was used. Cellular microfluorographs of (A) TCDD-exposed cells and (B) cells after dequenching with 1,10-phenanthroline. The white bar represents 50 μ m. The changes in intracellular iron was determined by the differences in cell fluorescence of control against [C] B[a]P- or [D] TCDD-exposed cells as described in Material and Methods. Data are expressed as percentage of iron levels found in unexposed cells, arbitrarily set to 100 %. The results correspond to the mean \pm S.D of four independent experiments. The level of significance relative to control was determined by using the t-test (***) $p < 0.0001$.

6.7 Possible involvement of nitric oxide (NO) in calmodulin-modulated iron content of cells

Finally, to analyze whether the changes in LIP of the cells was mediated by nitric oxide synthase (NOS) *via* calmodulin, the NO content of the cells was determined first. The measurement of the nitrite and nitrate concentrations (as a measure of NO) with the Griess reagent revealed an increase of NO in B[a]P-exposed cells by 153 % (compared to control) and in TCDD-exposed cells by 96 % (compared to control) (**Figure 34**). The experiments were also performed at higher concentrations of B[a]P (5 μ M) and TCDD (1000 pM). Here, NO production increased considerably at both concentrations (111 % and 78 %, respectively) when compared to that in control cells.

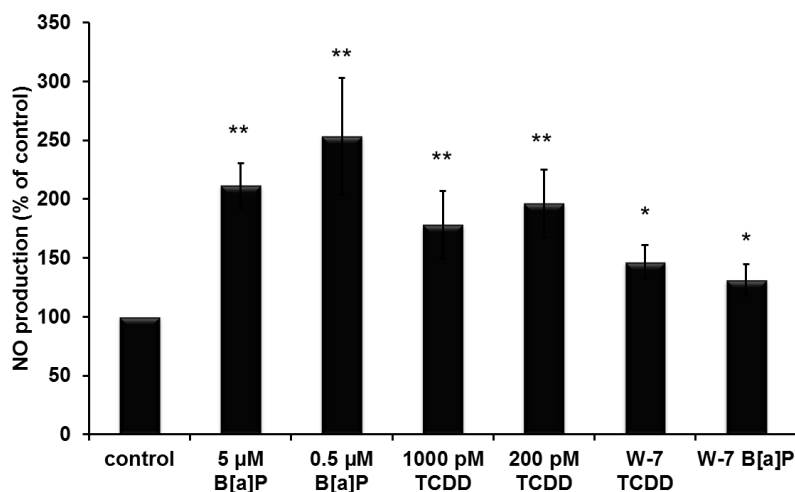


Figure 34: NO production after exposure to TCDD or B[a]P in normal and W-7-inhibited RT4 cells. 4.0×10^6 cells were exposed to TCDD or B[a]P alone or in a co-treatment with $10 \mu\text{M}$ W-7 (for 10 min). After 24 h of exposure, the medium was used for the determination of the NO content by using the Griess assay. Data are expressed as percentage of NO levels found in unexposed

cells, arbitrarily set to 100 %. The results correspond to the mean \pm S.D of four independent experiments. The level of significance relative to control was determined by using the t-test (** $p < 0.001$, * $p < 0.05$).

Also, as calmodulin is a key enzyme required for NOS activity, CaM was blocked by using its antagonist W-7. W-7 decreased the basal levels of NO both in (200 pM) TCDD- and (0.5 μM) B[a]P-exposed RT4 cells by 50 % and 122 %, respectively ($p < 0.05$, **Figure 34**) when compared to non-inhibited cells. These results suggest that CaM is a necessary signal for NOS that, in turn, is capable of regulating iron metabolism by producing NO.

7. Discussion

Benzo[a]pyrene (B[a]P), a five-ring polycyclic aromatic hydrocarbon, is a well-recognized environmental pollutant found in coal tar, automobile exhaust fumes (especially from diesel engines), in smoke resulting from the combustion of organic material (including cigarette smoke), and in charbroiled food. It is known to cause lung, breast, and cervical cancer; whether it plays a role in bladder cancer development is still discussed. The ubiquitous presence of B[a]P in the environment and its potential involvement in the most important urologic malignancy was the rationale to investigate how and to what extent it is taken up by urothelial cells and which are the effects induced by this environmental chemical, especially at the protein level. A well-established primary urinary bladder epithelial cell model (PUBEC), isolated from bladders of freshly slaughtered pigs were used for the major part of the studies. In addition, to investigate B[a]P-induced effects on protein complexes (by Blue Native PAGE analysis), the human urinary bladder epithelial cell line RT4 was utilized.

7.1 Uptake and subcellular distribution of B[a]P

As in many other instances of carcinogenic compounds, considerable attention has been given so far to the genotoxic effects of B[a]P and to its metabolic activation to reactive intermediates. In contrast, essentially no information has been gathered on its uptake and subcellular distribution, processes that necessarily precede all other biological events occurring after the exposure. Nevertheless, as the presence of small quantities of non-metabolized B[a]P in addition to that of its hydroxylated metabolites in urine has been demonstrated and because B[a]P is a highly lipophilic compound, the possibility that it is taken up by the urothelium cannot be ignored. In this thesis, the pattern of cellular uptake and distribution of B[a]P in pig urinary epithelial cells is reported for the first time.

In many studies the fluorescent properties of B[a]P, resulting from the multi-fused aromatic rings with delocalized π bonds, have been utilized to monitor the mixed-function oxygenase activity by applying flow cytometry, laser cytometry, and confocal microscopy [175-177]. Here, the uptake of B[a]P by pig bladder epithelial cells was analyzed by using confocal microscopy. This technique did not only allow to study and visualize the intracellular distribution of B[a]P but also helped in minimizing the photobleaching of B[a]P due to unwanted collateral non-confocal irradiation. In the cells exposed to 0.5 μ M B[a]P (for 2, 6, 12, 18, and 24 h), the first indication of cellular uptake of B[a]P was obtained after 6 h of

exposure (**Figure 16**), while no signs of B[a]P uptake were apparent after the initial 2 h (data not shown). Also, in contrast to studies with other cell lines in which a saturation of B[a]P uptake was observed as early as 5 min and 4 h, respectively [41, 178], there was no evidence of approaching uptake saturation in PUBEC during the entire exposure period of 24 h. Nevertheless, B[a]P uptake was markedly different in the various PUBEC pools used for the study (**Figure 16**). The variation in uptake kinetics of B[a]P in PUBEC seems to reflect the situation in humans where a wide variation in the toxic response to B[a]P and other PAH is observed.

As reported for other cell types [179], B[a]P rapidly distributes into the cell membrane (**Figure 17A**). This rapid uptake of B[a]P can be attributed to its highly lipophilic character and to the wide range of lipoproteins contained in the plasma membrane. It has been speculated that these proteins facilitate the rapid uptake of B[a]P into the cell membrane [180]. A small but significantly higher amount of B[a]P compared to control cells was also found in the cytosol and nucleus of PUBEC (**Figure 17B**). The uptake of B[a]P by these cell compartments has been reported in a few other studies [181]. There are some indications that B[a]P is not only metabolized by cytosolic enzymes but also in the nuclear compartment. It has been shown in various studies that monooxygenases/hydroxylases are not only active in the cytosol but are also present in the nuclear envelope [182-184].

After having analyzed the time-dependent uptake and subcellular distribution of B[a]P by using confocal microscopy, spectrofluorometric and GC-MS techniques were applied to quantitatively determine the uptake by PUBEC exposed to low (0.5 μM) and high (10 μM) B[a]P concentrations. An *ex situ* calibration method was applied for which standard solutions of B[a]P in a cytosolic medium (as described in the Materials and Methods chapter) were prepared to obtain a homogenous solution and to mimic the intracellular environment. B[a]P does not form homogenous solutions with various organic solvents. Similar to the initial uptake studies, two distinct subpopulations of PUBEC were found with regard to the intracellular B[a]P concentrations: In cells exposed to 0.5 μM B[a]P, the intracellular B[a]P concentrations ranged from 7.28 μM to 10.75 μM in one subpopulation and from 23.17 μM to 35.07 μM in the other one. The corresponding ranges of values for the two subpopulations of cells exposed to 10 μM B[a]P were 29.9 μM to 48.31 μM and 373.72 μM to 406.64 μM , respectively. An increased metabolic turnover originating in an increased induction of B[a]P-metabolizing enzymes may be the reason for the lower intracellular B[a]P concentrations in one of the PUBEC subpopulations. PUBEC have been shown to express inducible

cytochrome P450 isoenzymes, which is of particular relevance since these enzymes contribute to the activation of B[a]P to carcinogenic metabolites [171, 172, 185, 186]. The formation in PUBEC of 3-OH-B[a]P, one of the major B[a]P metabolites, is reported for the first time. 3-OH-B[a]P has often been used as biomarker for assessing internal exposure to PAH [187, 188]. GC-MS analysis revealed that this metabolite is present in all of the B[a]P-exposed PUBEC (**Figure 18B**). It is the first reported proof that oxygenated B[a]P metabolites are actually formed in this cell model.

In summary, the results of the uptake studies indicate that urinary bladder epithelial cells are able to incorporate B[a]P, which may come in contact with the epithelium either directly during urinary excretion or by diffusion from the capillaries in the *lamina propria*. The uptake of B[a]P by these cells and their ability to metabolize this chemical to reactive intermediates strongly supports the hypothesis that B[a]P may act as a urinary bladder carcinogen. Moreover, the uptake differences found in the studies may be one of the reasons for the varying carcinogenic response to PAH exposure observed in humans [189].

7.2 Development of a 2DE proteome map of PUBEC

Historically, the use of cell lines is well established in proteomic research. However, the most important disadvantage of note while using a cell line is the loss of some critical physiological traits that are inherent in the process of stable cell line creation [190]. Urinary bladders from freshly slaughtered pigs were used for generating the first 2DE reference proteome map of bladder epithelial cells as a valuable reference resource for comparative studies [191]. In total, 1000 protein spots with a molecular weight of 20-100 kDa and isoelectric points from 4-10 were detected by using a colloidal Coomassie brilliant blue staining protocol developed in our laboratory. 120 of these spots were identified by tryptic digest and subsequent MALDI-TOF-MS analysis of the peptides (Table 5). During Mascot analysis for protein identification, many proteins were not identified even though mass spectra of high quality were recorded. It became apparent that the available pig database is still incomplete and that homologous sequences from other species are not sufficiently identical to achieve a high enough score to produce a match [192]. The PANTHER classification revealed a broad range of biological processes in which the identified proteins were involved (**Figure 35**). Proteins taking part in biotransformation, energy metabolism, structural, signaling, and stress pathways were identified even under basal conditions. Of considerable interest were proteins associated with cell stress and detoxification (GSTP1, PRDX2, HSP60, HSP71, HSP70, HSP90, and HSP27).

GSTP1 and PRDX2 are proteins involved in detoxification processes (through redox regulation), and have emerged as significant candidates for cancer biomarker development [193-195]. Seven proteins related to carbohydrate metabolism were identified, which is of great interest for studying bladder-related diseases as there are distinct carbohydrate profiles in normal and tumor tissues [196]. Other than these, many cytoskeletal proteins (KRT7, KRT17, KRT10, KRT19) were identified which do not only provide structure stability to the cells but have also been implicated in malignant transformation *via* a differential regulation of the actin-based cytoskeleton [197].

Precipitation, a conventional and economical method of enriching proteins of interest, was used for isolating phosphoproteins. Phosphorylation is a posttranslational modification principally of serine, threonine, or tyrosine residues of proteins. Enrichment of phosphoproteins is essential because of their low abundance. Many methods involving enhancement of phosphoproteins by precipitation with calcium and barium phosphate have been suggested [198-200]. Often these methods are tedious and time-consuming, and the amount of precipitated proteins is not sufficient to be separated on gels. In our laboratory, a method for the enrichment of phosphoproteins by precipitation with lanthanum ions (La^{3+}) prior to 2DE separation and mass spectrometric identification was developed [160]. Because of its strong electropositive properties and its preference for oxygen-containing anions, lanthanum ions form very tight complexes with most common biological ligands such as carboxyl and phosphate groups [201]. By using this method, 31 phosphoproteins were identified in PUBEC (**Table 6**). Phosphorylation of many calcium-containing proteins (calumenin, clathrin, calpain, and calreticulin) was observed in these cells. Among them, the differential regulation of calreticulin (CALR) has been reported in several cancerous tissues such as breast, colon, and liver tumors [202-204]. CALR has also been discussed in many recent studies as a suitable marker for the diagnosis of bladder cancer [205, 206]. Other than that of calreticulin, the phosphorylation of clathrin, a protein involved in the transactivation of p53 target proteins [207-210], was observed. Moreover, three proteins of the electron transport chain (NADH-cytochrome b5 reductase 3, NADPH-cytochrome P450 reductase, cytochrome b5), required by the bladder for the energy-demanding maintenance of urine storage and removal, were discovered [211]. Collectively, with the current work a comprehensive 2DE proteome map along with a phosphoproteome map of healthy bladder epithelial cells were reported for the first time. The map can prove as a useful source of information for bladder cancer studies and especially for studies involving pigs (as model system) where information is still very scarce.

7.3 Toxicoproteomic analysis of B[a]P-mediated toxicity in PUBEC

After the 2DE map of PUBEC had been established, these cells were used for analyzing the protein-protein interactions involved in B[a]P-mediated toxicity. After B[a]P exposure for 24 h approx. 40 proteins showed significant changes in expression levels. Twenty-five of these proteins were successfully identified by MALDI-TOF-MS analysis (**Table 7**). When the biological networks of the identified and differentially expressed proteins were analyzed by using the STRING software, three nodes of interest involving TP53, XPC, and splicing genes were indicated (**Figure 24**). Four of the differentially associated proteins (RAD23A, RAD23B, PMSD5, and PMSD4) were related to the xeroderma pigmentosum, complementation group C (XPC) protein system. XPC is a part of the core incision complex of the mammalian nucleotide excision repair (NER) system that is involved in the elimination of a wide variety of DNA lesions, mostly of carcinogen-induced bulky DNA adducts related to tobacco smoke [212, 213]. B[a]P, one of the components of tobacco smoke, is known to cause DNA damage [214]. The sequence of events that occur during DNA repair can be divided into recognition, unwinding, incision, and repair synthesis [215]. RAD23, PMSD5, and PMSD4 play a crucial role in DNA repair [216] and are up-regulated after B[a]P exposure complexed with RAD4, another nuclear protein. The RAD4/RAD23 complex is involved in the recognition of DNA adducts [217]. The up-regulation of these proteins suggests that B[a]P exposure for 24 h leads to DNA damage in bladder epithelial cells. These findings were supported by the concentration-dependent increase in olive tail moments as determined by the comet assay. A significant increase ($p < 0.001$) was observed even at a low B[a]P exposure concentration (**Figure 25**). These findings were also in agreement with the results of the metabolism studies, where the formation of 3-OH-B[a]P, a likely precursor of genotoxic B[a]P metabolites, was demonstrated in PUBEC exposed to 0.5 and 10 μM B[a]P. Overall, the synopsis of the results obtained by the proteomic, genotoxicity, and metabolism studies substantiate the hypothesis that B[a]P is capable of causing DNA damage in bladder epithelial cells by generation of ultimate carcinogenic intermediates [218].

Interestingly, for the proteins differentially regulated in B[a]P-exposed PUBEC, one node of interest involving TP53 was observed. One of the most dramatic responses to p53 activation is the induction of apoptosis [219]. DNA damage induces cell cycle arrest that as well as apoptosis is related to the mutation status of p53 [220]. A lack of functional p53 inactivates the G1 checkpoint, and the cell proceeds to the G2/M phase arrest notwithstanding DNA

damage. The G2/M phase arrest is only transient, however, and the cell proceeds in the presence of the damaged DNA to an unscheduled premature mitosis that develops into a mitotic catastrophe and to apoptosis [221]. Two p53-induced apoptotic pathways have been proposed: the intrinsic mitochondrial and the extrinsic death receptor pathway [222]. Generally, the cells committed to die *via* p53-dependent apoptosis typically follow the intrinsic apoptotic mitochondrial pathway. The STRING pathway analysis indicated that four of the differentially regulated proteins (VDAC2, CTSD, HSP27, and HSP70) were related to this pathway. To validate these findings, the mitochondrial membrane potential (MMP) of PUBEC exposed to 0.5 μ M B[a]P for different time periods was measured (**Figure 26**). The MMP decreased within 2 h of exposure, however in contrast to the previous reports, it was nearly re-established after an exposure period of 24 h, thus indicating that B[a]P-mediated apoptosis is not entirely dependent on the intrinsic mitochondrial apoptotic pathway [223].

Consistent with the 2DE data, western blot analysis also revealed an up-regulated expression of VDAC2 and CTSD, while the expression of HSP27 and HSP70 was down-regulated (**Figure 28**) HSP27 and HSP70 are known for their anti-apoptotic regulation. Both proteins, when present in abundance, suppress mitochondrial damage and nuclear fragmentation, and hence apoptosis [224, 225]. Since the expression of both proteins was decreased in PUBEC after B[a]P exposure, they may be responsible for the B[a]P-mediated apoptosis in PUBEC. On the other hand, while the up-regulation of CTSD is in support of the observed B[a]P-induced apoptosis, the up-regulation of VDAC2 is not. In addition to its role as a porin ion channel protein, it is also known to be involved in apoptotic signaling. The down-regulation of VDAC2 leads to mitochondrial membrane permeabilization and to apoptosis [226]. The observed up-regulation of this protein, as also supported by the results of the MMP measurements points towards the struggle of the cells to avoid cell death. Similar results were reported for 5L rat hepatoma cells exposed to TCDD [227]. The exact role of VDAC2 in mitochondrial apoptosis remains controversial. On the one hand, this protein has been implicated in forming an open pore through which cytochrome c and other proteins can be released from the mitochondrial intermembrane space to the cytosol to induce apoptosis [228]. On the other hand, it has been suggested to form a closed pore that promotes the permeabilization of the MMP by completely block the flux of metabolites [229]. In either case, further studies are required to elucidate the precise role of VDAC2 in xenobiotic-induced apoptosis.

7.4 2D BN/SDS-PAGE analysis for the identification of protein complexes involved in B[a]P toxicity

Interactions between different protein complexes are responsible for many biological processes such as cell-cell signaling, cell cycling, folding, and transport [230]. These diverse structures operate to boost signaling efficiency, ensure specificity, and increase sensitivity of the biochemical circuitry [231]. There are a variety of conventional (liquid chromatography, ultracentrifugation, and sucrose density gradient centrifugation) and non-conventional (co-immunoprecipitation, epitope-tagging, tandem affinity purification, and GST-pulldown methods available for the isolation of these multiprotein complexes [232]. However, most of these techniques often separate a population of multiprotein complex assemblies. To isolate individual complexes, further separation is required which can be achieved by 2D BN/SDS-PAGE. This technique involves the use of the anionic dye Coomassie brilliant blue instead of an ionic detergent to introduce the negative charge on the multiprotein complex. As a result, the multiple protein complexes are separated due to the sieving effect of the polyacrylamide gel, but the protein-protein interaction is still retained [233].

This approach was used to analyze the multiprotein complex interactions in the cells exposed to B[a]P and TCDD, two classic inducers of the AhR pathway, in an effort to investigate potentially alternate cellular mechanisms that may respond to these two xenobiotics. As mentioned above, B[a]P itself is nontoxic but is converted to reactive DNA adduct-forming metabolites by the AhR-induced cytochrome P450 enzyme system [234]. Unlike B[a]P, TCDD is not a substrate of this enzyme. The toxicity of this xenobiotic is related to its ability to initiate the metabolism of other toxic compounds (such as B[a]P) and to its slow detoxification from the body [235].

Before the multiprotein complexes were separated by 2D BN/SDS-PAGE, a subcellular fractionation of the exposed cells (0.5 μ M B[a]P or 200 pM TCDD) was carried out by using a commercially available fractionation kit. The subcellular fractionation of the samples is necessary, because the multiprotein complexes are distributed in different subcellular compartments (such as mitochondria, Golgi apparatus, plasma membrane, and others) in addition to their presence in the cytoplasm. Subcellular fractionation leads to a concentration of these multiprotein complexes, otherwise they are difficult to identify. By using the kit, control, B[a]P- and TCDD-exposed RT4 cell lysates were separated into cytosolic proteins, membrane/organelle proteins, and nuclear proteins. Prior to the use of these fractions for

differential 2D BN/SDS-PAGE analysis, a proteome map of different fractions of non-exposed RT4 cells was generated.

MALDI-TOF-MS analysis revealed many typical protein complexes and monomeric proteins specific for these compartments (**Table 9, Table 10, Table 11 see annex II**). These proteins were classified according to the GO annotation of the PANTHER software and were found to be associated with a broad range of protein classes (**Figure 35**).

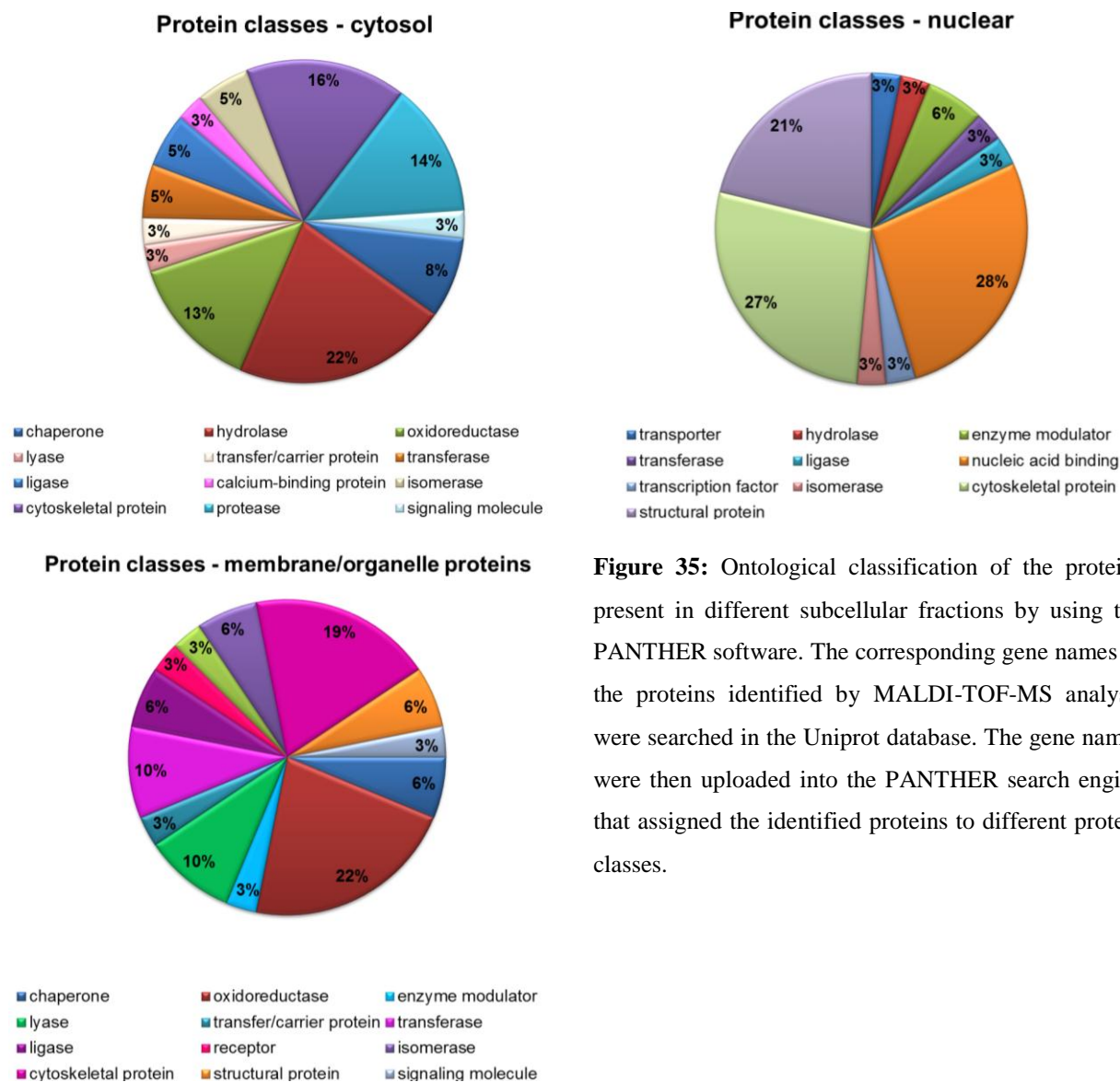


Figure 35: Ontological classification of the proteins present in different subcellular fractions by using the PANTHER software. The corresponding gene names of the proteins identified by MALDI-TOF-MS analysis were searched in the Uniprot database. The gene names were then uploaded into the PANTHER search engine that assigned the identified proteins to different protein classes.

After the proteome map had been generated, the gels obtained from different fractions of the exposed samples were compared with the respective control gels. By MALDI-TOF-MS analysis of the differentially regulated proteins, the expression of many calcium-containing (calmodulin, protein S100-A2, annexin A10, annexin A5, gelsolin isoform b) and iron-containing (ferritin, heme-binding protein 2, transferrin receptor protein 1) proteins were identified in TCDD-exposed subcellular fractions (**Table 8**), along with others proteins. Also, the expression of a unique cluster of three protein spots was observed in the cytosolic fraction of TCDD-exposed cells that was absent in control and B[a]P-exposed fractions. Two of these three protein spots were identified as calmodulin and protein S100A. Furthermore, a few calcium-containing proteins (cyclophilin B, cyclophilin A, and calreticulin) were identified in B[a]P-exposed fractions.

The modulation of intracellular calcium and iron homeostasis upon TCDD and B[a]P exposure has been observed in several studies [236-239]. The induction of CYP1A1 by AhR agonists has been shown to be abolished by inhibition of calcium movements [240, 241]. However, the mechanisms behind these interactions were largely unknown until recently, where a few studies indicated a role of the Ca^{2+} /CaM/CaMKI α pathway in AhR-dependent and -independent genomic responses [242-244]. The observed expression of calmodulin in TCDD-exposed samples is also in support of these findings. In another current study a TCDD-mediated impairment of the cellular iron homeostasis associated with a changed ferritin content coupled to TfR-1 induction was reported [245]. Similar differences in the expression of iron-containing proteins (ferritin (FTH1), heme-binding protein 2 (HEBP2), transferrin (TfR-1)) were found in the TCDD-exposed samples (**Table 11.1-11.2, see annex II**).

Apart from this, studies indicate a cross-link between calcium and nitric oxide signaling *via* nitric oxide synthases (NOSs) [246, 247]. NOSs are a family of enzymes consisting of a bi-domain structure: the N-terminal oxygenase and the C-terminal reductase domain [248-250]. These enzymes are involved in the production of NO from L-arginine for which they require calmodulin binding to its C-terminal reductase domain. By that, electrons could be transferred from the reductase domain to the oxygenase domain which subsequently generate NO and citrulline as products by oxygenation of arginine [251, 252]. NO, a very important signaling molecule, is the key mediator for a wide variety of physiological processes including vasodilation, neurotransmission, and platelet aggregation [253]. Other than these functions, its

role in Fe metabolism has also been recognized [254]. Increased production of NO species in cells exposed to TCDD or BaP has been reported [255, 256]

Based upon these studies and the observed differential expression of both calcium- and iron-containing proteins, the following hypothesis was developed (**Figure 36**). Upon exposure to TCDD or B[a]P, a rapid increase in intracellular calcium ion concentration occurs. CaM, the major sensor for these calcium ions, becomes active and binds to the constitutive forms of NOS.

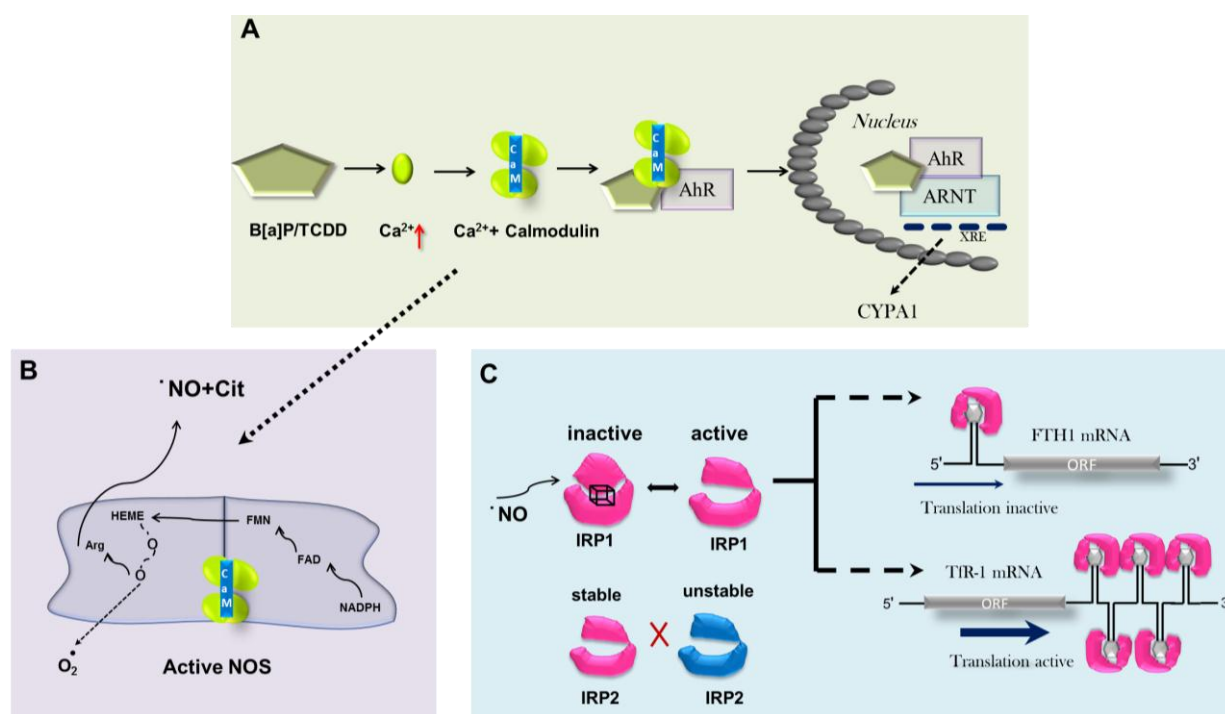


Figure 36: Pictorial representation of the hypothesis proposed for the interactions between calcium and iron. (A) Exposure to B[a]P/TCDD causes elevation of intracellular calcium which activates calmodulin (CaM). Activated CaM, along with the translocation of the aryl hydrocarbon receptor (AhR) for the induction of cytochrome P450 (CYP1A1) release, is also capable of causing conformation changes in nitric oxide synthase (NOS). Electrons are donated by NADPH to the reductase domain of the enzyme and proceed *via* FAD and FMN redox carriers to the oxygenase domain. There, they interact with the heme iron at the active site to catalyze the reaction of oxygen with L-arginine, generating citrulline and NO as products. NO by interacting with iron clusters of IRP1 stimulates its RNA-binding activity resulting in an increase in transferrin (TfR1) mRNA levels and a decrease in ferritin (FTH1) synthesis. The changed ferritin and TfR1 content impairs the cellular iron homeostasis, ultimately leading to significant changes in the labile iron pool (LIP).

This enzyme undergoes global conformational changes that enhance the rate of NO production. NO, except for causing cytotoxic effects, is also capable of modulating Fe-containing proteins such as the iron regulatory proteins IRPA1 and IRPA2 by direct coordination to the Fe centers of IRPA1 [254, 257]. The activated IRPA1 can promote the up-

regulation of transferrin by binding to the iron regulatory element in 3'UTR of TfR mRNA, whereas by binding to iron response element (IRE) in the 5'UTR of ferritin mRNA blocks the translation of ferritin. This ultimately leads to significant changes in the labile iron pool and hence in cellular toxicity [258, 259].

To prove this hypothesis at least in part, the intracellular calcium changes upon exposure to TCDD and B[a]P were monitored by using the fluorescence probes Fluo-4 and Rhod-2. As detailed in the results section, the transient increase in intracellular calcium concentration reported by several groups [113, 242, 243, 260, 261] was not observed during the exposure. The first changes in intracellular calcium levels were observed only after an exposure to these xenobiotics for 24 h. An intracellular calcium level elevated by 27 % was found in the TCDD-exposed samples, while a 21 % increase was observed in B[a]P-exposed cells (**Figure 32**). A sustained increase in intracellular calcium concentration involving cytochrome P450-mediated metabolism of xenobiotics with elevating intracellular activity was observed in some studies [179, 262, 263]. It was reported that the dihydrodiol and dihydrodiol-epoxide metabolites of B[a]P were more efficient in the up-regulation of intracellular calcium than the parent compound [254, 255 [264]. It is possible that alterations of calcium homeostasis in RT4 cells also depend on cytochrome P450-associated mechanisms: metabolic reactions in the case of B[a]P and changes in redox cycle in the case of TCDD. Moreover, it has also been reported that calmodulin is capable of performing its essential functions independent of intracellular calcium mobilization [265, 266]. In addition, the observed increases in Rhod-2 fluorescence intensity by 30 % in the TCDD-exposed RT4 cells and by 12 % in the B[a]P-exposed cells indicate an uptake of calcium from extracellular sources. The increased calcium levels in these stores may be responsible for the biological processes, which could result in cell death as observed by previous 2D proteomic studies on RT4 cells in our laboratory [267].

To find out, if the differential regulation of iron-containing proteins such as transferrin and ferritin leads to an alteration in iron homeostasis, the LIPs of B[a]P- and TCDD-exposed cells were analyzed by using the fluorescent dye PG SK. The measurements were performed after exposure periods of 3 h and 24 h, respectively, to ascertain a time-dependent effect. In B[a]P-exposed cells, the LIP was not affected after either time period, however, the LIP of TCDD-exposed cells was increased by 7 % and 13 %, respectively, after 3 h and 24 h of exposure (**Figure 33**). An AhR-mediated cellular iron load after exposure to TCDD has been observed in a few studies. In fact, it has been demonstrated that iron potentiates both hepatic porphyria and TCDD toxicity in susceptible mice in an oxidative process involving a disturbed activity

of iron regulatory proteins [236]. Moreover, significant changes in the expression of genes related to heme metabolism and iron homeostasis that were associated with liver injury were found in mice exposed for two or five weeks to TCDD [238, 268]. The changes in LIP as observed in RT4 cells are in support of these findings, although these changes were not as strong as reported by other groups, presumably because of the low TCDD concentrations of 200 pM used in the studies. Furthermore, the cells were blocked with the CaM antagonist W-7 to determine whether CaM was modulating the LIP. While the TCDD-mediated increase in LIP was completely inhibited in W-7-treated cells exposed to TCDD for 3 h, this inhibition was reverted in cells exposed for 24 h (**Figure 33**). The increase in intracellular calcium as observed after 24 h of TCDD exposure may be responsible for this effect. The experiment proved at least in part that CaM exerts some modulating effects on the LIP of the cells.

As discussed earlier, CaM is also capable of triggering the production of NO *via* the induction of conformational changes in NOS. The NO thus produced is capable of modulating the LIP of the cells by alternating the expression of the iron-containing proteins FTH1 and TfR-1. A quantitative measurement of NO is hard to perform as it has a half-life of only approx. 6 s [269]. However, NO is rapidly oxidized to NO_2^- and NO_3^- , which provides a means to indirectly measure NO production. Therefore, the increased NO_2^- production as measured by using the Griess assay was indicative of an NO release triggered by treatment of the cells with TCDD or B[a]P. The analyses revealed a substantial increase in NO production which amounted to 196 % in the cells exposed to B[a]P and to 253 % in the TCDD-exposed cells (**Figure 34**). Decreased basal levels of NO both in TCDD- and B[a]P-exposed RT4 cells after blocking the cells with W-7 indicated that the observed effects were CaM-controlled and thus a further support of the above hypothesis.

8. Summary

The major objective of this study was to evaluate whether the environmental contaminant benzo[a]pyrene B[a]P, one of the most important polycyclic aromatic hydrocarbons (PAH), is capable of mediating DNA damage in urinary bladder epithelial cells and hence potentially bladder carcinogenesis. To pursue this goal, effects of B[a]P on urinary bladder epithelial cells were investigated by applying a proteomic approach with the purpose of identifying proteins and pathways involved in B[a]P toxicity. First, the ability of bladder epithelial cells for B[a]P uptake and metabolism was determined. Secondly, a proteome map of primary porcine urinary bladder epithelial cells (PUBEC), the cell model used in the majority of the studies, was established as basis for comparative investigations. In the same model, investigations on time- and concentration-dependent expression changes of proteins after B[a]P exposure followed. The proteins were separated by using 2D gel electrophoresis and identified by MALDI-TOF-MS analysis in these studies. Finally, to elucidate mechanisms by which B[a]P mediates its toxicity, signaling pathways were studied in RT4 cells by using Blue Native PAGE analysis. Besides offering some insights into B[a]P-mediated toxic effects, the studies also point towards the possibility of bladder cancer development induced by B[a]P exposure.

B[a]P is a ubiquitous environmental pollutant formed during the combustion of fossil fuels, grilling, barbecuing, and smoking of food. Although much information is available on the carcinogenic properties of B[a]P, the mechanism by which this chemical is taken up by cells is still not known. In **Chapter 3** of this thesis, attempts were made to investigate the dynamics of B[a]P uptake, subcellular distribution, and metabolism in PUBEC. It was found that exposure to 0.5 μM B[a]P led to an increase in intracellular concentration of B[a]P in bladder epithelial cells in a time-dependent manner but without approaching saturation. Also, a marked difference in B[a]P uptake was observed among various PUBEC pools used for the studies. Subcellular partitioning studies of B[a]P by using confocal microscopy revealed that a significant amount of B[a]P accumulated in the cell membrane of PUBEC, while only a slight but significant increase in B[a]P fluorescence intensity was observed in the cytosol and nucleus. Quantification of B[a]P uptake by bladder epithelial cells by spectrofluorometric and gas chromatographic-mass spectrometric analysis yielded intracellular concentrations ranging from 7.28 μM to 35.07 μM in cells exposed to 0.5 μM B[a]P and from 29.9 μM to 406.64 μM in cells exposed to 10 μM B[a]P. The formation of 3-OH-B[a]P in all of the B[a]P-exposed PUBEC determined by GC-MS analysis demonstrated for the first time that oxygenated B[a]P

metabolites are actually formed in this cell model. These results indicate that bladder epithelial cells are capable of a strong accumulation and metabolic activation of B[a]P and suggest that B[a]P may act as a bladder cancer-inducing chemical. Also, the differences in B[a]P uptake by the various PUBEC pools is an explanation for the inter-individual variation in PAH toxicity as observed in humans.

Urinary bladder epithelial cells (also known as transitional epithelial cells) are the innermost cells of the bladder which are involved in accommodating the fluctuation of liquid volume in this organ and also help to protect it against caustic/toxic effects of urine. These cells are also the first ones to come in contact with urinary toxicants and thus account for 90 % of bladder cancers known as transitional cell carcinomas. As a prerequisite for proteomic studies, the first reference proteome and phosphoproteome maps of porcine bladder epithelia cells were generated by applying 2DE gel electrophoresis. This is discussed in **Chapter 4**. A total of 120 selected protein spots were identified by MALDI-TOF-MS analysis, among which 31 phosphoproteins were enriched by using a method based on the precipitation with lanthanum ions (La^{3+}). All identified proteins were bioinformatically annotated according to their physiochemical characteristic, subcellular location, and function. Most of the proteins were distributed in an area of pI 4-10 and a molecular mass range between 20 kDa and 100 kDa. The 2DE map with the complete range of expressed proteins, especially with information about phosphoproteins, provides a valuable resource for comparative proteomic analysis of normal and pathological conditions affecting the bladder function.

The studies described in **Chapter 5** of the thesis deal with a series of events leading from DNA damage to apoptosis that were investigated by using a proteomic approach. 2DE gel electrophoresis mapped the differences between cells exposed to 0.5 μM B[a]P and control cells. Twenty-five differentially expressed proteins involved in DNA repair, mitochondrial dysfunction, and apoptosis were identified by MALDI-TOF-MS analysis. A concentration-dependent increase in DNA damage was observed after an exposure period of 24 h. The expression of VDAC2, CTSD, HSP27, and HSP70 indicated towards the intrinsic apoptotic mitochondrial pathway, although the analysis of mitochondrial dysfunction pointed towards an alternate pathway of cell death: The mitochondrial membrane potential (MMP), although disturbed during the initial exposure period, was nearly retained after 24 h of B[a]P treatment. In conclusion, the studies indicated DNA damage caused by B[a]P at low concentrations during an exposure period of 24 h and also shed light on a possible apoptotic mechanism induced by DNA damage.

Studies on protein-protein interactions involved in B[a]P toxicity are described in **Chapter 6**. A comparative analysis of proteomic complexes involving the two AhR ligands B[a]P and TCDD was carried out by using 2D BN/SDS-PAGE. For the enrichment of the protein complexes, a subcellular fractionation of unexposed cells and cells exposed to B[a]P and TCDD was carried out. BN/SDS-PAGE of these fractions revealed an effective separation of protein species and complexes of various origins, including mitochondria, plasma membrane, and intracellular compartments. The major differences in the protein maps obtained from samples of control cells and cells exposed to B[a]P and TCDD, respectively, concerned the expression of many calcium- and iron-containing proteins. On the basis of these findings, the intracellular calcium content of cells exposed to TCDD and B[a]P was evaluated, revealing an increase only after 24 h of exposure but with no transient elevation. The cells exposed to TCDD also showed an alteration in the labile iron pool (LIP) of the cells, but no such changes were observed in B[a]P-exposed cells. The increase in the LIP was strongly inhibited by the calmodulin (CaM) antagonist W-7 (10 μ M). These results point towards a possible interaction between the iron and calcium signaling of the cells. The analysis of nitric oxide generation by using the Griess assay revealed a substantial increase in NO content of both B[a]P- and TCDD-exposed cells. Also in these cells, the basal NO generation was inhibited when the cells were blocked with the CaM antagonist W-7. The results led to the conclusion that alterations in calcium and iron homeostasis upon exposure to TCDD and B[a]P is linked by NO that is produced by CaM-activated nitric oxide synthase (NOS). The NO thus produced by interacting with the iron centers of IRPAs modulated the activity of TfR1 and FTH1 which in turn changed the LIP of the cells and hence the toxicity. Although some new mechanistic insights into the mechanisms of B[a]P- and TCDD-induced toxicity were provided by these studies, further investigations are still required for the validation of these initial results.

9. References

- [1] Juhasz, A. L., Naidu, R., Bioremediation of high molecular weight polycyclic aromatic hydrocarbons: a review of the microbial degradation of benzo[a]pyrene. *Int. Biodeterior. Biodegrad.* 2000, *45*, 57-88.
- [2] Phillips, D. H., Fifty years of benzo(a)pyrene. *Nature* 1983, *303*, 468-472.
- [3] Li, J. L., Chen, B. H., Solubilization of model polycyclic aromatic hydrocarbons by nonionic surfactants. *Chem. Eng. Sci.* 2002, *57*, 2825-2835.
- [4] U.S., Environmental protection agency. Locating and estimating air emissions from sources of polycyclic organic matter. EPA-454/R-98-014. Office of air quality planning and standards, research triangle park, NC. 1998.
- [5] ATSDR, (Agency for Toxic Substances and Disease Registry). Toxicological Profile for Polycyclic Aromatic Hydrocarbons (PAHs). *Public Health Service, U.S. Department of Health and Human Services, Atlanta, GA.* 1995.
- [6] Larsson, B. K., Sahlberg, G. P., Eriksson, A. T., Busk, L. A., Polycyclic aromatic hydrocarbons in grilled food. *J. Agric. Food Chem.* 1983, *31*, 867-873.
- [7] Ramesh, A., Inyang, F., Hood, D. B., Archibong, A. E., *et al.*, Metabolism, bioavailability, and toxicokinetics of benzo([alpha])pyrene in F-344 rats following oral administration. *Exp. Toxicol. Pathol.* 2001, *53*, 275-290.
- [8] Moody, R. P., Nadeau, B., Chu, I., In vivo and in vitro dermal absorption of benzo[a]pyrene in rat, guinea pig, human and tissue-cultured skin. *J. Dermatol. Sci.* 1995, *9*, 48-58.
- [9] Walle, T., Walle, U. K., Sedmera, D., Klausner, M., Benzo(a)pyrene induces oral carcinogenesis and chemoprevention: studies in bioengineered human tissue. *Drug Metab. Dispos.* 2006, *34*, 346-350.
- [10] Yamazaki, H., Terada, M., Tsuboi, A., Matsubara, C., *et al.*, Distribution and binding pattern of benzo(a)pyrene in rat liver, lung and kidney constituents after oral administration. *Toxicol. Environ. Chem.* 1987, *15*, 71-81.
- [11] Prough, R. A., Patrizi, V. W., Okita, R. T., Masters, B. S. S., Jakobsson, S. W., Characteristics of benzo(a)pyrene metabolism by kidney, liver, and lung microsomal fractions from rodents and humans. *Cancer Res.* 1979, *39*, 1199-1206.
- [12] Hoffman D., Schmeltz I., Hecht S.S., Wynder E.L., *Tobacco carcinogenesis. In Gelboin, HS, and Ts'o, POP, editors. Polycyclic hydrocarbons and cancer*, Academic Press : New York 1978, *1*, 85-117, *1*, pp. 85-117.
- [13] Douglas Rees, E., Mandelstam, P., Lowry, J. Q., Lipscomb, H., A study of the mechanism of intestinal absorption of benzo(a)pyrene. *Biochimica et Biophysica Acta (BBA) - Biomembranes* 1971, *225*, 96-107.

-
- [14] Sun, J. D., Wolff, R. K., Kanapilly, G. M., Deposition, retention, and biological fate of inhaled benzo(a)pyrene adsorbed onto ultrafine particles and as a pure aerosol. *Toxicol. Appl. Pharmacol.* 1982, 65, 231-244.
- [15] Sun, J. D., Wolff, R. K., Kanapilly, G. M., McClellan, R. O., Lung retention and metabolic fate of inhaled benzo(a)pyrene associated with diesel exhaust particles. *Toxicol. Appl. Pharmacol.* 1984, 73, 48-59.
- [16] Verma, N., Rettenmeier, A. W., Schmitz-Spanke, S., Exposure of primary porcine urothelial cells to benzo(a)pyrene: In vitro uptake, intracellular concentration and biological response. *Submitted* 2012.
- [17] Kelman, B. J., Springer, D. L., Movements of benzo[a]pyrene across the hemochorial placenta of the guinea pig. *Proc. Soc. Exp. Biol. Med.* 1982, 169, 58-62.
- [18] Denissenko, M. F., Pao, A., Tang, M.-s., Pfeifer, G. P., Preferential formation of benzo[a]pyrene adducts at lung cancer mutational hotspots in P53. *Science* 1996, 274, 430-432.
- [19] Vauhkonen, M., Kuusi, T., Kinnunen, P. K. J., Serum and tissue distribution of benzo[a]pyrene from intravenously injected chylomicrons in rat in vivo. *Cancer Lett.* 1980, 11, 113-119.
- [20] Schmidt, J. V., Bradfield, C. A., Ah receptor signaling pathways. *Annu. Rev. Cell Dev. Biol.* 1996, 12, 55-89.
- [21] Fujisawa-Sehara, A., Yamane, M., Fujii-Kuriyama, Y., A DNA-binding factor specific for xenobiotic responsive elements of P-450c gene exists as a cryptic form in cytoplasm: its possible translocation to nucleus. *Proceedings of the National Academy of Sciences* 1988, 85, 5859-5863.
- [22] Hakura, A., Tsutsui, Y., Sonoda, J., Kai, J., *et al.*, Comparison between in vivo mutagenicity and carcinogenicity in multiple organs by benzo[a]pyrene in the lacZ transgenic mouse (Muta(TM)Mouse). *Mutation Research/Fundamental and Molecular Mechanisms of Mutagenesis* 1998, 398, 123-130.
- [23] Levin, W., Wood, A. W., Wislocki, P. G., Chang, R. L., *et al.*, *Mutagenicity and carcinogenicity of benzo[a]pyrene derivatives.* In Gelboin, H.V., Ts'o, P.O.P., Eds. *Polycyclic hydrocarbons and cancer, academic press: New York*, 1978, 189-202.
- [24] Denison, M. S., Fisher, J. M., Whitlock, J. P., The DNA recognition site for the dioxin-Ah receptor complex. Nucleotide sequence and functional analysis. *J. Biol. Chem.* 1988, 263, 17221-17224.
- [25] Denison, M. S., Fisher, J. M., Whitlock, J. P., Inducible, receptor-dependent protein-DNA interactions at a dioxin-responsive transcriptional enhancer. *Proceedings of the National Academy of Sciences* 1988, 85, 2528-2532.
- [26] Denison, M. S., Nagy, S. R., Activation of the aryl hydrocarbon receptor by structurally diverse exogenous and endogenous chemicals. *Annu. Rev. Pharmacol. Toxicol.* 2003, 43, 309-334.

- [27] Selkirk, J. K., Croy, R. G., Gelboin, H. V., Isolation by high pressure liquid chromatography and characterization of benzo(a)pyrene-4,5-epoxide as a metabolite of benzo(a)pyrene. *Arch. Biochem. Biophys.* 1975, *168*, 322-326.
- [28] Chou, M. W., Evans, F. E., Yang, S. K., Fu, P. P., Evidence for a 2,3-epoxide as an intermediate in the microsomal metabolism of 6-nitrobenzo[a]pyrene. *Carcinogenesis* 1983, *4*, 699-702.
- [29] Sims, P., Grover, P. L., in: George Klein, S. W., Alexander, H. (Eds.), *Epoxides in polycyclic aromatic hydrocarbon metabolism and carcinogenesis*, Academic Press, United States 1974, pp 165-274.
- [30] Selkirk, J. K., Croy, R. G., Gelboin, H. V., High-pressure liquid chromatographic separation of 10 benzo(a)pyrene phenols and the identification of 1-phenol and 7-phenol as new metabolites. *Cancer Res.* 1976, *36*, 922-926.
- [31] Croy, R. G., Selkirk, J. K., Harvey, R. G., Engel, J. F., Gelboin, H. V., Separation of ten benzo(a)pyrene phenols by recycle high pressure liquid chromatography and identification of four phenols as metabolites. *Biochem. Pharmacol.* 1976, *25*, 227-230.
- [32] Yang, S. K., Roller, P. P., Gelboin, H. V., Enzymic mechanism of benzo[a]pyrene conversion to phenols and diols and an improved high-pressure liquid chromatographic separation of benzo[a]pyrene derivatives. *Biochemistry* 1977, *16*, 3680-3687.
- [33] Lorentzen, R. J., Caspary, W. J., Lesko, S. A., Ts'o, P. O. P., Autoxidation of 6-hydroxybenzo[a]pyrene and 6-oxobenzo[a]pyrene radical, reactive metabolites of benzo[a]pyrene. *Biochemistry* 1975, *14*, 3970-3977.
- [34] James, K. S., Robert, G. C., Harry, V. G., Benzo[a]pyrene metabolites: Efficient and rapid separation by high-pressure liquid chromatography. *Science* 1974, *184*, 169-171.
- [35] Burczynski, M. E., Harvey, R. G., Penning, T. M., Expression and characterization of four recombinant human dihydrodiol dehydrogenase isoforms: oxidation of trans-7, 8-dihydroxy-7,8-dihydrobenzo[a]pyrene to the activated o-quinone metabolite benzo[a]pyrene-7,8-dione. *Biochemistry* 1998, *37*, 6781-6790.
- [36] Penning, T. M., Burczynski, M. E., Hung, C. F., McCoull, K. D., *et al.*, Dihydrodiol dehydrogenases and polycyclic aromatic hydrocarbon activation: generation of reactive and redox active o-quinones. *Chem. Res. Toxicol.* 1999, *12*, 1-18.
- [37] Moore, B. P., Cohen, G. M., Metabolism of benzo(a)pyrene and Its major metabolites to ethyl acetate soluble and water-soluble metabolites by cultured rodent trachea. *Cancer Res.* 1978, *38*, 3066-3075.
- [38] Booth, J., Sims, P., Different pathways involved in the metabolism of the 7.8- and 9, 10-dihydrodiols of benzo(a)pyrene. *Biochem. Pharmacol.* 1976, *25*, 979-980.
- [39] Holder, G., Yagi, H., Dansette, P., Jerina, D. M., *et al.*, Effects of inducers and epoxide hydrase on the metabolism of benzo[a]pyrene by liver microsomes and a reconstituted system: analysis by high pressure liquid chromatography. *Proceedings of the National Academy of Sciences* 1974, *71*, 4356-4360.

-
- [40] Kinoshita, N., Shears, B., Gelboin, H. V., K-region and non-K-region metabolism of benzo(a)pyrene by rat liver microsomes. *Cancer Res.* 1973, 33, 1937-1944.
- [41] Swindle, M. M., swine in the laboratory: surgery, anesthesia, imaging and experimental techniques, FL: CRC press, Boca Raton 2007. .
- [42] Nemoto, N., Gelboin, H. V., Enzymatic conjugation of benzo(a)pyrene oxides, phenols and dihydrodiols with UDP glucuronic acid. *Biochem. Pharmacol.* 1976, 25, 1221-1226.
- [43] Nobuo, N., Shozo, T., Kinetics of glucuronidation of phenol-derivatives of benzo(a)pyrene with rat and mouse liver microsomes. *Toxicol. Lett.* 1982, 10, 75-79.
- [44] Wiebel, F. J., Metabolism of monohydroxybenzo(a)pyrenes by rat liver microsomes and mammalian cells in culture. *Arch. Biochem. Biophys.* 1975, 168, 609-621.
- [45] Nemoto, N., Takayama, S., Gelboin, H. V., Sulfate conjugation of benzo[a]pyrene metabolites and derivatives. *Chem-Biol. Interact.* 1978, 23, 19-30.
- [46] Nemoto, N., Takayama, S., Enzymatic formation and properties of a conjugate of sulfate with 3 hydroxybenzo(a)pyrene. *Biochem. Pharmacol.* 1977, 26, 679-684.
- [47] Nemoto, N., Gelboin, H., Assay and properties of glutathione-S-benzo(a)pyrene-4,5-oxide transferase. *Arch. Biochem. Biophys.* 1975, 170, 739-742.
- [48] Deutsch, J., Gelboin, H. V., Benzo[a]pyrene glucuronide and sulfate conjugate characterization by field desorption mass spectrometry. *Biol. Mass Spectrom.* 1982, 9, 99-102.
- [49] Nemoto, N., Gelboin, H. V., Habig, W. H., Ketley, J. N., Jakoby, W. B., K region benzo([alpha])pyrene-4,5-oxide is conjugated by homogeneous glutathione S-transferases. *Nature* 1975, 255, 512-512.
- [50] Jernström, B., Martinez, M., Meyer, D. J., Ketterer, B., Glutathione conjugation of the carcinogenic and mutagenic electrophile (\pm)-7 β ,8 α -dihydroxy-9 α ,10 α -oxy-7,8,9,10-tetrahydrobenzo[a]pyrene catalyzed by purified rat liver glutathione transferases. *Carcinogenesis* 1985, 6, 85-89.
- [51] Yang, S. K., McCourt, D. W., Leutz, J. C., Gelboin, H. V., *Benzo[a]pyrene diol epoxides: mechanism of enzymatic formation and optically active intermediates*, 1977, 196, pp. 1199-1201.
- [52] Huberman, E., Sachs, L., Yang, S. K., Gelboin, V., Identification of mutagenic metabolites of benzo(a)pyrene in mammalian cells. *Proc. Natl. Acad. Sci. U. S. A.* 1976, 73, 607-611.
- [53] Thakker, D. R., Yagi, H., Akagi, H., Koreeda, M., *et al.*, Metabolism of benzo[a]pyrene VI. Stereoselective metabolism of benzo[a]pyrene and benzo[a]pyrene 7,8-dihydrodiol to diol epoxides. *Chem-Biol. Interact.* 1977, 16, 281-300.
- [54] Yang, S. K., McCourt, D. W., Roller, P. P., Gelboin, H. V., Enzymatic conversion of benzo(a)pyrene leading predominantly to the diol-epoxide r-7,t-8-dihydroxy-t-9,10-oxy-7,8,9,10-tetrahydrobenzo(a)pyrene through a single enantiomer of r-7, t-8-dihydroxy-7,8-dihydrobenzo(a)pyrene. *Proceedings of the National Academy of Sciences* 1976, 73, 2594-2598.

-
- [55] Yang, S., McCourt, D., Leutz, J., Gelboin, H., Benzo[a]pyrene diol epoxides: mechanism of enzymatic formation and optically active intermediates. *Science* 1977, 196, 1199-1201.
- [56] Huberman, E., Sachs, L., Yang, S. K., Gelboin, V., Identification of mutagenic metabolites of benzo(a)pyrene in mammalian cells. *Proceedings of the National Academy of Sciences* 1976, 73, 607-611.
- [57] Conney, A. H., Pharmacological implications of microsomal enzyme induction. *Pharmacol. Rev.* 1967, 19, 317-366.
- [58] Gelboin, H. V., in: Alexander, H., Sidney, W. (Eds.), *Carcinogens, enzyme induction, and gene action*, Academic Press 1967, pp 1-81.
- [59] Mitchell, C. E., Fischer, J. P., Dahl, A. R., Differential induction of cytochrome P-450 catalyzed activities by polychlorinated biphenyls and benzo[a]pyrene in B6C3F1 mouse liver and lung. *Toxicology* 1987, 43, 315-323.
- [60] Ekström, G., von Bahr, C., Glaumann, H., Ingelman-Sundberg, M., Interindividual variation in benzo(a)pyrene metabolism and composition of isoenzymes of cytochrome P-450 as revealed by SDS-gel electrophoresis of human liver microsomal Fractions. *Acta Pharmacol. Toxicol.* 1982, 50, 251-260.
- [61] Levin, W., Wood, A. W., Chang, R. L., Slaga, T. J., *et al.*, Marked differences in the tumor-initiating activity of optically pure (+)- and (-)-trans-7,8-dihydroxy-7,8-dihydrobenzo(a)pyrene on mouse skin. *Cancer Res.* 1977, 37, 2721-2725.
- [62] Smithgall, T. E., Harvey, R. G., Penning, T. M., Spectroscopic identification of ortho-quinones as the products of polycyclic aromatic trans-dihydrodiol oxidation catalyzed by dihydrodiol dehydrogenase. A potential route of proximate carcinogen metabolism. *J. Biol. Chem.* 1988, 263, 1814-1820.
- [63] Pelkonen, O., Nebert, D. W., Metabolism of polycyclic aromatic hydrocarbons: etiologic role in carcinogenesis. *Pharmacol. Rev.* 1982, 34, 189-222.
- [64] Glatt, H. R., Oesch, F., Phenolic benzo(a)pyrene metabolites are mutagens. *Mutation Research/Fundamental and Molecular Mechanisms of Mutagenesis* 1976, 36, 379-383.
- [65] Gelboin, H. V., Benzo[alpha]pyrene metabolism, activation and carcinogenesis: role and regulation of mixed-function oxidases and related enzymes. *Physiol. Rev.* 1980, 60, 1107-1166.
- [66] Cavalieri, E. L., Rogan, E. G., The approach to understanding aromatic hydrocarbon carcinogenesis. The central role of radical cations in metabolic activation. *Pharmacol. Ther.* 1992, 55, 183-199.
- [67] Sullivan, P. D., Free radicals of benzo(a)pyrene and derivatives. *Environ. Health Perspect.* 1985, 64, 283-295.
- [68] Selkirk, J. K., Croy, R. G., Roller, P. P., Gelboin, H. V., High-Pressure Liquid Chromatographic Analysis of Benzo(a)pyrene Metabolism and Covalent Binding and the Mechanism of Action of 7,8-Benzoflavone and 1,2-Epoxy-3,3,3-trichloropropane. *Cancer Res.* 1974, 34, 3474-3480.

- [69] Wislocki, P. G., Wood, A. W., Chang, R. L., Levin, W., *et al.*, Mutagenicity and cytotoxicity of benzo(a)pyrene arene oxides, phenols, quinones, and dihydrodiols in bacterial and mammalian cells. *Cancer Res.* 1976, *36*, 3350-3357.
- [70] Zhu, H., Li, Y., Trush, M. A., Characterization of benzo[a]pyrene quinone-induced toxicity to primary cultured bone marrow stromal cells from DBA/2 mice: Potential role of mitochondrial dysfunction. *Toxicol. Appl. Pharmacol.* 1995, *130*, 108-120.
- [71] Slaga, T. J., Bracken, W. J., Gleason, G., Levin, W., *et al.*, Marked differences in the skin tumor-initiating activities of the optical enantiomers of the diastereomeric benzo(a)pyrene 7,8-diol-9,10-epoxides. *Cancer Res.* 1979, *39*, 67-71.
- [72] Phillips, D. H., Hewer, A., Seidel, A., Steinbrecher, T., *et al.*, Relationship between mutagenicity and DNA adduct formation in mammalian cells for fjord- and bay-region diol-epoxides of polycyclic aromatic hydrocarbons. *Chem-Biol. Interact.* 1991, *80*, 177-186.
- [73] Lehr, R. E., Jerina, D. M., Relationships of quantum mechanical calculations, relative mutagenicity of benzo[a]anthracene diol epoxides, and "bay region" concept of aromatic hydrocarbon carcinogenicity. *J. Toxicol. Environ. Health* 1977, *2*, 1259-1265.
- [74] Xue, W., Warshawsky, D., Metabolic activation of polycyclic and heterocyclic aromatic hydrocarbons and DNA damage: A review. *Toxicol. Appl. Pharmacol.* 2005, *206*, 73-93.
- [75] Szeliga, J., Dipple, A., DNA Adduct Formation by Polycyclic Aromatic Hydrocarbon Dihydrodiol Epoxides. *Chem. Res. Toxicol.* 1998, *11*, 1-11.
- [76] Meehan, T., Straub, K., Calvin, M., Benzo[a]pyrene diol epoxide covalently binds to deoxyguanosine and deoxyadenosine in DNA. *Nature* 1977, *269*, 725-727.
- [77] King, H. W. S., Thompson, M. H., Brookes, P., The role of 9-hydroxybenzo(a)pyrene in the microsome mediated binding of benzo(a)pyrene to DNA. *Int. J. Cancer* 1976, *18*, 339-344.
- [78] Zhang, Y., Wu, X., Guo, D., Rechkoblit, O., Wang, Z., Activities of human DNA polymerase κ in response to the major benzo[a]pyrene DNA adduct: error-free lesion bypass and extension synthesis from opposite the lesion. *DNA Repair* 2002, *1*, 559-569.
- [79] Zhang, Y., Wu, X., Guo, D., Rechkoblit, O., *et al.*, Two-step error-prone bypass of the (+)- and (-)-trans-anti-BPDE-N2-dG adducts by human DNA polymerases η and κ . *Mutation Research/Fundamental and Molecular Mechanisms of Mutagenesis* 2002, *510*, 23-35.
- [80] Plöttner, S., Borza, A., Wolf, A., Bolt, H. M., *et al.*, Evaluation of time dependence and interindividual differences in benzo[a]pyrene-mediated CYP1A1 induction and genotoxicity in porcine urinary bladder cell cultures. *Journal of Toxicology and Environmental Health, Part A: Current Issues* 2008, *71*, 969 - 975.
- [81] Blake, D. A., Martz, F., Gery-Martz, A., Gordon, G. B., Mellits, E. D., Fetal tissues from various strains of induced mice metabolize benzo(a)pyrene to mutagenic metabolites. *Teratology* 1979, *20*, 377-382.
- [82] Riva, C., Binelli, A., Rusconi, F., Colombo, G., *et al.*, A proteomic study using zebra mussels (*D. polymorpha*) exposed to benzo([alpha])pyrene: The role of gender and exposure concentrations. *Aquat. Toxicol.* 2011, *104*, 14-22.

- [83] Hockley, S. L., Arlt, V. M., Brewer, D., Giddings, I., Phillips, D. H., Time- and concentration-dependent changes in gene expression induced by benzo(a)pyrene in two human cell lines, MCF-7 and HepG2. *BMC Genomics* 2006, 7, 260-283.
- [84] Kafferlein, H. U., Marczyński, B., Mensing, T., Bruning, T., Albumin and hemoglobin adducts of benzo[a]pyrene in humans—Analytical methods, exposure assessment, and recommendations for future directions. *Crit. Rev. Toxicol.* 2010, 40, 126-150.
- [85] dell'Omo, M., Lauwerys, R. R., Adducts to macromolecules in the biological monitoring of workers exposed to polycyclic aromatic hydrocarbons. *Crit. Rev. Toxicol.* 1993, 23, 111-126.
- [86] Nielsen, P. S., Okkels, H., Sigsgaard, T., Kyrtopoulos, S., Autrup, H., Exposure to urban and rural air pollution: DNA and protein adducts and effect of glutathione-S-transferase genotype on adduct levels. *Int. Arch. Occup. Environ. Health* 1996, 68, 170-176.
- [87] Lee, B. M., Yin, B. Y., Herbert, R., Hemminki, K., *et al.*, Immunologic measurement of polycyclic aromatic hydrocarbon-albumin adducts in foundry workers and roofers. *Scand. J. Work. Environ. Health* 1991, 17, 190-194.
- [88] Kure, E. H., Benzo(a)pyrene-albumin adducts in humans exposed to polycyclic aromatic hydrocarbons in an industrial area of Poland. *Fuel and Energy Abstracts* 1998, 39, 58-58.
- [89] Hemminki, K., Zhang, L. F., Kruger, J., Autrup, H., *et al.*, Exposure of bus and taxi drivers to urban air pollutants as measured by DNA and protein adducts. *Toxicol. Lett.* 1994, 72, 171-174.
- [90] Binkova, B., Lewtas, J., Mıškova, I., Rossner, P., *et al.*, Biomarker studies in Northern Bohemia. *Environ. Health Perspect.* 1996, 104, 591-597.
- [91] Crawford, F. G., Mayer, J., Santella, R. M., Cooper, T. B., *et al.*, Biomarkers of environmental tobacco smoke in preschool children and their mothers. *J. Natl. Cancer Inst.* 1994, 86, 1398-1402.
- [92] Tang, D., Warburton, D., Tannenbaum, S. R., Skipper, P., *et al.*, Molecular and genetic damage from environmental tobacco smoke in young children. *Cancer Epidemiol. Biomark. Prev.* 1999, 8, 427-431.
- [93] Ruchirawat, M., Mahidol, C., Tangjarukij, C., Pui-ock, S., *et al.*, Exposure to genotoxins present in ambient air in Bangkok, Thailand - particle associated polycyclic aromatic hydrocarbons and biomarkers. *The Science of the Total Environment* 2002, 287, 121-132.
- [94] Pastorelli, R., Guanci, M., Restano, J., Berri, A., *et al.*, Seasonal effect on airborne pyrene, urinary 1-hydroxypyrene, and benzo[a]pyrene diol epoxide-hemoglobin adducts in the general population. *Cancer Epidemiol. Biomark. Prev.* 1999, 8, 561-565.
- [95] Chung, M. K., Riby, J., Li, H., Iavarone, A. T., *et al.*, A sandwich enzyme-linked immunosorbent assay for adducts of polycyclic aromatic hydrocarbons with human serum albumin. *Anal. Biochem.* 2010, 400, 123-129.
- [96] Wang, H., Chen, W., Zheng, H., Guo, L., *et al.*, Association between plasma BPDE-Alb adduct concentrations and DNA damage of peripheral blood lymphocytes among coke oven workers. *Occup. Environ. Med.* 2007, 64, 753-758.

- [97] Autrup, H., Daneshvar, B., Dragsted, L. O., Gamborg, M., *et al.*, *Biomarkers for exposure to ambient air pollution--comparison of carcinogen-DNA adduct levels with other exposure markers and markers for oxidative stress*, 1999, 107, pp. 233-238.
- [98] Scherer, G., Frank, S., Riedel, K., Meger-Kossien, I., Renner, T., Biomonitoring of exposure to polycyclic aromatic hydrocarbons of nonoccupationally exposed persons. *Cancer Epidemiol. Biomark. Prev.* 2000, 9, 373-380.
- [99] Sherson, D., Sabro, P., Sigsgaard, T., Johansen, F., Autrup, H., Biological monitoring of foundry workers exposed to polycyclic aromatic hydrocarbons. *Br. J. Ind. Med.* 1990, 47, 448-453.
- [100] Omland, O., Sherson, D., Hansen, A. M., Sigsgaard, T., *et al.*, Exposure of iron foundry workers to polycyclic aromatic hydrocarbons: benzo(a)pyrene-albumin adducts and 1-hydroxypyrene as biomarkers for exposure. *Occup. Environ. Med.* 1994, 51, 513-518.
- [101] Ferreira Júnior, M. F., Tas, S., dell'Omo, M., Goormans, G., *et al.*, Determinants of benzo(a)pyrenediol epoxide adducts to haemoglobin in workers exposed to polycyclic aromatic hydrocarbons. *Occup. Environ. Med.* 1994, 51, 451-455.
- [102] Frank, S., Renner, T., Ruppert, T., Scherer, G., Determination of albumin adducts of (+)-anti-benzo[a]pyrene-diol-epoxide using an high-performance liquid chromatographic column switching technique for sample preparation and gas chromatography-mass spectrometry for the final detection. *Journal of Chromatography B: Biomedical Sciences and Applications* 1998, 713, 331-337.
- [103] Penning, T. M., Ohnishi, S. T., Ohnishi, T., Harvey, R. G., Generation of reactive oxygen species during the enzymatic oxidation of polycyclic aromatic hydrocarbon trans-dihydrodiols catalyzed by dihydrodiol dehydrogenase. *Chem. Res. Toxicol.* 1996, 9, 84-92.
- [104] Shou, M., Harvey, R. G., Penning, T. M., Contribution of dihydrodiol dehydrogenase to the metabolism of (\pm)-trans;-7,8-dihydroxy-7,8-dihydrobenzo[a]pyrene in fortified rat liver subcellular fractions. *Carcinogenesis* 1992, 13, 1575-1582.
- [105] Flowers-Geary, L., Harvey, R. G., Penning, T. M., Identification of benzo[a]pyrene-7,8-dione as an authentic metabolite of (\pm)-trans-7,8-dihydroxy-7,8-dihydrobenzo[a]pyrene in isolated rat hepatocytes. *Carcinogenesis* 1995, 16, 2707-2715.
- [106] Penning, T. M., in: Helmut, S., Lester, P. (Eds.), *Aldo-keto reductases and formation of polycyclic aromatic hydrocarbon o-quinones*, Academic Press 2004, pp 31-67.
- [107] Shou, M., Harvey, R. G., Penning, T. M., Reactivity of benzo[a]pyrene-7,8-dione with DNA. Evidence for the formation of deoxyguanosine adducts. *Carcinogenesis* 1993, 14, 475-482.
- [108] Burczynski, M. E., Penning, T. M., Genotoxic polycyclic aromatic hydrocarbon ortho-quinones generated by aldo-keto reductases induce CYP1A1 via nuclear translocation of the aryl hydrocarbon receptor. *Cancer Res.* 2000, 60, 908-915.
- [109] Kasai, H., Crain, P. F., Kuchino, Y., Nishimura, S., *et al.*, Formation of 8-hydroxyguanine moiety in cellular DNA by agents producing oxygen radicals and evidence for its repair. *Carcinogenesis* 1986, 7, 1849-1851.

-
- [110] Benamira, M., Johnson, K., Chaudhary, A., Bruner, K., *et al.*, Induction of mutations by replication of malondialdehyde-modified M13 DNA in *Escherichia coli*: determination of the extent of DNA modification, genetic requirements for mutagenesis, and types of mutations induced. *Carcinogenesis* 1995, *16*, 93-99.
- [111] Carafoli, E., Intracellular calcium homeostasis. *Annu. Rev. Biochem.* 1987, *56*, 395-433.
- [112] DiGiovanni, J., Gill, R. D., Nettikumara, A. N., Colby, A. B., Reiners, J. J., Effect of extracellular calcium concentration on the metabolism of polycyclic aromatic hydrocarbons by cultured mouse keratinocytes. *Cancer Res.* 1989, *49*, 5567-5574.
- [113] N'Diaye, M., Le Ferrec, E., Lagadic-Gossmann, D., Corre, S., *et al.*, Aryl hydrocarbon receptor- and calcium-dependent induction of the chemokine CCL1 by the environmental contaminant benzo[a]pyrene. *J. Biol. Chem.* 2006, *281*, 19906-19915.
- [114] Ou, X. L., Weber, T. J., Chapkin, R. S., Ramos, K. S., Interference with protein kinase C-related signal Transduction in vascular smooth muscle cells by benzo[a]pyrene. *Arch. Biochem. Biophys.* 1995, *318*, 122-130.
- [115] Webb, B. L. J., Hirst, S. J., Giembycz, M. A., Protein kinase C isoenzymes: a review of their structure, regulation and role in regulating airways smooth muscle tone and mitogenesis. *Br. J. Pharmacol.* 2000, *130*, 1433-1452.
- [116] Ou, X., Ramos, K. S., Benzo[a]pyrene inhibits protein kinase C activity in subcultured rat aortic smooth muscle cells. *Chem-Biol. Interact.* 1994, *93*, 29-40.
- [117] Liyan, Z., Connor, E. E., Chegini, N., Shiverick, K. T., Modulation by benzo[a]pyrene of epidermal growth factor receptors, cell proliferation, and secretion of human chorionic gonadotropin in human placental cell lines. *Biochem. Pharmacol.* 1995, *50*, 1171-1180.
- [118] Carpenter, G., Cohen, S., Epidermal growth factor. *J. Biol. Chem.* 1990, *265*, 7709-7712.
- [119] Guyda, H. J., Mathieu, L., Lai, W., Manchester, D., *et al.*, Benzo(a)pyrene inhibits epidermal growth factor binding and receptor autophosphorylation in human placental cell cultures. *Mol. Pharmacol.* 1990, *37*, 137-143.
- [120] Zhang, L., Shiverick, K. T., Benzo(a)pyrene, but Not 2,3,7,8-Tetrachlorodibenzo-p-dioxin, Alters Cell Proliferation and c-Myc and Growth Factor Expression in Human Placental Choriocarcinoma JEG-3 Cells. *Biochem. Biophys. Res. Commun.* 1997, *231*, 117-120.
- [121] Kaufman, D. S., Shipley, W. U., Feldman, A. S., Bladder cancer. *The Lancet* 2009, *374*, 239-249.
- [122] Zeegers, M. P. A., Tan, F. E. S., Dorant, E., van den Brandt, P. A., The impact of characteristics of cigarette smoking on urinary tract cancer risk. *Cancer* 2000, *89*, 630-639.
- [123] Boffetta, P., Tobacco smoking and risk of bladder cancer. *Scand. J. Urol. Nephrol.* 2008, *42*, 45-54.

-
- [124] Rodgman, A., Smith, C. J., Perfetti, T. A., The composition of cigarette smoke: a retrospective, with emphasis on polycyclic components. *Hum. Exp. Toxicol.* 2000, *19*, 573-595.
- [125] Kogevinas, M., Mannetje, A., Cordier, S., Ranft, U., *et al.*, Occupation and bladder cancer among men in Western Europe. *Cancer Causes Control* 2003, *14*, 907-914.
- [126] Wolf, A., Kutz, A., Plottner, S., Behm, C., *et al.*, The effect of benzo(a)pyrene on porcine urinary bladder epithelial cells analyzed for the expression of selected genes and cellular toxicological endpoints. *Toxicology* 2005, *207*, 255-269.
- [127] Valen, G., Öwall, A., Takeshima, S., Goiny, M., *et al.*, Metabolic changes induced by ischemia and cardioplegia: a study employing cardiac microdialysis in pigs. *Eur. J. Cardiothorac. Surg.* 2004, *25*, 69-75.
- [128] Thomas, S. A., Fallavollita, J. A., Lee, T.-C., Feng, J., Canty, J. M., Jr, Absence of troponin I degradation or altered sarcoplasmic reticulum uptake protein expression after reversible ischemia in swine. *Circ. Res.* 1999, *85*, 446-456.
- [129] Ambrose, J. A., Myocardial ischemia and infarction. *J. Am. Coll. Cardiol.* 2006, *47*, D13-17.
- [130] Boluyt, M. O., Cirrincione, G. M., Loyd, A. M., Korzick, D. H., *et al.*, Effects of gradual coronary artery occlusion and exercise training on gene expression in swine heart. *Mol. Cell. Biochem.* 2007, *294*, 87-96.
- [131] Turk, J. R., Henderson, K. K., Vanvickle, G. D., Watkins, J., Laughlin, M. H., Arterial endothelial function in a porcine model of early stage atherosclerotic vascular disease. *Int. J. Exp. Pathol.* 2005, *86*, 335-345.
- [132] Turk, J. R., Laughlin, M. H., Physical activity and atherosclerosis: which animal model? *Can. J. Appl. Physiol.* 2004, *29*, 657-683.
- [133] Castles, L. A., Terblanche, J., van Hoorn-Hickman, R. V., Vinik, A. I., Peptic ulcer and gastrin in pigs. *Aust. N. Z. J. Surg.* 1978, *48*, 214-219.
- [134] Kimura, K., LaRosa, C. A., Blank, M. A., Jaffe, B. M., Successful segmental intestinal transplantation in enterectomized pigs. *Ann. Surg.* 1990, *211*, 158-164.
- [135] Van Kruiningen, H. J., Colombel, J.-F., The forgotten role of lymphangitis in Crohn's disease. *Gut* 2008, *57*, 1-4.
- [136] Schouten, J. A., Beynen, A. C., Meijer, S., Hoitsma, H. F., Effect of partial ileal bypass on ileum morphology in cholesterol-fed pigs. *Lab. Anim.* 1986, *20*, 155-157.
- [137] Baskerville, A., Animal model of human disease: chronic bronchitis. *Am. J. Pathol.* 1976, *82*, 237-240.
- [138] Welsh, M. J., Rogers, C. S., Stoltz, D. A., Meyerholz, D. K., Prather, R. S., Development of a porcine model of cystic fibrosis. *Trans. Am. Clin. Climatol. Assoc.* 2009, *120*, 149-162.

-
- [139] Stern, M., Longaker, M. T., Adzick, N. S., Harrison, M. R., Stern, R., Hyaluronidase levels in urine from Wilms' tumor patients. *J. Natl. Cancer Inst.* 1991, *83*, 1569-1574.
- [140] Booyse, F. M., Quarfoot, A. J., Bell, S., Fass, D. N., *et al.*, Cultured aortic endothelial cells from pigs with von Willebrand disease: in vitro model for studying the molecular defect(s) of the disease. *Proc. Natl. Acad. Sci. U. S. A.* 1977, *74*, 5702-5706.
- [141] Szebeni, J., Baranyi, L., Savay, S., Bodo, M., *et al.*, Complement activation-related cardiac anaphylaxis in pigs: role of C5a anaphylatoxin and adenosine in liposome-induced abnormalities in ECG and heart function. *Am. J. Physiol. Heart Circ. Physiol.* 2006, *290*, H1050-1058.
- [142] Drew, R. A., Erysipelothrix arthritis in pigs as a comparative model for rheumatoid arthritis. *Proc. R. Soc. Med.* 1972, *65*, 994-998.
- [143] Skavlen, P. A., Stills, H. F., Jr., Caldwell, C. W., Middleton, C. C., Malignant lymphoma in a Sinclair miniature pig. *Am. J. Vet. Res.* 1986, *47*, 389-393.
- [144] Troisi, R., Maene, L., Jacobs, B., Berrevoet, F., *et al.*, Segmental porcine pancreatic autotransplantation as model for pancreas preservation studies using two different techniques for vascular reconstruction. *J. Invest. Surg.* 2000, *13*, 203-211.
- [145] Kin, T., Korbitt, G. S., Kobayashi, T., Dufour, J. M., Rajotte, R. V., Reversal of diabetes in pancreatectomized pigs after transplantation of neonatal porcine islets. *Diabetes* 2005, *54*, 1032-1039.
- [146] Hainsworth, D. P., Katz, M. L., Sanders, D. A., Sanders, D. N., *et al.*, Retinal capillary basement membrane thickening in a porcine model of diabetes mellitus. *Comp. Med.* 2002, *52*, 523-529.
- [147] Koopmans, S. J., Mroz, Z., Dekker, R., Corbijn, H., *et al.*, Association of insulin resistance with hyperglycemia in streptozotocin-diabetic pigs: effects of metformin at isoenergetic feeding in a type 2-like diabetic pig model. *Metabolism.* 2006, *55*, 960-971.
- [148] Chavany, C., Jendoubi, M., Biology and potential strategies for the treatment of GM2 gangliosidosis. *Mol. Med. Today* 1998, *4*, 158-165.
- [149] Short, C. E., Paddleford, R. R., McGrath, C. J., Williams, C. H., Preanesthetic evaluation and management of malignant hyperthermia in the pig experimental model. *Anesth. Analg.* 1976, *55*, 643-653.
- [150] Brambilla, G., Cantafora, A., Metabolic and cardiovascular disorders in highly inbred lines for intensive pig farming: how animal welfare evaluation could improve the basic knowledge of human obesity. *Ann. Ist. Super. Sanita* 2004, *40*, 241-244.
- [151] Spurlock, M. E., Gabler, N. K., The development of porcine models of obesity and the metabolic syndrome. *J. Nutr.* 2008, *138*, 397-402.
- [152] Ekser, B., Rigotti, P., Gridelli, B., Cooper, D. K., Xenotransplantation of solid organs in the pig-to-primate model. *Transpl. Immunol.* 2009, *21*, 87-92.
- [153] Bergh, A., Söder, O., Studies of cryptorchidism in experimental animal models. *Acta Paediatrica* 2007, *96*, 617-621.

-
- [154] Green, J. A., Kim, J. G., Whitworth, K. M., Agca, C., Prather, R. S., The use of microarrays to define functionally-related genes that are differentially expressed in the cycling pig uterus. *Soc. Reprod. Fertil. Suppl.* 2006, 62, 163-176.
- [155] Strzezek, J., Wysocki, P., Kordan, W., Kuklinska, M., Proteomics of boar seminal plasma - current studies and possibility of their application in biotechnology of animal reproduction. *Reprod. Biol.* 2005, 5, 279-290.
- [156] Rohrer, G. A., Wise, T. H., Ford, J. J., Deciphering the pig genome to understand gamete production. *Soc. Reprod. Fertil. Suppl.* 2006, 62, 293-301.
- [157] Sun, Q. Y., Nagai, T., Molecular mechanisms underlying pig oocyte maturation and fertilization. *J. Reprod. Dev.* 2003, 49, 347-359.
- [158] Guhe, C., Föllmann, W., Growth and characterization of porcine urinary bladder epithelial cells in vitro. *Am. J. Physiol.* 1994, 266, F298-308.
- [159] Petrat, F., de Groot, H., Rauen, U., Determination of the chelatable iron pool of single intact cells by laser scanning microscopy. *Arch. Biochem. Biophys.* 2000, 376, 74-81.
- [160] Pink, M., Verma, N., Polato, F., Bonn, G. K., *et al.*, Precipitation by lanthanum ions: A straightforward approach to isolating phosphoproteins. *Journal of Proteomics* 2011, 75, 375-383.
- [161] Pink, M., Verma, N., Rettenmeier, A. W., Schmitz-Spanke, S., CBB staining protocol with higher sensitivity and mass spectrometric compatibility. *Electrophoresis* 2010, 31, 593-598.
- [162] Chazotte, B., Labeling mitochondria with rhodamine 123. *Cold Spring Harbor Protocols* 2011, 2011, pdb.prot5640.
- [163] Camacho-Carvajal, M. M., Wollscheid, B., Aebersold, R., Steimle, V., Schamel, W. W. A., Two-dimensional blue native/SDS gel electrophoresis of multi-protein complexes from whole cellular lysates. *Mol. Cell. Proteomics* 2004, 3, 176-182.
- [164] Kakhlon, O., Cabantchik, Z. I., The labile iron pool: characterization, measurement, and participation in cellular processes. *Free Radic. Biol. Med.* 2002, 33, 1037-1046.
- [165] Sun, J., Zhang, X., Broderick, M., Fein, H., Measurement of Nitric Oxide Production in Biological Systems by Using Griess Reaction Assay. *Sensors* 2003, 3, 276-284.
- [166] Thomas, P. D., Kejariwal, A., Guo, N., Mi, H., *et al.*, Applications for protein sequence-function evolution data: mRNA/protein expression analysis and coding SNP scoring tools. *Nucleic Acids Res.* 2006, 34, W645-W650.
- [167] Huang, D. W., Sherman, B. T., Lempicki, R. A., Systematic and integrative analysis of large gene lists using DAVID bioinformatics resources. *Nat. Protocols* 2008, 4, 44-57.
- [168] Alexander, M., Behm, C., Föllmann, W., Kuhlmann, J., Miniaturization of primary porcine urinary bladder epithelial cell cultures and application for gene expression studies after exposure to benzo[a]pyrene. *J. Toxicol. Environ. Health A* 2008, 71, 915-922.

-
- [169] Flieger, A., Golka, K., Schulze, H., Föllmann, W., Primary cultures of human urothelial cells for genotoxicity testing. *J Toxicol Environ Health A* 2008, *71*, 930-935.
- [170] Föllmann, W., Guhe, C., A cell culture model of isolated porcine urinary bladder epithelial cells for genotoxicity studies. *Toxicol. In Vitro* 1994, *8*, 763-765.
- [171] Plöttner, S., Selinski, S., Bolt, H., Degen, G., *et al.*, Distinct subtypes of urinary bladder epithelial cells with inducible and non-inducible cytochrome P450 1A1. *Arch. Toxicol.* 2009, *83*, 131-138.
- [172] Wolf, A., Kutz, A., Plöttner, S., Behm, C., *et al.*, The effect of benzo(a)pyrene on porcine urinary bladder epithelial cells analyzed for the expression of selected genes and cellular toxicological endpoints. *Toxicology* 2005, *207*, 255-269.
- [173] Verma, N., Bäuerlein, C., Pink, M., Rettenmeier, A. W., Schmitz-Spanke, S., Proteome and phosphoproteome of primary cultured pig urothelial cells. *Electrophoresis* 2011, *32*, 3600-3611.
- [174] Kyte, J., Doolittle, R. F., A simple method for displaying the hydropathic character of a protein. *J. Mol. Biol.* 1982, *157*, 105-132.
- [175] Miller, A. G., Israel, D., Whitlock, J. P., Biochemical and genetic analysis of variant mouse hepatoma cells defective in the induction of benzo(a)pyrene-metabolizing enzyme activity. *J. Biol. Chem.* 1983, *258*, 3523-3527.
- [176] Moore, M., Wang, X., Lu, Y. F., Wormke, M., *et al.*, Benzo[a]pyrene-resistant MCF-7 human breast cancer cells. A unique aryl hydrocarbon-nonresponsive clone. *J. Biol. Chem.* 1994, *269*, 11751-11759.
- [177] Heinonen, J. T., Sidhu, J. S., Reilly, M. T., Farin, F. M., *et al.*, Assessment of regional cytochrome P450 activities in rat liver slices using resorufin substrates and fluorescence confocal laser cytometry. *Environ. Health Perspect.* 1996, *104*, 536-543.
- [178] Plant, A. L., Benson, D. M., Smith, L. C., Cellular uptake and intracellular localization of benzo(a)pyrene by digital fluorescence imaging microscopy. *J. Cell Biol.* 1985, *100*, 1295-1308.
- [179] Barhoumi, R., Mouneimne, Y., Ramos, K. S., Safe, S. H., *et al.*, Analysis of benzo[a]pyrene partitioning and cellular homeostasis in a rat Liver cell line. *Toxicol. Sci.* 2000, *53*, 264-270.
- [180] Shu, H. P., Nichols, A. V., Benzo(a)pyrene uptake by human plasma lipoproteins in vitro. *Cancer Res.* 1979, *39*, 1224-1230.
- [181] Ekelman, K. B., Milo, G. E., Cellular uptake, transport, and macromolecular binding of benzo(a)pyrene and 7,12-dimethylbenz(a)anthracene by human cells in vitro. *Cancer Res.* 1978, *38*, 3026-3032.
- [182] Fahl, W. E., Jefcoate, C. R., Kasper, C. B., Characteristics of benzo(a)pyrene metabolism and cytochrome P-450 heterogeneity in rat liver nuclear envelope and comparison to microsomal membrane. *J. Biol. Chem.* 1978, *253*, 3106-3113.

-
- [183] Kasper, C. B., Biochemical distinctions between the nuclear and microsomal membranes from rat hepatocytes. *J. Biol. Chem.* 1971, *246*, 577-581.
- [184] Khandwala, A. S., Kasper, C. B., Preferential induction of aryl hydroxylase activity in rat liver nuclear envelope by 3-methylcholanthrene. *Biochem. Biophys. Res. Commun.* 1973, *54*, 1241-1246.
- [185] Guhe, C., Degen, G. H., Schuhmacher, U. S., Kiefer, F., Föllmann, W., Drug metabolizing enzyme activities in porcine urinary bladder epithelial cell cultures (PUBEC). *Arch. Toxicol.* 1996, *70*, 599-606.
- [186] Borza, A., Plöttner, S., Wolf, A., Behm, C., *et al.*, Synergism of aromatic amines and benzo[a]pyrene in induction of Ah receptor-dependent genes. *Arch. Toxicol.* 2008, *82*, 973-980.
- [187] Ariese, F., Verkaik, M., Hoornweg, G. P., van de Nesse, R. J., *et al.*, Trace analysis of 3-hydroxy benzo[a]pyrene in urine for the biomonitoring of human exposure to polycyclic aromatic hydrocarbons. *J. Anal. Toxicol.* 1994, *18*, 195-204.
- [188] Förster, K., Preuss, R., Roßbach, B., Brüning, T., *et al.*, 3-Hydroxybenzo[a]pyrene in the urine of workers with occupational exposure to polycyclic aromatic hydrocarbons in different industries. *Occup. Environ. Med.* 2008, *65*, 224-229.
- [189] Verma, N., Pink, M., Petrat, F., Rettenmeier, A., Schmitz-Spanke, S., Exposure of primary porcine urothelial cells to benzo(a)pyrene: in vitro uptake, intracellular concentration, and biological response. *Arch. Toxicol.*, 1-11.
- [190] Chatterjee, R., Cell biology: cases of mistaken identity. *Science* 2007, *315*, 928-931.
- [191] Verma, N., Bauerlein, C., Pink, M., Rettenmeier, A. W., Schmitz-Spanke, S., Proteome and phosphoproteome of primary cultured pig urothelial cells. *Electrophoresis* 2011, *32*, 3600-3611.
- [192] Verma, N., Rettenmeier, A. W., Schmitz-Spanke, S., Pig as a model organism for toxicoproteomic studies on bladder cancer. *Toxicol. Lett.* 2009, *189*, S194-S194.
- [193] Zhang, R., Xu, G., Chen, W., Zhang, W., Genetic polymorphisms of glutathione S-transferase P1 and bladder cancer susceptibility in a chinese population. *Genet Test Mol Biomarkers.* 2011, *15*, 85-88.
- [194] Chen, Y.-T., Chen, C.-L., Chen, H.-W., Chung, T., *et al.*, Discovery of novel bladder cancer biomarkers by comparative urine proteomics using iTRAQ technology. *J. Proteome Res.* 2010, *9*, 5803-5815.
- [195] Hofmann, B., Hecht, H. J., Flohé, L., Peroxiredoxins. *Biol. Chem.* 2002, *383*, 347-364.
- [196] Ohyama, C., Glycosylation in bladder cancer. *Int. J. Clin. Oncol.* 2008, *13*, 308-313.
- [197] Mertz, K. D., Demichelis, F., Sboner, A., Hirsch, M. S., *et al.*, Association of cytokeratin 7 and 19 expression with genomic stability and favorable prognosis in clear cell renal cell cancer. *Int. J. Cancer* 2008, *123*, 569-576.

-
- [198] Xia, Q., Cheng, D., Duong, D. M., Gearing, M., *et al.*, Phosphoproteomic analysis of human brain by calcium phosphate precipitation and mass spectrometry. *J. Proteome Res.* 2008, 7, 2845-2851.
- [199] Zhang, X., Ye, J., Jensen, O. N., Roepstorff, P., Highly efficient phosphopeptide enrichment by calcium phosphate precipitation combined with subsequent IMAC enrichment. *Mol. Cell. Proteomics* 2007, 6, 2032-2042.
- [200] Ruse, C. I., McClatchy, D. B., Lu, B., Cociorva, D., *et al.*, Motif-specific sampling of phosphoproteomes. *J. Proteome Res.* 2008, 7, 2140-2150.
- [201] Persy, V. P., Behets, G. J., Bervoets, A. R., De Broe, M. E., D'Haese, P. C., Lanthanum: A safe phosphate binder. *Semin. Dial.* 2006, 19, 195-199.
- [202] Bini, L., Magi, B., Marzocchi, B., Arcuri, F., *et al.*, Protein expression profiles in human breast ductal carcinoma and histologically normal tissue. *Electrophoresis* 1997, 18, 2832-2841.
- [203] Brünagel, G., Shah, U., Schoen, R. E., Getzenberg, R. H., Identification of calreticulin as a nuclear matrix protein associated with human colon cancer. *J. Cell. Biochem.* 2003, 89, 238-243.
- [204] Yoon, G.-S., Lee, H., Jung, Y., Yu, E., *et al.*, Nuclear matrix of calreticulin in hepatocellular carcinoma. *Cancer Res.* 2000, 60, 1117-1120.
- [205] Kageyama, S., Isono, T., Matsuda, S., Ushio, Y., *et al.*, Urinary calreticulin in the diagnosis of bladder urothelial carcinoma. *Int. J. Urol.* 2009, 16, 481-486.
- [206] Kageyama, S., Isono, T., Iwaki, H., Wakabayashi, Y., *et al.*, Identification by proteomic analysis of calreticulin as a marker for bladder cancer and evaluation of the diagnostic accuracy of its detection in urine. *Clin. Chem.* 2004, 50, 857-866.
- [207] Kirchhausen, T., Clathrin. *Annu. Rev. Biochem.* 2000, 69, 699-727.
- [208] Royle, S. J., Bright, N. A., Lagnado, L., Clathrin is required for the function of the mitotic spindle. *Nature* 2005, 434, 1152-1157.
- [209] Conner, S. D., Schmid, S. L., Regulated portals of entry into the cell. *Nature* 2003, 422, 37-44.
- [210] Enari, M., Ohmori, K., Kitabayashi, I., Taya, Y., Requirement of clathrin heavy chain for p53-mediated transcription. *Genes Dev.* 2006, 20, 1087-1099
- [211] Levin, R. M., Ruggieri, M. R., Gill, H. S., Haugaard, N., Wein, A. J., Studies on the biphasic nature of urinary bladder contraction and function. *Neurourol. Urodyn.* 1987, 6, 339-350.
- [212] Sugasawa, K., Shimizu, Y., Iwai, S., Hanaoka, F., A molecular mechanism for DNA damage recognition by the xeroderma pigmentosum group C protein complex. *DNA Repair* 2002, 1, 95-107.

-
- [213] Hang, B., Formation and repair of tobacco carcinogen-derived bulky DNA adducts. *Journal of Nucleic Acids* 2010, 2010.
- [214] Kaiserman, M. J., Rickert, W. S., Carcinogens in tobacco smoke: benzo[a]pyrene from Canadian cigarettes and cigarette tobacco. *Am. J. Public Health* 1992, 82, 1023-1026.
- [215] Hoeijmakers, J. H. J., Genome maintenance mechanisms for preventing cancer. *Nature* 2001, 411, 366-374.
- [216] Staton, L. W., David, T., The Rad23 ubiquitin receptor, the proteasome and functional specificity in transcriptional control. *Transcription* 2010, 1, 22–26. .
- [217] Min, J.-H., Pavletich, N. P., Recognition of DNA damage by the Rad4 nucleotide excision repair protein. *Nature* 2007, 449, 570-575.
- [218] Verma, N., Pink, M., Petrat, F., Rettenmeier, A. W., Schmitz-Spanke, S., Exposure of primary porcine urothelial cells to benzo(a)pyrene: in vitro uptake, intracellular concentration, and biological response. *Arch. Toxicol.* 2012.
- [219] Shen, Y., White, E., *p53-Dependent apoptosis pathways*, Academic Press 2001, pp 55-84.
- [220] Amundson, S. A., Myers, T. G., Fornace, A. J., Jr., Roles for p53 in growth arrest and apoptosis: putting on the brakes after genotoxic stress. *Oncogene* 1998, 17, 3287-3299.
- [221] Bunz, F., Hwang, P. M., Torrance, C., Waldman, T., *et al.*, Disruption of p53 in human cancer cells alters the responses to therapeutic agents. *J. Clin. Investig.* 1999, 104, 263-269.
- [222] Elmore, S., Apoptosis: A review of programmed cell death. *Toxicol. Pathol.* 2007, 35, 495-516.
- [223] Kim, J. Y., Chung, J.-Y., Park, J.-E., Lee, S. G., *et al.*, Benzo[a]pyrene induces apoptosis in RL95-2 human endometrial cancer cells by cytochrome P450 1A1 activation. *Endocrinology* 2007, 148, 5112-5122.
- [224] Rane, M. J., Pan, Y., Singh, S., Powell, D. W., *et al.*, Heat shock protein 27 controls apoptosis by regulating Akt activation. *J. Biol. Chem.* 2003, 278, 27828-27835.
- [225] Li, C.-Y., Lee, J.-S., Ko, Y.-G., Kim, J.-I., Seo, J.-S., Heat shock protein 70 inhibits apoptosis downstream of cytochrome c release and upstream of caspase-3 activation. *J. Biol. Chem.* 2000, 275, 25665-25671.
- [226] Shoshan-Barmatz, V., Keinan, N., Zaid, H., Uncovering the role of VDAC in the regulation of cell life and death. *J. Bioenerg. Biomembr.* 2008, 40, 183-191.
- [227] Sarioglu, H., Brandner, S., Habegger, M., Jacobsen, C., *et al.*, Analysis of 2,3,7,8-tetrachlorodibenzo-p-dioxin-induced proteome changes in 5L rat hepatoma cells reveals novel targets of dioxin action including the mitochondrial apoptosis regulator VDAC2. *Mol. Cell. Proteomics* 2008, 7, 394-410.
- [228] Shimizu, S., Narita, M., Tsujimoto, Y., Bcl-2 family proteins regulate the release of apoptogenic cytochrome c by the mitochondrial channel VDAC. *Nature* 1999, 399, 483-487.

- [229] Heiden, M. G. V., Chandel, N. S., Schumacker, P. T., Thompson, C. B., Bcl-xL Prevents cell death following growth factor withdrawal by facilitating mitochondrial ATP/ADP exchange. *Mol. Cell* 1999, 3, 159-167.
- [230] Nooren, I. M. A., Thornton, J. M., Diversity of protein-protein interactions. *EMBO J.* 2003, 22, 3486-3492.
- [231] Pereira-Leal, J. B., Levy, E. D., Teichmann, S. A., The origins and evolution of functional modules: lessons from protein complexes. *Philosophical Transactions of the Royal Society B: Biological Sciences* 2006, 361, 507-517.
- [232] Yang, W., Steen, H., Freeman, M. R., Proteomic approaches to the analysis of multiprotein signaling complexes. *Proteomics* 2008, 8, 832-851.
- [233] Schägger, H., von Jagow, G., Blue native electrophoresis for isolation of membrane protein complexes in enzymatically active form. *Anal. Biochem.* 1991, 199, 223-231.
- [234] Sayer, J. M., Whalen, D. L., Jerina, D. M., Chemical Strategies for the Inactivation of Bay-Region Diol Epoxides. Ultimate Carcinogens Derived from Polycyclic Aromatic Hydrocarbons'. *Drug Metab. Rev.* 1989, 20, 155-182.
- [235] Landers, J. P., Bunce, N. J., The Ah receptor and the mechanism of dioxin toxicity. *Biochem. J.* 1991, 276 (Pt 2), 273-287.
- [236] Davila, D. R., Davis, D. P., Campbell, K., Cambier, J. C., *et al.*, Role of alterations in Ca^{2+} -associated signaling pathways in the immunotoxicity of polycyclic aromatic hydrocarbons. *J. Toxicol. Environ. Health* 1995, 45, 101-126.
- [237] Tannheimer, S. L., Barton, S. L., Ethier, S. P., Burchiel, S. W., Carcinogenic polycyclic aromatic hydrocarbons increase intracellular Ca^{2+} and cell proliferation in primary human mammary epithelial cells. *Carcinogenesis* 1997, 18, 1177-1182.
- [238] Smith, A. G., Clothier, B., Robinson, S., Scullion, M. J., *et al.*, Interaction between iron metabolism and 2,3,7,8-tetrachlorodibenzo-p-dioxin in mice with variants of the Ahr gene: a hepatic oxidative mechanism. *Mol. Pharmacol.* 1998, 53, 52-61.
- [239] Robinson, S. W., Clothier, B., Akhtar, R. A., Yang, A. L., *et al.*, Non-Ahr gene susceptibility loci for porphyria and liver injury induced by the interaction of 'Dioxin' with iron overload in mice. *Mol. Pharmacol.* 2002, 61, 674-681.
- [240] Le Ferrec, E., Lagadic-Gossmann, D., Rauch, C., Bardiau, C., *et al.*, Transcriptional induction of CYP1A1 by oltipraz in human Caco-2 cells is aryl hydrocarbon receptor- and calcium-dependent. *J. Biol. Chem.* 2002, 277, 24780-24787.
- [241] N'Diaye, M., Le Ferrec, E., Lagadic-Gossmann, D., Corre, S., *et al.*, Aryl hydrocarbon receptor- and calcium-dependent induction of the chemokine CCL1 by the environmental contaminant benzo[a]pyrene. *J. Biol. Chem.* 2006, 281, 19906-19915.
- [242] Monteiro, P., Gilot, D., Le Ferrec, E., Rauch, C., *et al.*, Dioxin-mediated up-regulation of aryl hydrocarbon receptor target genes is dependent on the calcium/calmodulin/CaMKI α pathway. *Mol. Pharmacol.* 2008, 73, 769-777.

- [243] Kobayashi, D., Ahmed, S., Ishida, M., Kasai, S., Kikuchi, H., Calcium/calmodulin signaling elicits release of cytochrome c during 2,3,7,8-tetrachlorodibenzo-p-dioxin-induced apoptosis in the human lymphoblastic T-cell line, L-MAT. *Toxicology* 2009, 258, 25-32.
- [244] He, C., Wang, C., Zhou, Y., Li, J., Zuo, Z., Embryonic exposure to benzo(a)pyrene influences neural development and function in rockfish (*Sebastes marmoratus*). *Neurotoxicology* 2012, 33, 758-762.
- [245] Santamaria, R., Fiorito, F., Irace, C., De Martino, L., *et al.*, 2,3,7,8-Tetrachlorodibenzo-p-dioxin impairs iron homeostasis by modulating iron-related proteins expression and increasing the labile iron pool in mammalian cells. *Biochimica et Biophysica Acta (BBA) - Molecular Cell Research* 2011, 1813, 704-712.
- [246] Kakizawa, S., Yamazawa, T., Chen, Y., Ito, A., *et al.*, Nitric oxide-induced calcium release via ryanodine receptors regulates neuronal function. *EMBO J.* 2012, 31, 417-428.
- [247] Bal-Price, A., Moneer, Z., Brown, G. C., Nitric oxide induces rapid, calcium-dependent release of vesicular glutamate and ATP from cultured rat astrocytes. *Glia* 2002, 40, 312-323.
- [248] Stuehr, D. J., Structure-function aspects in the nitric oxide synthases. *Annu. Rev. Pharmacol. Toxicol.* 1997, 37, 339-359.
- [249] Masters, B. S., McMillan, K., Sheta, E. A., Nishimura, J. S., *et al.*, Neuronal nitric oxide synthase, a modular enzyme formed by convergent evolution: structure studies of a cysteine thiolate-liganded heme protein that hydroxylates L-arginine to produce NO. as a cellular signal. *The FASEB Journal* 1996, 10, 552-558.
- [250] Xie, Q. W., Leung, M., Fuortes, M., Sassa, S., Nathan, C., Complementation analysis of mutants of nitric oxide synthase reveals that the active site requires two hemes. *Proceedings of the National Academy of Sciences* 1996, 93, 4891-4896.
- [251] Abu-Soud, H. M., Stuehr, D. J., Nitric oxide synthases reveal a role for calmodulin in controlling electron transfer. *Proceedings of the National Academy of Sciences* 1993, 90, 10769-10772.
- [252] Chen, P. F., Tsai, A. L., Wu, K. K., Cysteine 184 of endothelial nitric oxide synthase is involved in heme coordination and catalytic activity. *J. Biol. Chem.* 1994, 269, 25062-25066.
- [253] Hofseth, L. J., Hussain, S. P., Wogan, G. N., Harris, C. C., Nitric oxide in cancer and chemoprevention. *Free Radic. Biol. Med.* 2003, 34, 955-968.
- [254] Kim, S., Ponka, P., Role of nitric oxide in cellular iron metabolism. *Biometals* 2003, 16, 125-135.
- [255] Dutta, K., Ghosh, D., Nazmi, A., Kumawat, K. L., Basu, A., A Common Carcinogen Benzo[a]pyrene Causes Neuronal Death in Mouse via Microglial Activation. *PLoS One* 2010, 5, e9984.
- [256] Kopf, P. G., Walker, M. K., 2,3,7,8-Tetrachlorodibenzo-p-dioxin increases reactive oxygen species production in human endothelial cells via induction of cytochrome P4501A1. *Toxicol. Appl. Pharmacol.* 2010, 245, 91-99.

- [257] Styś, A., Galy, B., Starzyński, R. R., Smuda, E., *et al.*, Iron Regulatory Protein 1 Outcompetes Iron Regulatory Protein 2 in Regulating Cellular Iron Homeostasis in Response to Nitric Oxide. *J. Biol. Chem.* 2011, 286, 22846-22854.
- [258] Kim, S., Ponka, P., Control of Transferrin Receptor Expression via Nitric Oxide-mediated Modulation of Iron-regulatory Protein 2. *J. Biol. Chem.* 1999, 274, 33035-33042.
- [259] Pantopoulos, K., Hentze, M. W., Nitric oxide signaling to iron-regulatory protein: direct control of ferritin mRNA translation and transferrin receptor mRNA stability in transfected fibroblasts. *Proceedings of the National Academy of Sciences* 1995, 92, 1267-1271.
- [260] Mounho, B. J., Davila, D. R., Burchiel, S. W., Characterization of Intracellular Calcium Responses Produced by Polycyclic Aromatic Hydrocarbons in Surface Marker-Defined Human Peripheral Blood Mononuclear Cells. *Toxicol. Appl. Pharmacol.* 1997, 145, 323-330.
- [261] Mayati, A., Levoine, N., Paris, H., N'Diaye, M., *et al.*, Induction of Intracellular Calcium Concentration by Environmental Benzo(a)pyrene Involves a β 2-Adrenergic Receptor/Adenylyl Cyclase/Epac-1/Inositol 1,4,5-Trisphosphate Pathway in Endothelial Cells. *J. Biol. Chem.* 2012, 287, 4041-4052.
- [262] Tannheimer, S. L., Lauer, F. T., Lane, J., Burchiel, S. W., Factors influencing elevation of intracellular Ca²⁺ in the MCF-10A human mammary epithelial cell line by carcinogenic polycyclic aromatic hydrocarbons. *Mol. Carcinog.* 1999, 25, 48-54.
- [263] Romero, D. L., Mounho, B. J., Lauer, F. T., Born, J. L., Burchiel, S. W., Depletion of Glutathione by Benzo(a)pyrene Metabolites, Ionomycin, Thapsigargin, and Phorbol Myristate in Human Peripheral Blood Mononuclear Cells. *Toxicol. Appl. Pharmacol.* 1997, 144, 62-69.
- [264] Mounho, B. J., Burchiel, S. W., Alterations in human B cell calcium homeostasis by polycyclic aromatic hydrocarbons: possible associations with cytochrome P450 metabolism and increased protein tyrosine phosphorylation. *Toxicol. Appl. Pharmacol.* 1998, 149, 80-89.
- [265] Tvermoes, B. E., Bird, G. S., Freedman, J. H., Cadmium induces transcription independently of intracellular calcium mobilization. *PLoS One* 2011, 6, e20542.
- [266] Geiser, J. R., van Tuinen, D., Brockerhoff, S. E., Neff, M. M., Davis, T. N., Can calmodulin function without binding calcium? *Cell* 1991, 65, 949-959.
- [267] Schmitz-Spanke S. , Pink M. , Jeske E. , Stempelmann K. , *et al.*, Deutsche gesellschaft für experimentelle und klinische pharmakologie und toxikologie e.V. *Naunyn-Schmiedeberg's Arch. Pharmacol.* 2012, 385, 1-116.
- [268] Davies, R., Clothier, B., Robinson, S. W., Edwards, R. E., *et al.*, Essential role of the AH receptor in the dysfunction of heme metabolism induced by 2,3,7,8-tetrachlorodibenzo-p-dioxin. *Chem. Res. Toxicol.* 2007, 21, 330-340.
- [269] Beckman, J. S., Koppenol, W. H., Nitric oxide, superoxide, and peroxynitrite: the good, the bad, and ugly. *Am. J. Physiol. Cell Physiol.* 1996, 271, C1424-C1437.

10. Annex

10.1 Annex I - Representative 2D-gel image after B[a]P exposure

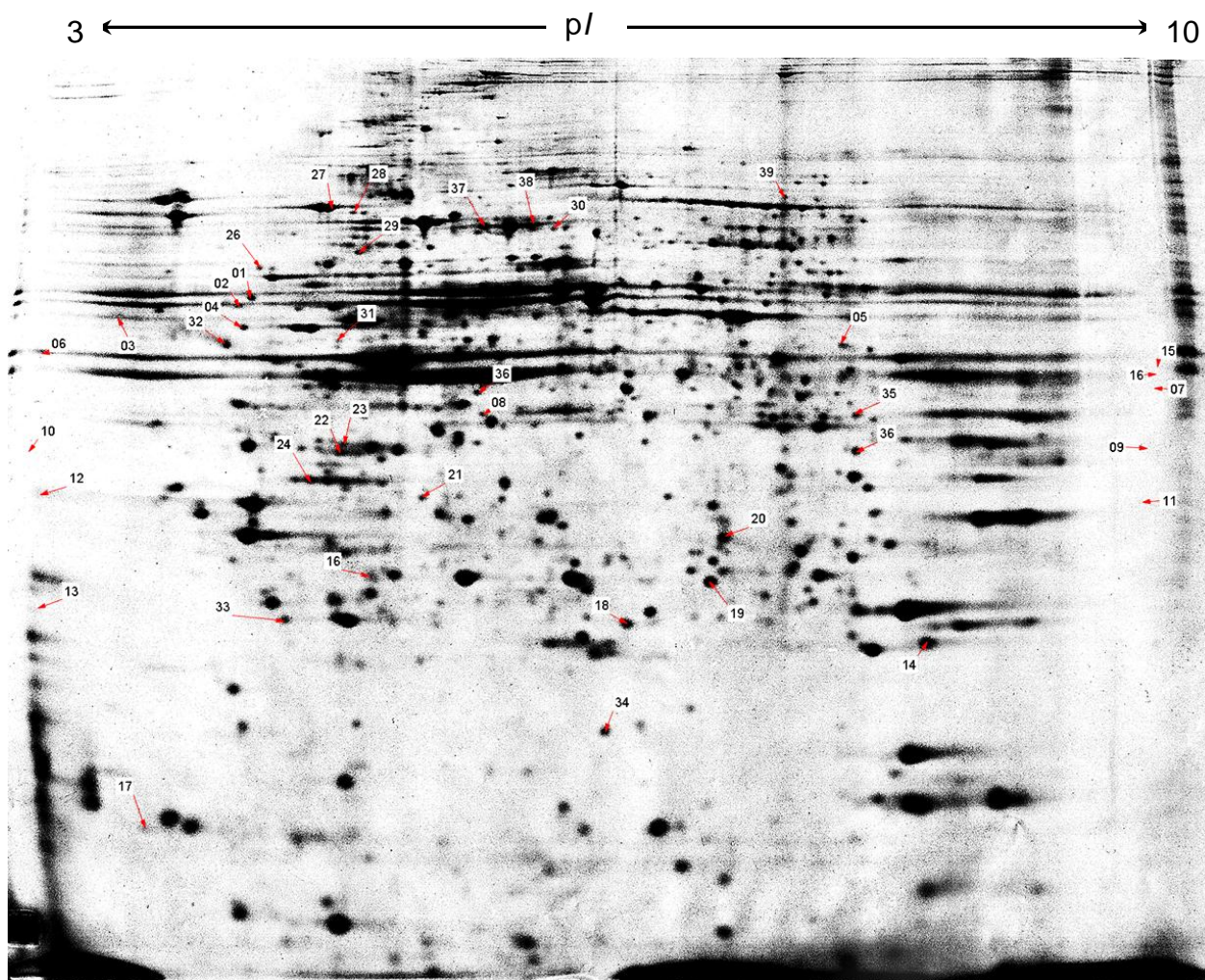


Figure 37: Representative 2D-gel image representing the differentially expressed proteins after B[a]P (0.5 μ M) exposure. 450 μ g of proteins from whole cell extract of control and B[a]P-exposed cells were separated by IEF (pH 3-10) and 12 % SDS-PAGE, and the resulting two dimensional protein arrays were detected by applying a Coomassie brilliant blue protocol developed in our laboratory. By using the Delta2D v4.0 image analysis software, 40 proteins (numbered spots) were identified as differentially expressed. For assigning the identity of these proteins as identified by MALDI-TOF-MS, protein peptide mass matching was performed on Mascot by searching the MSDB and NCBI nr protein databases with the taxonomy pig. The proteins identified by MALDI-TOF-MS are listed in **Table 7**.

10.2 Annex II – Protein complexes of subcellular fractions of RT4 cells identified by using MALDI-TOF-MS

Table 9: Mass spectrometric data of proteins identified in the cytosolic fraction of RT4 cells, used for the generation of a proteome map (see map with ID numbers in **Figure 29**).

Uniprot accession no ^a	Spot no ^c	Protein name ^a	Gene name ^a	Theoretical molecular weight / pI ^a	Score ^b	Peptide match ^b
Q01469	ID-1	Fatty acid-binding protein, epidermal	FABP5	15164.43/6.59	129	62
P15090	ID-2	Human adipocyte fatty acid binding protein	FABP4	14718.89/6.59	127	60
P49069	ID-3	Calcium signal-modulating cyclophilin ligand	CAMLG	32952.55/8.20	171	66
P60174	ID-4	Triosephosphate isomerase isoform 1	TPI1	30791.00/5.65	262	84
Q9UL46	ID-5	Proteasome activator complex subunit 1 isoform 2	PSME2	27401.63/5.54	85	45
P61289	ID-6	Proteasome activator complex subunit 1 isoform 1	PSME3	29506.06/5.69	71	50
Q9UL46	ID-7	Proteasome subunit alpha type-2	PSME2	27401.63/5.54	124	56
Q9UL46	ID-8	Proteasome subunit alpha type-2	PSME2	27401.63/5.54	75	42
P04792	ID-9	Heat shock protein 27	HSPB1	22782.52/5.98	103	39
P20618	ID-10	Proteasome (prosome, macropain) subunit, beta type, 1	PSMB1	26489.37/8.27	120	65
P49721	ID-11	Proteasome (prosome, macropain) subunit, beta type, 2	PSMB2	22836.28/6.52	103	40
P28074	ID-12	Proteasome subunit MB1	PSMB5	21844.60/9.23	79	46
P28074	ID-13	Proteasome subunit beta type-5 isoform 2	PSMB5	21844.60/9.23	79	64
O14818	ID-14	Proteasome subunit alpha type-7	PSMA7	20193.01/8.54	107	48
O14818	ID-15	Proteasome subunit alpha type-7	PSMA7	20193.01/8.54	125	57
Q9UL46	ID-16	Proteasome activator complex subunit 2	PSME2	27401.63/5.54	130	56
Q9UL46	ID-17	Proteasome activator complex subunit 2	PSME2	27401.63/5.54	180	49
Q06323	ID-18	Proteasome activator complex subunit 1 isoform 1	PSME1	28723.10/5.78	135	35
O43865	ID-19	Adenosylhomocysteinase isoform 1	AHCYL1	58951.43/6.49	138	32
P35527	ID-20	Keratin 9	KRT9	62064.32/5.14	270	41
P46926	ID-21	Glucosamine-6-phosphate isomerase 1	GNPDA1	32668.52/6.42	151	63
P07195	ID-23	*L-Lactate Dehydrogenase B	LDHB	36638.49/5.71	173	43

Uniprot accession no ^a	Spot no ^c	Protein name ^a	Gene name ^a	Theoretical molecular weight / pI ^a	Score ^b	Peptide match ^b
P07195	ID-24	*L-Lactate dehydrogenase B	LDHB	36638.49/5.71	140	35
P07195	ID-25	*L-Lactate dehydrogenase B	LDHB	36638.49/5.71	125	25
P07195	ID-26	*L-Lactate dehydrogenase B	LDHB	36638.49/5.71	166	43
P07195	ID-27	*L-Lactate dehydrogenase B	LDHB	36638.49/5.71	148	46
P07195	ID-28	*L-Lactate dehydrogenase B	LDHB	36638.49/5.71	99	27
P00338	ID-29	Lactate dehydrogenase A variant	LDHA	36688.72/8.44	165	38
P00338	ID-30	Lactate dehydrogenase A variant	LDHA	36688.72/8.44	104	35
P53396	ID-31	ATP:citrate lyase	ACLY	120839.23/6.95	165	27
P55072	ID-32	Transitional endoplasmic reticulum ATPase	VCP	89321.80/5.14	130	30
O75891	ID-33	10-formyltetrahydrofolate dehydrogenase	ALDH1L1	98829.24/5.63	284	44
P40925	ID-34	Malate dehydrogenase 1, NAD (soluble), isoform CRA_d	MDH1	27025.01/9.18	110	40
P62258	ID-35	14-3-3 protein epsilon	YWHAE	29173.90/4.63	111	49
P31947	ID-35-2	14-3-3 protein sigma	SFN	24336.24/4.77	166	68
O60701	ID-36	UDP-glucose 6-dehydrogenase isoform 1	UDGH	55024.09/6.73	206	45
P22234	ID-37	Multifunctional protein phosphoribosylaminoimidazole-succinocarboxamide synthase isoform 2	PAICS	47079.22/6.94	173	36
P22234	ID-38	Phosphoribosylaminoimidazole-succinocarboxamide synthase	PAICS	47079.22/6.94	148	30
Q32Q12	ID-39	Nucleoside diphosphate kinase	NME1-NME2	32641.97/8.70	158	40
P07737	ID-40	Human platelet profilin complexed with an L-pro10-iodotyrosine peptide	PFN1	15054.23/8.44	121	66
O76070	ID-41	Synuclein gamma	SNCG	13330.80/4.86	89	60
P60660	ID-44	Myosin light polypeptide 6	MYL6	16961.12/4.46	123	67
P04406	ID-45	Human liver glyceraldehyde-3-phosphate dehydrogenase	GAPDH	36053.21/8.57	114	31
P35579	ID-46	Myosin-9	MYH9	226532.24/5.50	205	22
P06744	ID-47	Glucose-6-phosphate isomerase isoform 1	GPI	63147.13/8.42	245	22
P13798	ID-48	Acylamino-acid-releasing enzyme	APEH	81224.55/5.29	134	28
O14818	ID-49	Proteasome subunit alpha type-7	PSMA7	20193.01/8.54	167	34
O75874	ID-51	Isocitrate Dehydrogenase	IDH1	46659.30/6.53	145	44

Uniprot accession no ^a	Spot no ^c	Protein name ^a	Gene name ^a	Theoretical molecular weight / pI ^a	Score ^b	Peptide match ^b
P07205	ID-52	Human phosphoglycerate kinase	PGK2	44796.12/8.74	170	67
A0AUL6	ID-53	Actin	ACTB	11464.13/6.94	150	47
P15121	ID-54	Human aldose reductase	AKR1B1	35853.40/6.52	199	64
A8K202	ID-55	AICAR formyltransferase/IMP cyclohydrolase bifunctional	ATIC	64509.70/6.27	166	38
P31939	ID-56	Bi-functional purine biosynthesis protein PURH	PURH	64615.87/6.27	215	46
P08238	ID-57	Heat shock protein HSP 90-beta	HSPB1	83264.20/4.96	218	43
O43707	ID-58	Actinin, alpha 4	ACTN4	104854.04/5.27	260	40
P08237	ID-59	Phosphofructokinase	PFKM	85182.52/8.23	113	32
Q9BUK9	ID-60	Heat shock 70kDa protein 4	HSPA4	15689.43/4.62	186	38
P18669	ID-61	*Phosphoglycerate mutase 1	PGAM1	28803.93/6.67	102	47
P18669	ID-62	*Phosphoglycerate mutase 1	PGAM1	28803.93/6.67	92	44
P18669	ID-63	*Phosphoglycerate mutase 1	PGAM1	28803.93/6.67	116	48
P26639	ID-64	Threonyl-tRNA synthetase	TARS	83435.10/6.23	95	22

a Gene name, protein name, theoretical molecular weight, and pI entries in Uniprot database for the each protein identified by MALDI-TOF-MS.

b Score and peptides matches in Mascot search engine.

c Experimental ID numbers.

* If multiple spots were identified as the same protein, the protein is marked with an asterisk.

Table 10: Mass spectrometric data of proteins identified in the membrane/organelle fraction of RT4 cells, used for the generation of a proteome map (see map with ID numbers in **Figure 30**).

Uniprot accession no ^a	Spot No ^c	Protein name ^a	Gene name ^a	Theoretical molecular weight / pI ^a	Score ^b	Peptide match ^b
Q9UNM1	ID-1	Chaperonin 10-related protein	EPFP1	10294.93/8.98	105	49
Q6BCY4	ID-2	Cytochrome b5 isoform 2	CYB5R2	31458.27/8.49	80	77
Q01105	ID-3	*HLA-DR-associated protein II	SET	33488.88/4.22	72	21
Q01105	ID-5	*HLA-DR-associated protein II	SET	33488.88/4.22	87	68
P30084	ID-6	Enoyl-Coenzyme A (Coa) hydratase 1	ECHS1	31387.39/8.34	172	60
P13645	ID-7	Actin-related protein 2/3 complex subunit 3	ARPC3	26011.07/5.67	106	48
Q92747	ID-9	Actin-related protein 2/3 complex subunit 1	ARPC1	41568.29/8.46	144	59
O15144	ID8	Actin-related protein 2/3 complex subunit 2	ARPC2	34333.02/6.84	158	33
HOYM70	ID-10	Keratin 10	KRT10	58827.09/5.13	125	28
P59998	ID-12	Actin-related protein 2/3 complex subunit 4 isoform a	ARPC4	19667.01/8.3	130	23
P06753	ID-13	Tropomyosin alpha-3 chain isoform 2	TPM3	32818.79/4.68	158	44
P00491	ID-14	Purine nucleoside phosphorylase	PNP	32117.87/6.45	153	62
P40925	ID-15	Malate dehydrogenase 1, NAD (soluble)	MDH1	36426.12/6.91	155	50
P38117	ID-16	Electron transfer flavoprotein	ETFB	27843.61/8.25	132	60
P38117	ID-17	Mitochondrial malate dehydrogenase 2, NAD	ETFB	27843.61/8.25	193	58
P08779	ID-21	Keratin, type I cytoskeletal 16	KRT16	51267.82/4.98	103	31
Q06830	ID-22	Peroxiredoxin-1	PRDX1	22110.36/8.27	90	49
P22570	ID-23	NADPH:adrenodoxin oxidoreductase, mitochondrial	FDXR	53836.79/8.72	82	65
P23284	ID-24	Chain A, Cyclophilin B complexed with [d-(Cholinylester)ser8]- cyclosporin	CYPB	23742.54/9.49	86	57
P62937	ID-25	Chain A, Cyclophilin A complexed with dipeptide gly-pro	CYPA	18012.49/7.68	163	75
Q01469	ID-26	Fatty acid-binding protein, epidermal	FABP5	15164.43/6.59	84	57
P07737	ID-27	Human profilin 1	PFN1	15054.23/8.44	157	66
P15090	ID-28	Adipocyte fatty acid binding protein in complex with a non-covalent ligand	FABP4	14718.89/6.59	105	53
P13674	ID-29	Procollagen-proline, 2-oxoglutarate 4-dioxygenase	P4HA1	61049.30/5.69	87	34

Uniprot accession no ^a	Spot No ^c	Protein name ^a	Gene name ^a	Theoretical molecular weight / pI ^a	Score ^b	Peptide match ^b
Q96L12	ID-30	Calreticulin precursor variant	CALR3	44995.61/6.19	177	43
P60709	ID-31	Actin	ACTB	11464.13/6.94	197	44
P53396	ID-35	ATP citrate lyase	ACLY	120839.23/6.95	187	27
O75369	ID-38	Filamin B	FLNB	278164.04/5.47	371	24
P14625	ID-39	Heat shock protein gp96 precursor	HSP90B1	92468.87/4.76	236	32
P18206	ID-43	Vinculin isoform VCL	VCL	123799.30/5.50	94	23
P13798	ID-42	*Acylamino-acid-releasing enzyme	APEH	81224.55/5.29	102	33
P13798	ID-41	*Acylamino-acid-releasing enzyme	APEH	81224.55/5.29	78	26
P38117	ID-44	Electron transfer flavoprotein subunit beta isoform 1	ETFB	27843.61(8.25)	73	40
P05062	ID-45	Muscle fructose 1,6-bisphosphate aldolase complexed with fructose 1,6-bisphosphate	ALDOB	39473.02/8.01	293	74
P13807	ID-46	Electron transfer flavoprotein subunit alpha	ETFBA	35080/8.62-	92	28
P51553	ID-47	Heterodimeric R132h mutant of human NADP(+)-dependent isocitrate dehydrogenase in complex with NADP and isocitrate	IDH3G	42794.30/8.75	197	52
P10809	ID-48	60 kDa Heat shock protein, mitochondrial	HSPD1	61054.64/5.70	170	38
P68402	ID-52	Platelet-activating factor acetylhydrolase IB subunit gamma	PAFAH1B2	17833.14/4.92	92	48
P00367	ID-53	Glutamate dehydrogenase 1, mitochondrial	GLUD1	61397.87/7.76	224	44
O15533	ID-54	Chain A, Tapasin ERP57	TAPBP	47625.77/6.67	160	34
P11021	ID-55	78 kDa glucose-regulated protein	HSPA5	72332.96/5.07	98	22
P15090	ID-57	Adipocyte fatty acid binding protein in complex with a non-covalent ligand	FABP4	14718.89/6.59	116	60
P26639	ID-58	Threonyl-tRNA synthetase, cytoplasmic	TARS	83435.10/6.23	127	28
IP25705	ID-62	Mitochondrial ATP synthase, H ⁺ transporting F1 complex beta subunit	ATP5A1	59750.63/9.16	128	32
P07437	ID-65	Tubulin, beta	TUBB	49670.82/4.78	139	30

a Gene name, protein name, theoretical molecular weight, and pI entries in Uniprot database for the each protein identified by MALDI-TOF-MS.

b Score and peptides matches in Mascot search engine.

c Experimental ID numbers.

* If multiple spots were identified as the same protein, the protein is marked with an asterisk.

Table 11: Mass spectrometric data of proteins identified in the nuclear fraction of RT4 cells, used for the generation of a proteome map.

Uniprot accession no ^a	Spot no ^c	Protein name ^a	Gene name ^a	Theoretical molecular weight / pI ^a	Score ^b	Peptide match ^b
P62805	ID-1	Histone 4	HIST2H4B	11367.34/11.36	89	51
Q0D2M2	ID-2	Histone 2	HIST1H2BC	13834.08/10.39	72	41
Q0D2M2	ID-3	Histone2	HIST1H2BC	13834.08/10.39	80	34
Q0D2M2	ID-4	Histone 2	HIST1H2BC	13834.08/10.39	102	45
P08727	ID-5	*Keratin, type I cytoskeletal 19	KRT19	44106.00/5.05	393	68
P08727	ID-6	*Keratin, type I cytoskeletal 19	KRT19	44106.00/5.05	377	56
P05783	ID-7	Cytokeratin 18	KRT18	48057.81/5.34	121	32
Q04695	ID-8	*Keratin, type II cytoskeletal 7	KRT17	48105.67/4.97	287	44
Q04695	ID-9	*Keratin, type II cytoskeletal 7	KRT17	48105.67/4.97	178	27
P05787	ID-10	Cytokeratin 8	KRT8	53704.25 /5.52	140	28
P08727	ID-11	Keratin, type I cytoskeletal 19	KRT19	44106.00/5.05	360	66
Q04695	ID-11	Keratin 17 protein	KRT17	48105.67/4.97	119	42
P08729	ID-12	*Keratin, type II cytoskeletal 7	KRT7	48105.67/4.97	296	53
P08729	ID-13	*Keratin, type II cytoskeletal 7	KRT7	48105.67/4.97	135	29
P02545	ID-14	Prelamin-A/C isoform 2	LMNA	74139.49/6.57	256	47
P08729	ID-15	*Keratin, type II cytoskeletal 7	KRT7	48105.67/4.97	142	25
Q96910	ID-16	Keratin 8	KRT8	53704.25 /5.52	120	36
P13645	ID-17	Keratin 10	KRT10	58827.09/5.13	91	23
Q9UHB6	ID-18	LIM domain and actin-binding protein 1	LIMA1	85225.55/6.41	106	23
P51530	ID-19	DNA2-like helicase	DNA2	120414.71/7.95	150	20
Q02880	ID-20	DNA topoisomerase 2-beta	TOP2B	183267.17/8.14	202	36
P08727	ID-21	*Keratin, type I cytoskeletal 19	KRT19	44106.00/5.05	107	67
Q08211	ID-22	Plectin isoform 1e	DHX9	140958.48/6.41	318	13
P08727	ID-23	*Keratin, type I cytoskeletal 19	KRT19	44106.00/5.05	413	68
P05783	ID-24	Cytokeratin 18	KRT18	48057.81/5.34	143	35

Uniprot accession no ^a	Spot no ^c	Protein name ^a	Gene name ^a	Theoretical molecular weight / pI ^a	Score ^b	Peptide match ^b
Q04695	ID-25	Keratin, type I cytoskeletal 17	KRT17	48105.67/4.97	154	28
Q04695	ID-26	Keratin, type II cytoskeletal 7	KRT7	48105.67/4.97	240	46
P05787	ID-27	Keratin 8	KRT8	53704.25 /5.52	239	67
P21796	ID-28	Porin 31HM	VDAC1	30772.60/8.62	135	52
Q9UNA4	ID-29	Human polymerase iota	POLI	83005.97/5.73	156	54
Q71DI3	ID-30	*Chain C, structure of the H3-H4 chaperone Asf1 bound to Histones H3 and H4	Histone H3.2	15388.03/11.27	70	48
Q71DI3	ID-31	*Chain C, structure of the H3-H4 chaperone Asf1 bound to histones H3 and H4	Histone H3.2	15388.03/11.27	102	64
Q71DI3	ID-32	*Chain C, structure of the H3-H4 chaperone Asf1 bound to histones H3 and H4	Histone H3.2	15388.03/11.27	91	64
Q0D2M2	ID-33	HIST1H2BC protein	HIST1H2BC	13834.08/10.39	74	50
Q99879	ID-34	Histone H2B type 1-M [Homo sapiens]	HIST1H2BM	13989.27/10.31	200	48
P19338	ID-35	Nucleolin	NCL	76614.41/4.60	287	29
Q3MI39	ID-36	Heterogeneous nuclear ribonucleoprotein A1	HNRPA1	16759.51/9.71	99	19
P62906	ID-37	*60S ribosomal protein L10a	RPL10A	24831.31/9.94	104	26
P35579	ID-38	Myosin-9	MYH9	226532.24/5.50	272	41
F5GWA7	ID-39	Prohibitin 2	PHB2	29226.59/9.21	137	37
P62906	ID-40	60S ribosomal protein L10a	RPL10A	24831.31/9.94	266	48
P0C0S8	ID-41	Histone H2A type 1-B/E	HIST1H2AG	14091.48/10.90	107	20
P55036	ID-42	S5a Uim-1 ubiquitin complex	PSMD4	40736.66/4.68	177	43
Q13242	ID-43	Serine/arginine-rich splicing factor 9	SRSF9	25542.24/8.74	199	27
Q99816	ID-44	Chain B, Tsg101(Uev) domain in complex with ubiquitin	TSG101	43944.32/6.06	259	17
Q9UNA4	ID-45	Chain B, solution structure of the human polymerase iota Ubm2- ubiquitin complex	POLI	43944.32/6.06	104	45
P0CG47	ID-46	Polyubiquitin-B	UBB	25761.64/6.86	158	23
P09629	ID-47	Homeobox B7	HOXB7	24014.62/8.83	240	34
Q9UHB6	ID-48	LIM domain and actin-binding protein 1 isoform a	LIMA1	85225.55/6.41	178	28

Uniprot accession no ^a	Spot no ^c	Protein name ^a	Gene name ^a	Theoretical molecular weight / pI ^a	Score ^b	Peptide match ^b
Q9BWF3	ID-49	RNA-binding protein 4 isoform 3	RBM4	40313.84/6.61	167	26
P21796	ID-50	Voltage-dependent anion channel	VDAC1		188	21
P22626	ID-51	Heterogeneous nuclear ribonucleoproteins A2/B1 isoform A2	HNRNPA2B	37429.70/8.97	106	31
Q9UNA4	ID-52	Human polymerase iota Ubm2- ubiquitin complex	POLI	83005.97/5.73	78	23
Q08211	ID-53	ATP-dependent RNA helicase A	DHX9	140958.48/6.41	209	34
Q15149	ID-54	Plectin isoform 1e	PLEC	531790.73/5.74	89	15
P62805	ID-55	Histone H4	HIST1H4A	11367.34/11.36	101	40

a Gene name, protein name, theoretical molecular weight, and pI entries in Uniprot database for the each protein identified by MALDI-TOF-MS.

b Score and peptides matches in Mascot search engine.

c Experimental ID numbers.

* If multiple spots were identified as the same protein, the protein is marked with an asterisk.

10.3 Annex III – List of protein complexes of subcellular fraction identified after exposure to B[a]P and TCDD

Table 11 1: List of proteins differentially expressed in the cytosolic fraction of RT4 cells identified by MALDI-TOF-MS after exposure to 200 pM TCDD for 24 h.

Spot no ¹	Gene name ²	Protein name ²	Score ³	Peptide match ³	Up or down regulated	Regulation ⁴
ID9	FLNB	Filamin B	416	26	down	-3.22999
ID1755	FTH1	Chain A, recombinant human H Ferritin, K86q mutant, soaked with Zn	83	27	down	-2,68431
ID34	NPEPPS	Aminopeptidase puromycin sensitive, isoform CRA_a	326	43	up	1.07601
ID203	S100A2	Protein S100-A2	73	53	up	3.8684
ID 231	CALM1	Chain A, trapped intermediate of calmodulin	71	31	up	2.13139
ID12	FASN	Fatty acid synthase	465	26	down	-2,16001
ID82	RBBP7	Histone-binding protein RBBP7	127	43	up	3,65179
ID148	ANP32A	ANP32A protein	160	49	up	1,75938
ID216	KRT10	Keratin 10	144	29	up	2,15201
ID68	TCP1	Chaperonin containing TCP1, subunit 3	93	26	up	2,32344
ID162	CLTA	Clathrin light chain A isoform a	112	32	up	3,28302
ID172	HEBP2	Heme-binding protein 2	86	37	up	2,03805
ID580	TCP1	Chaperonin containing TCP1, subunit 3	151	46	up	2,17571
ID205	ARPC4	Actin-related protein 2/3 complex subunit 4 isoform a	94	46	down	-2,45396
ID117	KRT2	Keratin, type II cytoskeletal 2 epidermal	93	26	up	2,28700
ID1756	IQGAP1	Ras GTPase-activating-like protein IQGAP1	288	26	down	-2,04209
ID1757	IQGAP1	Ras GTPase-activating-like protein IQGAP1	324	29	down	-1,72557
ID291	TSG101	Chain B, Tsg101(Uev) domain In complex with ubiquitin	83	61	up	3,12498
ID229	KRT16	Keratin, type I cytoskeletal 16	127	47	up	1,75034

¹: Experimental ID number.

²: Gene name and protein name entries in Uniprot database.

³: Score and peptides matches in Mascot search engine.

⁴ The values represent the ratio of the relative spot volume of treated and control cells as determined by using Delta2D v4.0 software.

Table 11 2: List of proteins differentially expressed in the membrane/organelle fraction of RT4 cells identified by MALDI-TOF-MS after exposure to 200 pM TCDD for 24 h.

Spot no ¹	Gene name ²	Protein name ²	Score ³	Peptide match ³	Up or down regulated	Regulation ⁴
13	NPEPPL1	PREDICTED: aminopeptidase puromycin sensitive isoform 2	250	26	up	1.13788
37	ACTB	ACTB protein	169	51	up	2.63077
24	ANXA10	Annexin A10	129	47	up	1.02979
25	ANXA5	Annexin A5	142	46	up	1.34865
23	AKR1B1	Chain A, fidarestat bound to human aldose reductase	201	59	up	2.02283
26	ANP32A	Acidic (leucine-rich) nuclear phosphoprotein 32 family, member A	166	48	up	2.30848
12	UBA1	Ubiquitin-like modifier-activating enzyme 1	325	40	up	1.01613
15	KRT9	Cytokeratin 9	103	50	up	1.30835
16	GSN	Gelsolin isoform b	96	23	up	1.08039
17	PDIA4	Protein disulfide-isomerase A4 precursor	303	45	up	1.18829
19	ERO1LB	Endoplasmic reticulum oxidoreductin 1	132	43	up	1.72305
18	CHRNB1	Cholinergic receptor, nicotinic, epsilon, isoform CRA_a			up	1.49665
20	GLUD1	Chain A, structure Of human glutamate dehydrogenase-apo form	245	51	up	1.16010
21	SHMT2	Serine hydroxymethyltransferase, mitochondrial isoform 3	139	43	down	-2.27026
42	EIF3A	Eukaryotic translation initiation factor 3, subunit A	135	19	down	-2.14621
3	NME2	Nm23 human nucleoside diphosphate kinase B complexed with Gdp	161	78	down	-1.09288
5	TFRC	Transferrin receptor protein 1	91	17	up	1.35857
6	TFRC	Transferrin receptor protein 1	113	24	up	1.35857
7	KRT1	Keratin 1	83	23	up	1.15404
33	PSMB9	Proteasome (prosome, macropain) subunit, beta type, 1	90	51	down	-1.42373
34	PRDX1	Peroxiredoxin-1	77	49	down	-1,93899
40	PSMA3	Proteasome (prosome, macropain) subunit, alpha type, 3	78	45	down	-2.34886

¹: Experimental ID number.

²: Gene name and protein name entries in Uniprot database.

³: Score and peptides matches in Mascot search engine.

⁴ The values represent the ratio of the relative spot volume of treated and control cells as determined by using Delta2D v4.0 software

Table 11 3: : List of proteins differentially expressed in the nuclear fraction of RT4 cells identified by MALDI-TOF-MS after exposure to 200 pM TCDD for 24 h.

Spot no ¹	Gene name ²	Protein name ²	Score ³	Peptide match ³	Up or down regulated	Regulation ⁴
ID-359867	MYH9	Myosin-9	166	20	up	3.57206
ID-359670	HIST1H1E	Histone H1.4	79	36	up	2.45941
ID-359484	POLI	Human polymerase Iota Ubm2- ubiquitin complex	83	77	up	6.25469
ID-359483	TSG101	Chain B, Tsg101(Uev) domain in complex with ubiquitin	73	61	up	3.05263
ID-359479	PHB	Prohibitin	89	42	up	2.10602
ID-359476	VDAC1	Porin 31HM	121	58	up	1.89122
ID-359470	RPL10A	60S ribosomal protein L7	91	35	up	2.35149
ID-359480	SRSF9	Serine/arginine-rich splicing factor 9	90	42	up	2.83745

¹: Experimental ID number.

²: Gene name and protein name entries in Uniprot database.

³: Score and peptides matches in Mascot search engine.

⁴ The values represent the ratio of the relative spot volume of treated and control cells as determined by using Delta2D v4.0 software

Table 11 4 : List of proteins differentially expressed in the cytosolic fraction of RT4 cells identified by MALDI-TOF-MS after exposure to 0.5 μ M B[a]P for 24 h.

Spot no ¹	Gene name ²	Protein name ²	Score ³	Peptide match ³	Up or down regulated	Regulation ⁴
ID22326	PFN1	Profilin-1	147	58	down	1.87683
ID22471	TBCD	Tubulin-specific chaperone d, isoform CRA_c	161	24	up	1.88427
ID22486	VCP	Transitional endoplasmic reticulum ATPase	234	46	up	1.92522
ID22491	ALDH1L1	10-formyltetrahydrofolate dehydrogenase	423	51	up	2.1961
ID22515	KRT2	Keratin, type II cytoskeletal 2 epidermal	68	17	down	-2.29904
ID22516	CCT2	T-complex protein 1 subunit beta isoform 2	131	44	up	2.12253
ID22545	IDH1	Heterodimeric R132h mutant of human cytosolic NADP(+)-dependent isocitrate dehydrogenase in complex with NADP and isocitrate	240	53	down	-1.81488
ID22596	NME2	Nucleoside diphosphate kinase B isoform a	154	73	down	-1.7242
ID22613	FABP4	Human adipocyte fatty acid binding protein	91	59	up	4.13207
ID24295	PREP	Prolyl endopeptidase	213	44	up	2.25443
ID24958	ATIC	Bifunctional purine biosynthesis protein PURH	203	50	up	-2.04968
ID25983	LDHA	Lactate dehydrogenase A variant	113	31	down	-1.20712
ID22033	PRDX6	Peroxiredoxin-6	92	48	up	2.25032
ID22510	TCP1	T-complex protein 1 subunit alpha isoform a	111	31	up	3.59029
ID26273	PRDX6	Peroxiredoxin-6	153	64	down	-2.27703

¹: Experimental ID number.

²: Gene name and protein name entries in Uniprot database.

³: Score and peptides matches in Mascot search engine.

⁴ The values represent the ratio of the relative spot volume of treated and control cells as determined by using Delta2D v4.0 software

Table 11 5: List of proteins differentially expressed in the cytosolic fraction of RT4 cells identified by MALDI-TOF-MS after exposure to 0.5 μ M B[a]P for 24 h.

Spot no ¹	Gene name ²	Protein name ²	Score ³	Peptide match ³	Up or down regulated	Regulation ⁴
BaP2-06	CLTC	Clathrin heavy chain 1 isoform 6	342	27	up	1.73274
BaP2-15	PDIA4	Protein disulfide-isomerase A4 precursor	329	47	up	2.39697
BaP2-23	UGDH	UDP-glucose 6-dehydrogenase isoform 1	167	48	up	1.82155
BaP2-26	ALDOA	Fructose 1,6-bisphosphate aldolase complexed with fructose 1,6-bisphosphate	273	66	down	-1.82195
BaP2-30	ANXA10	Annexin A10	82	30	down	-3.95467
BaP2-33	TPM3	Tropomyosin alpha-3 chain isoform 3	103	45	down	-2.92923
BaP2-39	PPIB	Cyclophilin B complexed with cyclosporin	116	57	up	1.74984
BaP2-43	PPIA	Cyclophilin A complexed with dipeptide Gly-Pro	85	67	up	3.41278
BaP2-47	PFN1	Profilin complexed with An L-Pro10-iodotyrosine peptide	113	58	up	1.76324
BaP2-07	UBA1	Ubiquitin-like modifier-activating enzyme 1	279	36	up	2.67377
BaP2-16	P4HA1	Procollagen-proline, 2-oxoglutarate 4-dioxygenase	251	57	up	7.82073
BaP2-18	UBA1	Ubiquitin-like modifier-activating enzyme 1	287	34	down	-1.7525
BaP2-19	CALR	Calreticulin precursor variant	125	43	up	2,15407
BaP2-20	GPI	Glucose-6-phosphate isomerase isoform 1	123	27	down	-3.0432
BaP2-22	ATP5A1	ATP synthase, H+ transporting, mitochondrial F1 complex, alpha subunit 1	182	33	up	2.54415
BaP2-24	ATP5B	Mitochondrial ATP synthase, H+ transporting F1 complex beta subunit	155	47	up	1.82857
Bap2-31	GNPDA1	Glucosamine-6-phosphate isomerase 1	150	64	down	-3.95467
Bap2-08	UBA1	Ubiquitin-like modifier-activating enzyme 1	331	37	up	2.59967
Bap2-42	PPIA	Cyclophilin A complexed with dipeptide Gly-Pro	134	82	up	3.74312
Bap2-45	PPIA	Cyclophilin A complexed with dipeptide Gly-Pro	157	75	up	3.07921
Bap2-48	KRT9	Keratin, type I cytoskeletal 9	108	32	up	2.62558

¹: Experimental ID number.

²: Gene name and protein name entries in Uniprot database.

³: Score and peptides matches in Mascot search engine.

⁴ The values represent the ratio of the relative spot volume of treated and control cells as determined by using Delta2D v4.0 software

Table 11 6: : List of proteins differentially expressed in the nuclear fraction of RT4 cells identified by MALDI-TOF-MS after exposure to 0.5 μ M B[a]P for 24 h.

Spot no ¹	Gene name ²	Protein name ²	Score ³	Peptide match ³	Up or down regulated	Regulation ⁴
2	KRT8	Keratin 8 protein	261	77	down	-1.90642
3	KRT7	Keratin, type II cytoskeletal 7	330	53	down	-1.95532
4	KRT19	Keratin, type I cytoskeletal 19	416	74	down	-2.7945
5	HNRPA1	Heterogeneous nuclear ribonucleoprotein A1	96	42	up	2.65593
6	VDAC1	Porin 31HM [human, skeletal muscle membranes	107	53	up	2.32705
7	HIST1H1B	Histone H1.5	100	43	up	4.05107
8	PHB	Prohibitin	77	38	up	4,03869
9	NDUFV1	NADH dehydrogenase [ubiquinone] iron-sulfur protein 3, mitochondrial precursor	70	27	up	8.73903
10	HECTD3	Chain X, E2~ubiquitin-Hect	75	77	up	8.73204
11	RPL10A	60S ribosomal protein L10a	77	50	up	2.13607
15	UBE2K	Ubiquitin-conjugating enzyme E2 K	79	59	up	3.61185
22	PSMB9	Proteasome (prosome, macropain) subunit, beta type, 9	74	32	up	2.27713
23	HIST1H2BM	Histone H2B type 1-M	76	50	down	-3.83119
24	HIST1H2AG	Histone H2A type 1-B/E	70	30	down	-4.15894
25	HIST2H3A	TH3-H4 chaperone Asf1 bound to histones H3 and H4	120	66	down	-3.16213
26	MYH9	Myosin-9	253	23	up	3.06755
27	DHX9	Nuclear DNA helicase II	152	19	up	3.10872

¹:Experimental ID number.

²: Gene name and protein name entries in Uniprot database.

³: Score and peptides matches in Mascot search engine.

⁴ The values represent the ratio of the relative spot volume of treated and control cells as determined by using Delta2D v4.0 software

10.4 Annex IV – Representative 2D BN/PAGE gel images after exposure to B[a]P and TCDD

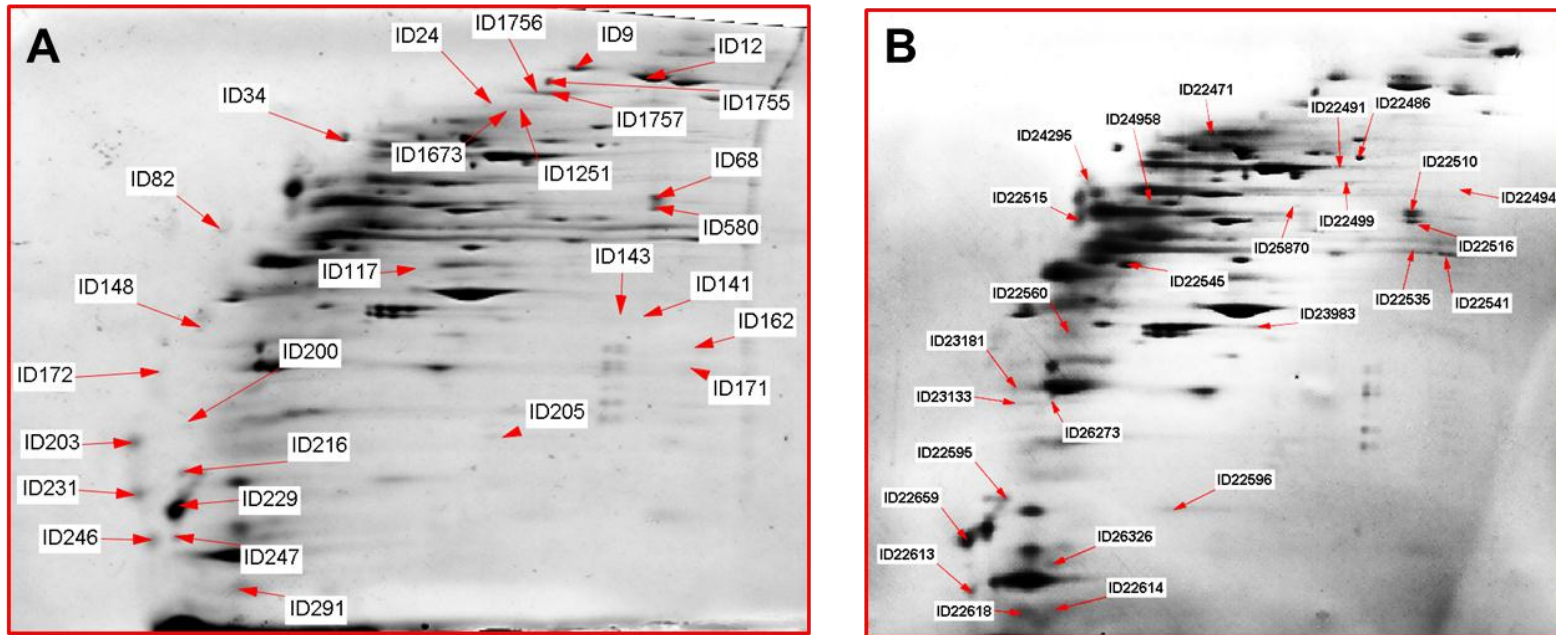


Figure 38: 2D BN/PAGE gels representing proteins differentially expressed in the cytosolic fraction of RT4 cells after 24 h exposure to [A] TCDD (200 pM) or [B] B[a]P (0.5 μ M). 75 μ g of proteins from cytosolic fraction of control, B[a]P- and TCDD-exposed cells were separated by 4-12 % BN-PAGE and 12 % SDS-PAGE. The resulting protein arrays were detected by applying a Coomassie brilliant blue protocol developed in our laboratory. By using the Delta2D v4.0 image analysis software, numbered spots with arrows were identified as differentially expressed. For assigning the identity of these proteins, protein peptide mass matching was performed on Mascot by searching MSDB and NCBIr protein databases with the taxonomy *homo sapiens*. The proteins identified by MALDI-TOF-MS are listed in **Table 11.1** (TCDD) and **11.4** (B[a]P).

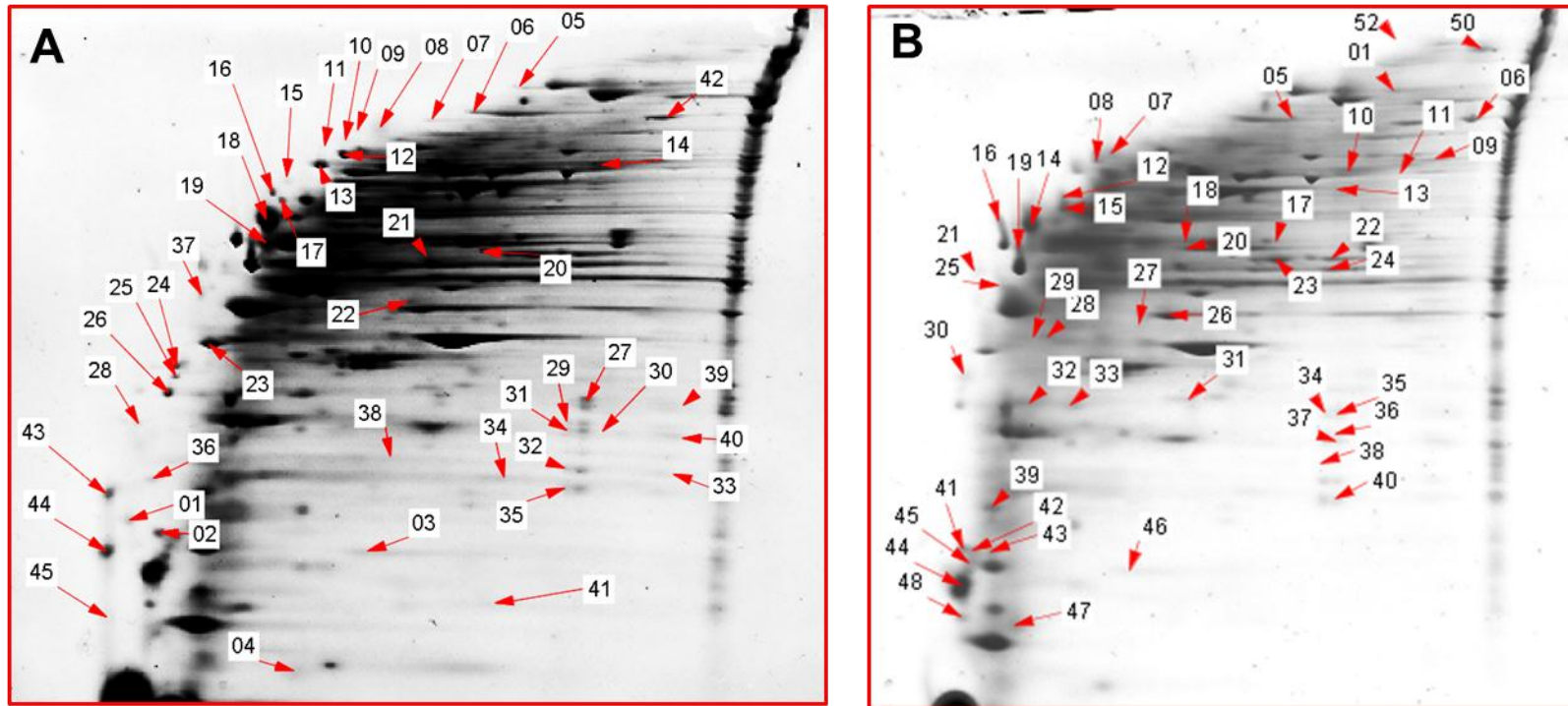


Figure 39: 2D BN/PAGE gels representing proteins differentially expressed in the membrane/organelle fraction of RT4 cells after 24 h exposure to [A] TCDD (200 pM) or [B] B[a]P (0.5 μ M). 75 μ g of proteins from cytosolic fraction of control, B[a]P- and TCDD-exposed cells were separated by 4-12 % BN-PAGE and 12 % SDS-PAGE. The resulting protein arrays were detected by applying a Coomassie brilliant blue protocol developed in our laboratory. By using the Delta2D v4.0 image analysis software, numbered spots with arrows were identified as differentially expressed. For assigning the identity of these proteins, protein peptide mass matching was performed on Mascot by searching MSDB and NCBIr protein databases with the taxonomy *homo sapiens*. The proteins identified by MALDI-TOF-MS are listed in **Table 11.2** (TCDD) and **11.5** (B[a]P)

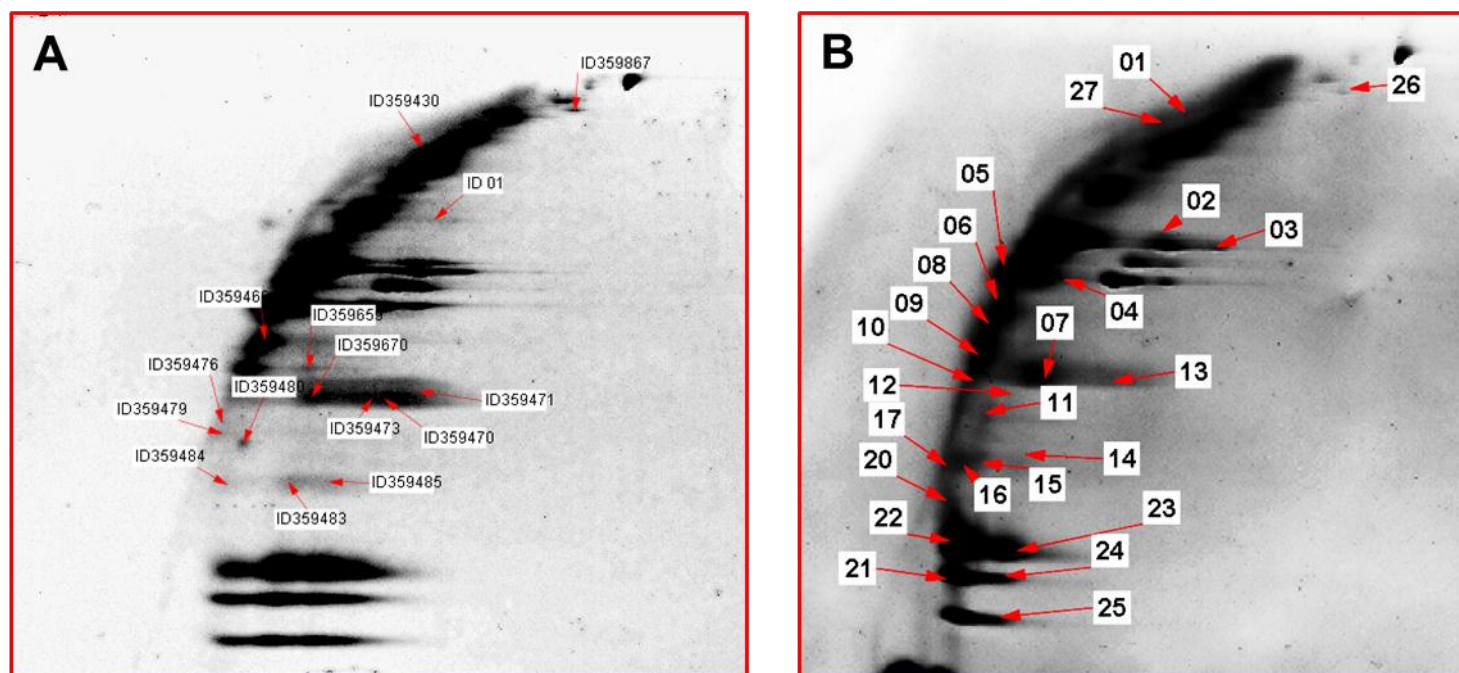


Figure 40: 2D BN/PAGE gels representing proteins differentially expressed in the nuclear fraction of RT4 cells after 24 h exposure to [A] TCDD (200 pM) or [B] B[a]P (0.5 μ M). 75 μ g of proteins from cytosolic fraction of control, B[a]P- and TCDD-exposed cells were separated by 4-12 % BN-PAGE and 12 % SDS-PAGE. The resulting protein arrays were detected by applying a Coomassie brilliant blue protocol developed in our laboratory. By using the Delta2D v4.0 image analysis software, numbered spots with arrows were identified as differentially expressed. For assigning the identity of these proteins, protein peptide mass matching was performed on Mascot by searching MSDB and NCBI nr protein databases with the taxonomy *homo sapiens*. The proteins identified by MALDI-TOF-MS are listed in **Table 11.3** (TCDD) and **11.6** (B[a]P)

10.5 Annex V - Cell culture media, reagents, and instrumentation

Medium for PUBEC

Medium	
472 ml (500 – 28 mL) F-12 medium	C.C. Pro GmbH, Oberdorla, Germany
Supplements	
2.5 ml Amphotericin (1.25 µg/mL)	C.C. Pro GmbH, Oberdorla, Germany
2.5 ml L-Glutamine (146 µg/mL)	PAA GmbH, Cölbe, Germany
2.5 mL Transferrin (5 µg/mL)	Sigma, Taufkirchen, Germany
5.0 mL NEAA (0.1 mM)	GIBCO, Darmstadt, Germany
5.0 mL Insulin (10 µg/mL)	PAA GmbH, Cölbe, Germany
5.0 mL Glucose (2.7 mg/mL)	Sigma, Taufkirchen, Germany
5.0 mL Penicillin-streptomycin (100 U/100 µg/mL)	GIBCO, Darmstadt, Germany
0.5 mL Hydrocortisone (1 µg/mL)	Sigma, Taufkirchen, Germany
50 µL Epidermal growth factor (20 ng/mL)	Sigma, Taufkirchen, Germany

Medium for RT4 cell line

Medium	
441.3 ml (500 – 58.7 mL) McCoy's medium	C.C. Pro GmbH, Oberdorla, Germany
Supplements	
3.7 ml L-Glutamine (1.5 mM)	Sigma, Taufkirchen, Germany
5.0 mL Penicillin-streptomycin (100 U/100 µg/mL)	GIBCO, Darmstadt, Germany
50 mL Fetal bovine serum (10 %)	GIBCO, Darmstadt, Germany

Instrumentation	
IPGphor isoelectric focusing unit (IEF) Ettan DALTsix electrophoresis system IPG-Stripe (3-10 NL) Isoelectric focusing system Gel-Custer	Amersham Bioscience, Freiburg, Germany
MALDI-TOF-MS (Voyager-STR)	Applied Biosystems, Foster City (USA)
Mass Spec Turbo 192 CHCA Chip	Qiagen, Hilden
Centrifuges: Allegra 6R Allegra X15R Ultracentrifuge L8-M	Beckman Coulter, Krefeld, Germany
Scanner (ScanMaker 9800XL)	Mikrotek, Willich, Germany
Genios Multi-Detection Microplate Reader	Tecan, Mainz, Germany
Confocal microscope	LSM 510, Zeiss, Oberkochen, Germany
Gas Chromatograph	HP 6890/5973, Agilent Technologies, Waldbronn, Germany
Leica DMLB, Fluorescence Microscope	Bensheim, Germany
Spectrofluorometer	Varian Cary Eclipse, Varian, Palo Alto, CA

Software	Version	Firm
Silverfast	6.6.0r3	LaserSoft Imaging AG, Kiel, Germany
Delta2D	4.0	Decodon, Greifswald, Germany
Voyager Instrument Control Panel	5.1	Applied Biosystems, Foster City, USA
Data Explorer	4.0	
Mascot	2.2	Matrix Science, London, England
Comet assay IV	4.3	Perspective Instruments, UK
Leica application suite	3.5.0	Leica Microsystems CMS GmbH, Switzerland

Kits and dyes used for the study

Kit	
Subcellular Proteome Extraction Kit	Cat no 539790, ProteoExtract [®] , Merck KGaA, Darmstadt, Germany
Dyes	
Phen Green [™] SK, diacetate	Cat no P14313, Molecular Probes [®] , Invitrogen, Darmstadt, Germany
Calcein, AM	Cat no C3100MP, Molecular Probes [®] , Invitrogen, Darmstadt, Germany
Fluo-4/AM	Cat no F-14201, Molecular Probes [®] , Invitrogen, Darmstadt, Germany
Rhod-2/AM	Cat no PK-CA707-50024, PromoKine, Heidelberg, Germany
Rhodamine 123	Cat no R302, Molecular Probes [®] , Invitrogen, Darmstadt, Germany

Chemicals	
1,4-Dithiothreitol (DTT)	
Bromphenol blue	
Glycine	
Agarose	Amersham Bioscience, Freiburg, Germany
Ammonium persulphate (APS)	
Glycerine	
N,N,N',N'-Tetramethylethylenediamine (TEMED)	
Pharmalyt 3-10	
Calibration-Standard (MALDI-TOF)	Applied Biosystems, Foster City, USA
Acrylamid-Bis solution (30 % Acrylamid, 0,4 % Bis)	BioRad, München, Germany
Penicillin-streptomycin	C-C-Pro, Neustadt, Germany
Trypsin (cell culture)	
Benzo[a]pyrene (B[a]P)	Fluka, Buchs, Switserland
Iodacetamide (IAA)	GE-Healthcare, München, Germany
Phosphate-buffered saline	Gibco, Karlsruhe, Germany
1-Butanol	
Coomassie brilliant blue G 250	
Ethanol	Merck, Darmstadt, Germany
Phosphoric acid 85 %	
Trifluoroacetic acid (TFA)	
Fetal calf serum (FCS)	PAA Laboratories, Pasching, Austria
Dry strip cover fluid (oil for IEF)	Pharmacia Biotech, Uppsala, Sweden
Aluminium sulfate	Riedel de Haën, Seelze Sigma, Taufkirchen, Germany
Complete [™] , Protease Inhibitor Cocktail tablets	Roche, Mannheim, Germany
Bovine serum albumin (BSA)	SERVA, Heidelberg, Germany
Acetonitrile	
Ammonium bicarbonate	
Dimethyl sulfoxide (DMSO)	
Ethylene diamine tetraacetate (EDTA)	Sigma, Taufkirchen, Germany
Sodium dodecyl sulfate (SDS)	
Sucrose	

Chemicals	
Thiourea	
Trypsin (proteomic grade)	
Tris(hydroxymethyl-)aminomethan (Tris)	Sigma, Taufkirchen, Germany USB Corporation, Cleveland, USA
Urea	
3-[(3-Cholamidopropyl)-dimethylammonio]-1-propanesulfonate (CHAPS)	USB Corporation, Cleveland, USA

10.6 Annex VI - Curriculum Vitae

Dr. rer. Nat. Nisha Verma

M.Sc. (Biotechnology), M.Phil. (Biotechnology),

PhD in Natural Sciences

CORRESPONDENCE:

Removed for reasons of data protection

PUBLICATIONS

Published / Accepted for publication

1. Verma N., Pink M., Petrat F., Rettenmeier A.W. & Schmitz-Spanke S. (2012) **Exposure of primary porcine urothelial cells to benzo[a]pyrene: *In vitro* uptake, intracellular concentration and biological response.** *Archives of Toxicology* 86(12): 1861-1871.
2. Verma N., Pink M., Rettenmeier A.W. & Schmitz-Spanke S. (2012) **Review on proteomic analyses of benzo[a]pyrene toxicity.** *Proteomics* 12(11): 1731-1755.
3. Verma N., Bäuerlein C., Pink M., Rettenmeier A.W. & Schmitz-Spanke S. (2011) **Analysis of the proteome and phosphoproteome of primitively cultured pig urothelial cells.** *Electrophoresis* 32(24): 3600-3611.
4. Verma N., Rettenmeier A.W. & Schmitz-Spanke S. (2011) **Recent advances in the use of *Sus scrofa* (pig) as a model system for proteomic studies.** *Proteomics* 11(4): 776-793.
5. Pink M., Verma N., Polato F., Hideo B.A., Rettenmeier W.A., & Spanke- Schmitz S. (2011) **Precipitation by lanthanum ions: an improved approach to isolate phosphoproteins.** *Journal of Proteome Research* 10(2): 375-83.
6. Pink M., Verma N., Rettenmeier A.W. & Schmitz-Spanke S. (2010) **CBB staining protocol with higher sensitivity and mass spectrometric compatibility.** *Electrophoresis* 31(4): 593-598.
7. Pink M, Stein C, Verma N, ., Rettenmeier A.W. & Schmitz-Spanke S. (2012) Gel-based separation of phosphoproteins in samples stored in urea/thiourea after precipitation by lanthanum chloride. *Electrophoresis* (doi: 10.1002/elps.201200278).

Submitted

8. Pink M., Verma N., Rettenmeier A.W. & Schmitz-Spanke S. (2012) **Integrated proteomic and metabolomics analysis to assess the effects of carbon black nanoparticles on energy metabolism in the human endothelial cell line EA.hy926.** (submitted)

Abstracts

1. **Verma N., Pink M., Rettenmeier A. W., Schmitz-Spanke S. (2012) Identification of protein complexes involved in calcium and iron homeostasis after TCDD exposure.** *Naunyn-Schmiedeberg's Archives of Pharmacology*, 385 (1), pp 99-99.
2. Schmitz-Spanke S., Pink M., Jeske E., Stempelmann K., Rehn S., Verma N., Rettenmeier A. W. (2012) **Protein expression changes in B[a]P-exposed human bladder cancer cells from spliceosome activation towards redistribution of the cytoskeleton after long-term exposure to subacute concentration.** *Naunyn-Schmiedeberg's Archives of Pharmacology*, 385 (1), pp 83-84.
3. **Verma N., Rettenmeier A.W. & Schmitz-Spanke S. (2010) Proteomic analysis of primary porcine bladder epithelial cells after B[a]P exposure.** *Toxicology Letters*; 196: S571-S571.
4. **Verma N., Rettenmeier A.W. & Schmitz-Spanke S. (2009) Pig as a model organism for toxicoproteomic studies on bladder cancer.** *Toxicology Letters*; 189: S194-S194.
5. Chand D., Vitzthum F., Sogani M., Pandey D., Singh R., Verma N. & Bhalla T.C. (2007) **Synthesis of acetohydroxamic acid in batch and fed-batch mode using acyltransferase activity of resting cells of *Nocardia globerula* entrapped in alginate gel beads.** *XVth International Workshop on Bioencapsulation*, Vienna, Austria: S1-05.
6. **Verma N., Chand D. & Pandey D. (2006) Isolation and screening of Glutaminase producing microbes.** *47th Annual Conference of Association of Microbiologists (AMI)*, Barakatullah University, Bhopal, Madhya Pradesh: p 188.
7. Chand D., Kumar D.K., Pandey D., Verma N. & Singh R. (2006) **Production of wide-spectrum amidase from *Bacillus* sp. APB 6.** *47th Annual Conference of Association of Microbiologists (AMI)*, Barakatullah University, Bhopal, Madhya Pradesh: p 180.
8. Singh K.S., Chand D., Pandey D., Verma N., Kumar D., Tyagi N. & Bhalla T.C. (2005) **Isolation and screening of acyltransferase producing bacterial strains and optimization of production and reaction conditions.** *46th Annual Conference of Association of Microbiologists (AMI)*, Osmania University, Hyderabad, Andhra Pradesh: p 75.
9. Pandey D., Chand D., Verma N., Singh K.S. & Bhalla T.C. (2005) **Purification and characterization of acyltransferase from *Nocardia globerula*.** *46th Annual Conference of Associations of Microbiologist (AMI)*, Osmania University, Hyderabad, Andhra Pradesh: p 75.
10. Tyagi N., Chand D., Pandey D., Verma N., Singh K.S., Kumar D. & Bhalla T.C. (2005) **Purification and characterization of amidase from *Nocardia globerula*.** *46th Annual Conference of Association of Microbiologists (AMI)*, Osmania University, Hyderabad, Andhra Pradesh: p 47.

Oral* / Poster Presentations**

1. ****Verma N., Pink M., Rettenmeier A.W. & Schmitz-Spanke S. (2012) Identification of protein complexes involved in calcium and iron homeostasis after TCDD exposure.** *Deutsche Gesellschaft für Experimentelle und Klinische Pharmakologie und Toxikologie*, Dresden, Germany
2. ***Verma N. (2011) Protein complexes as downstream targets of AhR signaling and the possible role of calcium and iron in TCDD mediated toxicity.** *17 Workshop of*

Zell- und Gewebeschädigung: Mechanismen, Protektion und Therapie, Xanthen, Germany.

3. ****Verma N., Rettenmeier A.W. & Schmitz-Spanke S. (2011) Studies on the analysis of Benzo(a)pyrene uptake and distribution using laser scanning microscopy.** *Deutsche Gesellschaft für Arbeitmedizin Und Umweltmedizin*, Heidelberg, Germany.
4. ****Verma N., Rettenmeier A.W. & Schmitz-Spanke S. (2010) Proteomic analysis of primary porcine bladder epithelial cells after B[a]P exposure.** *XII International Congress of Toxicology*, Barcelona, Spain.
5. ****Verma N., Rettenmeier A.W. & Schmitz-Spanke S. (2009) Pig as a model organism for toxicoproteomic studies on bladder cancer.** *46th Congress of European Society of Toxicology*, Dresden, Germany.
6. ****Verma N., Rettenmeier A.W. & Schmitz-Spanke S. (2008) Proteomics of porcine urinary bladder epithelial cells (PUBEC): The role of aryl hydrocarbon receptor.** *Forschungstag der Medizinischen Fakultät*, Essen, Germany.
7. ****Verma N., Chand D. & Pandey D. (2006) Isolation and Screening of Glutaminase producing microbes.** *47th Annual Conference of Association of Microbiologists (AMI)*, Barakatullah University, Bhopal, Madhya Pradesh.

Conferences* / Workshops Attended**

1. ****Membrane proteomics by Blue Native PAGE** (26-28th May, 2010) Hannover University, Germany.
2. ****Workshop on protein analysis of tissues** (06-07th March, 2009) Helmholtz Zentrum, München, Germany.
3. ***Nanotechnology & Biotechnology** (26-29th March, 2006) ASSOCHAM global knowledge millennium summit-IV, New Delhi, India.
4. ***Strategy for sustainable development of Himachal Pradesh with special emphasis on industry, tourism, Biotech & IT** (6-7th November, 2006) Shimla, India.
5. ***Entrepreneurship development programme in Biotechnology** (11-15th June, 2007) Shimla, India.

RESEARCH EXPERIENCES

1. PhD Thesis title: Proteomic Analysis of Benzo[a]pyrene-Mediated Bladder Toxicity.

Research Advisors: Prof. A.W. Rettenmeier & Dr. S. Schmitz-Spanke, Institute of Hygiene and Occupational Medicine, University Hospital Essen, Essen, Germany

2. M.Phil. Thesis title: Isolation and screening of Glutaminase producing microbes

Research Advisors: Dr. Duni Chand, Department of Biotechnology, H.P. University, Shimla.

3. M.Sc. Dissertation title :Molecular diagnostics of plant viruses

Supervisor: Dr. I.D. Garg, Head of the Department, Department of Plant Pathology, Central Potato Research Institute (CPRI), Shimla-171001.

PROJECT COMPLETED

- 1. Wastewater and solid waste management in hill region** (December 2005- May 2006).
- 2. Optimization of production and reaction parameters for Nitrilase from *Bacillus sp.* APB-6 isolated from soil of Himachal Himalaya** (August 2007-March 2008).

SPECIAL TRAININGS

- 1. Deutsch I (A1/1) language course** (completed). Institute für Optional Studien, Universität Duisburg-Essen, Germany (September 2008 to February 2009).
- 2. Training on Tools & Techniques used in Biotechnology.** Department of Experimental Medical Education, Post Graduate Institute of Research and Education, Chandigarh (PGIMER), India (June-2003 to July 2003).

10.7 Annex VII - Acknowledgement

It gives me immense pleasure to express my heartiest thanks and deep sense of gratitude to my esteemed guides Prof. Rettenmeier and Dr. Schmitz-Spanke for their intellectual stimulation, expert guidance, continued encouragement, and constructive suggestions, throughout the course of this investigation. I am extremely grateful to them for their keen interest, ever available help and unstained support which were a source of great inspiration and helped me a lot in conducting this work successfully.

I owe my deepest thank to all the members of our working group. I would specially like to thank Fr. Rehn, Fr. Stempelmann, Fr. Jeske, Fr. Biermann, and Hr. Diedrich for their technical support.

I am also thankful to Dr. Mosel, Prof. Dopp and all the non-technical staff of Institute for Hygiene and Occupational medicine for their cooperation throughout my work.

I extend my sincere thanks to Prof. de Groot and Dr. Petrat, Institute of Physiological Chemistry for opening the door of their institute for me. I specially would like to thank Dr. Petrat for his excellent scientific guidance. His exhaustive knowledge about iron metabolism and expertise in confocal microscopy has supported me throughout this work. I would also like to thank Dr. Effenberger-Neidnicht for introducing me to the Griess assay.

I also wish to express my sincere appreciation to Prof. Iliakis, Institute of Radiation Biology, for letting me use the facilities of his institute. I would specifically like to thank Dr. Mladenov for his technical assistance.

Special thanks go to my colleague and friend Mario, for all the help, all the work we've done together and all the great scientific and nonscientific debate we had. PhD work would never have been so much exciting without him.

Thanks go to Ricarda, Jessica, Heeda and Anna for your friendship and great environment during my stay in the department. I would particularly like to thank Ricarda for your valuable friendship, long walks, many relaxing moments, and enjoyable conversations.

I am also thankful to my friends Kunal, Aashish, Neru, Satyender, Savita, Rohit, Aparaná, Janapriya, Pooja, Stefan, and Deepa for many enjoyable evenings and a wonderful time in Germany. I felt like home with all you people around.

My dearest thanks are due to my revered parents, loving sisters and brother for their affection, inspiration, and moral support.

Last but not the least I fall short of words to thanks my husband, my best friend Shree for giving me the confidence to explore my research interests and for believing in me. I am intellectually indebted to his ideas and our conversations. None of this could have happened without him. This thesis is dedicated to him.

10.8 Annex VIII - Declaration

Erklärung:

Hiermit erkläre ich, gem. § 6 Abs. 2, Nr. f der Promotionsordnung der Math.-Nat. Fakultäten zur Erlangung des Dr. rer. nat., dass ich das Arbeitsgebiet, dem das Thema: **“Proteomic Analysis of Benzo[a]pyrene-Mediated Bladder Toxicity“** zuzuordnen ist, in Forschung und Lehre vertrete und den Antrag von Frau Nisha Verma befürworte.

Essen, den 4. September 2012

.....
(Prof A.W.Rettenmeier)

Erklärung:

Hiermit erkläre ich, gem. § 7 Abs. 2, c und e der Promotionsordnung der Math.-Nat. Fakultäten zur Erlangung des Dr. rer. nat., dass ich die vorliegende Dissertation selbständig verfasst und mich keiner anderen als der angegebenen Hilfsmittel bedient habe und alle wörtlich oder inhaltlich übernommenen Stellen als solche gekennzeichnet habe.

Essen, den 4. September 2012

.....
(Nisha Verma)

Erklärung:

Hiermit erkläre ich, gem. § 7 Abs. 2, d und f der Promotionsordnung der Math.-Nat. Fakultäten zur Erlangung des Dr. rer. nat., dass ich keine anderen Promotionen bzw. Promotionsversuche in der Vergangenheit durchgeführt habe, dass diese Arbeit von keiner anderen Fakultät abgelehnt worden ist, und dass ich die Dissertation nur in diesem Verfahren einreiche.

Essen, den 4. September 2012

.....
(Nisha Verma)